Construction, Operation, and Performance Evaluation of a Continuous Supercritical Fluid Extraction Process for the Recovery of Hydrocarbons from Drill Cuttings

by

Christianne Gwendolyn Street

A thesis submitted in partial fulfillment of the requirements for the degree of

Doctor of Philosophy
in
Environmental Engineering

Department of Civil and Environmental Engineering
University of Alberta

Abstract

The primary outcome of this research is the design, construction, commissioning, and operation of a novel, pilot-scale, continuous supercritical fluid extraction (SFE) process for recovering drilling fluid hydrocarbons from drill cuttings-water slurries. Counter-current flow of slurry and supercritical carbon dioxide (SC CO_2) was successfully demonstrated, and hydrocarbon was extracted from the cuttings.

The performance of the SFE process was measured by extraction efficiency and overall mass transfer coefficients of which a maximum 95.8 % and 9.69×10^{-4} s^{-1}, respectively, were achieved. Calculation of the extraction efficiency and overall mass transfer coefficient required the adaptation of a cold-shake solvent extraction method from the literature to determine the hydrocarbon content of cuttings. Additionally, the solubility of a drilling fluid hydrocarbon in SC CO_2 was experimentally measured, and the data was fit to the Chrastil correlation, in order to calculate the overall volumetric mass transfer coefficients.

Analysis of the operating and performance results provides recommendations for prioritizing future work, including introducing a slurry level measurement device for the bottom of the vessel, increasing the flow rates of SC CO_2 and slurry, and increasing the density by testing higher pressures.

The outcomes of this thesis demonstrate that the SFE process can extract hydrocarbons from drill cuttings-water slurries. The performance results provide useful recommendations towards the future commercialization of the process.

Preface

Chapter 2 of this thesis is a joint effort between Maedeh Roodpeyma and Christianne Street and it is available in both theses of the authors. Chapter 2 is associated with the continued design, build, and commission/operation of the continuous pilot-scale SFE process for treatment of drill cuttings. The three stated stages were conducted and completed as a collaboration between Maedeh Roodpeyma and Christianne Street. Department technicians (Civil & Environmental and Chemical & Materials Engineering) Perry Fedun, Todd Kinnee and Les Dean contributed to the build stage of the process. Eleisha Underwood and Warren Stiver contributed to the data collection and analysis in Chapter 3. The remainder of the thesis is the original work of the author, Christianne Street.

For Michael, Hanna, and Emily

Acknowledgements

The author would like to acknowledge the scholarly and personal support of the thesis supervisory committee: Dr. Selma Guigard, Dr. Warren Stiver, and Dr. Ergun Kuru. The author also gratefully acknowledges Maedeh Roodpeyma for her partnership in all aspects of this project.

Funding for the project was jointly provided by the Natural Sciences and Engineering Research Council (NSERC) of Canada and M-I SWACO. Scholarship support for the author was provided from the University of Alberta, the Government of Alberta, and NSERC. Drill cuttings samples for the project were provided by M-I SWACO and Ramdar Resource Management Ltd.

Technical support was provided by technicians in the Departments of Civil & Environmental Engineering and Chemical & Materials Engineering at the University of Alberta, including: Eleisha Underwood, Perry Fedun, Todd Kinnee, Les Dean, Jela Burkus, Maria Demeter, Steve Gamble, David (Yupeng) Zhao, Chen Liang, and Elena Dlusskaya.

For Chapter 3, Eleisha Underwood assisted in the development of the experimental method and completion of the measurements. Dr. Warren Stiver completed the Chrastil fitting of the experimental and literature data.

The work of Angelique Rosenthal at the University of Guelph in documenting the system preliminary design and operation, as well as completing the safety analysis, was key to the project's success. The prior slurry extraction and solubility results of Christopher Jones at the University of Alberta were the starting point for the efficiency and mass transfer analysis. Kory Auch and Alexandra Couillard assisted during the design and construction phases of the project, with funding provided by NSERC Undergraduate Student Research Awards. Marianne Barrier, an undergraduate student from INSA Lyon, completed chromatography work for early mass transfer samples.

Table of Contents

List of Tables

List of Figures

List of Abbreviations and Nomenclature

Abbreviations

AARD	Average absolute relative deviation
BTEX	Benzene, toluene, ethylbenzene, and xylene
CO_2	Carbon dioxide
D822	Distillate 822
GUI	Graphical user interface
HAZOP	Hazard and operability study
PAC	Programmable automation controller
P&ID	Piping and instrumentation diagram
RT	Real time
SC CO_2	Supercritical carbon dioxide
SFE	Supercritical fluid extraction
VFD	Variable frequency drive

Nomenclature

A	Constant (Chrastil 1982), K
A_x	Cross sectional area of extraction column, m^2
α	Constant (Evans et al. 1979)
B	Constant (Chrastil 1982), dimensionless
β	Constant (Evans et al. 1979)
C	Constant (Chrastil 1982), dimensionless; or Concentration, $g \cdot g^{-1}$
C_1	Constant (Fair 1993), dimensionless
C_p	Gas specific heat (Fair 1993), $BTU \cdot lb^{-1} \cdot °F^{-1}$
C^*	Interfacial concentration of oil in CO_2, $g \cdot g^{-1}$
D_{12}	Diffusion coefficient (Evans et al. 1979), $m^2 \cdot s^{-1}$
dz	Height of infinitesimal slice of column, m
H	Height of column, m
η	Extraction efficiency, %

η_2	Dynamic viscosity of solvent (Evans et al. 1979), Pa·s
HTU	Height of transfer unit (Fair 1993), ft
ka	Overall volumetric mass transfer coefficient, s^{-1}
$\dot{m}_L$	Liquid mass velocity (Fair 1993), $lb \cdot h^{-1} \cdot ft^{-2}$
n	Rate of mass transfer, $g \cdot s^{-1}$
ρ	Density of the supercritical solvent, $kg \cdot m^{-3}$
Pr	Prandtl number (Fair 1993), unitless
Q	Flow, $g \cdot s^{-1}$
Sc	Schmidt number (Fair 1993), unitless
T	Temperature (Evans et al. 1979), K
y	Solubility of the solute in the supercritical solvent, $g \cdot g^{-1}$

Subscripts

sl	Slurry
in	Flow into the vessel or infinitesimal slice of column
out	Flow out of the vessel or infinitesimal slice of column
oil	Oil
z, z+1	Position along height of infinitesimal slice of column
int	Interface between CO_2 and oil
CO2	Carbon dioxide
bulk	Bulk CO_2 (away from the interface)

Chapter 1: Introduction and Background Information

Chapter 1 provides the introduction and background information for the thesis including the problem definition, an overview of previous research, the objectives, the role of the thesis in the larger project, and thesis organization. Background information is provided on the drilling process; cuttings production; regulations regarding the treatment and disposal of cuttings; supercritical fluids; previous supercritical fluid extraction (SFE) research for the treatment of cuttings; and previous development of a fully continuous baffle column for the SFE of soil slurries.

1.1 Problem Definition

In rotary drilling for petroleum resources, drilling fluids, or "muds", are used as a circulating fluid. Drilling muds serve several purposes in the drilling process including cooling and lubricating the drill string and bit; preventing ingress of formation fluids to the wellbore by maintaining hydrostatic pressure; forming a filter cake on the wellbore wall to prevent drilling mud infiltration to lower pressure formations; reducing friction and drag of the drill string in the wellbore; preventing stuck pipe; and carrying the drilled solids, or "cuttings", from the active drilling surface to the surface (IAOGP 2003).

Drilling muds are typically composed of bentonite and barite solids suspended in a continuous liquid base, which may be either water or a non-aqueous fluid (IAOGP 2003). Water-based muds are inexpensive compared with non-aqueous-based muds, but water-based muds are not suitable for drilling wells that are deep, highly deviated, or are susceptible to hole enlargement through the reaction of the fluid with the drilled formation (IAOGP 2003). In these cases, non-aqueous-based muds are better suited through their inherent higher level of lubrication, decreased reactivity, and better thermal stability (IAOGP 2003). Non-aqueous-based muds can use either oil (such as diesel) or a synthetic hydrocarbon (such as refined mineral oil) as the base fluid (IAOGP 2003). Synthetic base fluids are typically used where a more biodegradable or less toxic non-aqueous-based fluid is needed. However, their cost can be 3 to 5 times that of oil-based fluids.

Figure 1.1 is a schematic of the mud circulation and cuttings recovery system of a drilling rig.

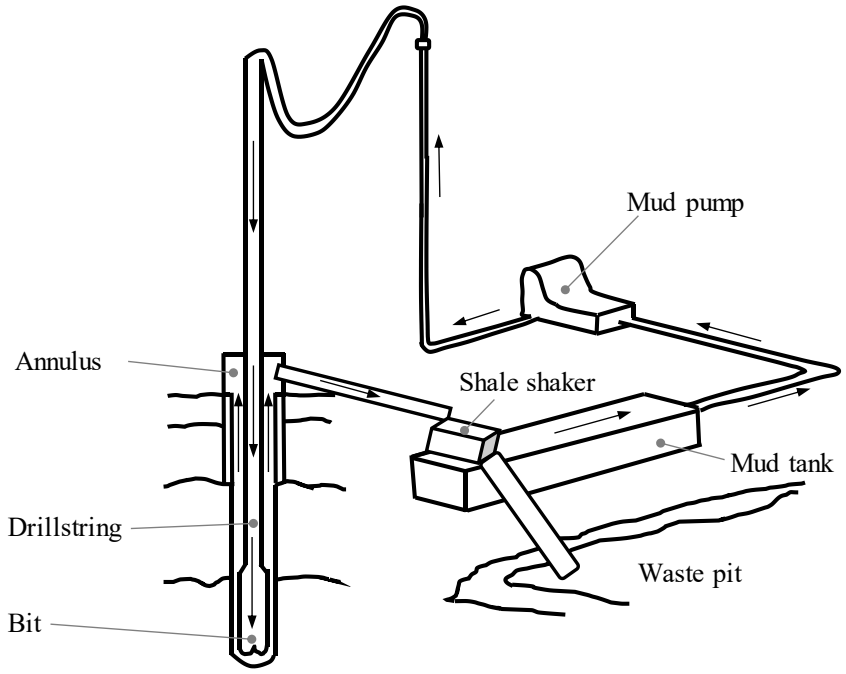

Figure 1.1: Drilling rig mud circulation system, adapted from Whittaker (1985)

Following the circulation path in Figure 1.1, first the drilling mud is pumped by the mud pumps from the mud pit, down the drillstring and out of the nozzles on the drill bit (IAOGP 2003; Whittaker 1985). The mud lifts the cuttings from the active drilling surface, up the annulus, and out of the wellbore. Then, the mud and cuttings pass through solids control equipment, such as a shale shaker, where the mud and cuttings are separated so that the mud can be recirculated, and the cuttings can be collected in a pit or container for disposal.

The quantity and composition of the cuttings depends on the wellbore dimensions; the efficiency of the solids control equipment; the drilling mud formulation; and the well subsurface, including the types of formations that are drilled through (USEPA 2019; USEPA 2000). Drill cuttings are a significant waste stream but there is very limited information on the exact quantities produced because the information is not regularly collected, or if it is collected, the methods used are not uniform to allow for aggregation or comparison (USEPA 2019). However, some estimates regarding the quantities of cuttings produced are available. For example, the United States Environmental Protection Agency (USEPA) estimated that

1500 million litres of cuttings were produced in the United States in 1995 (USEPA 2000). That estimate increased to 5300 million litres in 2016 (USEPA 2019). Of interest to this thesis are cuttings generated from the use of non-aqueous-based muds. Depending to the drilling location, anywhere from 20 to 75 % of wells drilled are drilled with non-aqueous-based muds, amounting to at least 530 million litres of hydrocarbon contaminated cuttings requiring treatment, in the United States alone (Burke and Veil 1995; USEPA 2000). In Canada, in 2018, just over 7300 wells were drilled (CAPP 2019). If 20 % of those wells were drilled with non-aqueous-based muds and approximately 640 m^3 of cuttings were produced per well, then the total amount of contaminated cuttings equals just over 460 million litres for 2018 (Burke and Veil 1995; USEPA 2000).

Drilling waste management practices have improved significantly since the beginnings of the petroleum resource industry 160 years ago. In the past, drill cuttings were a nuisance by-product of drilling that were disposed of in the most convenient method without regard for the environment or public health (Veil 2002). Onshore drilling wastes were typically discarded on the well site or nearby roads, and offshore wastes were typically discharged to the ocean. By the 1980s, regulators began to recognize the environmental impacts of the direct release of cuttings and began placing restrictions on drilling waste disposal (Veil 2002). Regarding cuttings generated from the use of non-aqueous-based muds, the current most stringent offshore disposal regulations do not allow direct discharge (eg., offshore Norway, above the 68^{th} parallel) (USEPA 2011). Below the 68^{th} parallel in Norway, discharge of cuttings from non-aqueous-based muds is allowed, but the cuttings hydrocarbon content must be below 1 % by weight (USEPA 2011). Canada does not permit the offshore discharge of cuttings produced from the use of oil-based fluids, but cuttings produced from the use of synthetic-based fluids can be discharged provided they contain less than 6.9 g of hydrocarbon per 100 g of wet solids (AER 2019).

As with offshore regulations, onshore disposal of cuttings is regulated differently depending on the jurisdiction. As an example, in Alberta the management of cuttings is regulated in *Directive 050: Drilling Waste Management* (AER 2019). Approved management methods include: storage at a well-site, pipeline right-of-way, or remote site; land applications such

as spraying, pump-off to surface soils, landspreading, or mix-bury-cover; biodegradation either as part of land treatment or in a contained system; subsurface disposal (or, "reinjection"); thermal treatment; and transferring the waste to an approved waste management facility (e.g., landfill). Each management method has its own regulations regarding waste and site suitability. *Directive 050* focusses on the end point hydrocarbon content of the soil after the cuttings are applied, the most stringent being in coarse-grained soils in agricultural or residential land at 0.3 g total hydrocarbon per 100 g of dry soil (with specific endpoints for the hydrocarbon carbon number fractions and benzene, toluene, ethylbenzene, and xylene) (AER 2019).

With millions of litres of hydrocarbon-contaminated cuttings being produced and ever-tightening regulations around their disposal, the petroleum industry has a need for better options in cuttings management. Each currently available disposal option and treatment technology, while effective, has some drawback. The main disadvantage being that most of them do not recover the valuable hydrocarbon for reuse (for example landfilling, biodegradation, and reinjection). Thermal desorption is the only commercially available technology which can recover the hydrocarbon from the base fluid. In thermal desorption, the cuttings are heated and the hydrocarbons are removed by volatilization (IAOGP 2003). Thermal desorption can reduce the hydrocarbon content of the solids to less than 1 % (Seaton et al. 2006). The main disadvantage of thermal desorption is its high operating cost, due to the energy used for heating (IAOGP 2003). Also, heating the cuttings can negatively impact the quality of the recovered hydrocarbons by the production of aromatic compounds through thermal degradation or "cracking" (Zupan and Kapila 2000; Seaton et al. 2006). In conclusion, there are currently very limited options for a technology that will fill the need for both a significant reduction in the hydrocarbon content of cuttings while recovering the valuable base fluid, at a high quality, for reuse.

One such technology is SFE. SFE is a technology that uses a substance above its critical pressure and temperature as a solvent. Above this point, the liquid and vapour phases of the substance merge, producing a supercritical fluid that has liquid-like density, gas-like diffusivity and viscosity, as well as a near-zero surface tension, making it an ideal solvent

(McHugh and Krukonis 1994). Supercritical fluids may be 'tuned' in terms of solvent power by changing operating pressure and temperature so that one supercritical fluid may replace multiple common liquid solvents that are typically less friendly to the environment and public health (Phelps et al. 1996). Carbon dioxide (CO_2) is the supercritical fluid of choice for many applications. In general, CO_2 is inexpensive, readily available, non-toxic, non-flammable, and has an easily attainable critical point of 31°C and 7.38 MPa (McHugh and Krukonis 1994).

Supercritical fluid technology, primarily using CO_2, has already been successfully commercialized, most notably since the 1970s for the decaffeination of coffee and tea (Phelps et al. 1996). Since that time, there are numerous successful commercial applications processing thousands of litres of feedstock per day, including production of hops extracts, recovery of essential oils from herbs and spices, extraction and fractionation of edible oils, and contaminant removal (Brunner 2010; Brunner 2005). Very recently, a 1.6 million $kg \cdot y^{-1}$ SFE system using CO_2 for the processing of cannabis for oil was announced to be built in Lethbridge, Alberta (Thar Process 2019). Many of the applications are operated in a semi-continuous mode, which has allowed the cost of the SFE process to become competitive (Brunner 2005).

Several lab scale, batch studies have investigated the use of various supercritical or near-supercritical fluids for the extraction of hydrocarbons from drill cuttings. These are summarized in Table 1.1.

Table 1.1: Summary of batch supercritical and near-supercritical extractions for the removal of hydrocarbons from cuttings

Ref.	Contaminant Oil Type	Sample Size (g)	Supercritical Fluid	Extraction Pressure (MPa)	Extraction Temperature (°C)
Eppig et al. (1984)	Diesel, Asphalt, No. 4 fuel oil	10 – 300	CO_2	9.7 – 22.1	30 – 70
			Freon	3.4 – 8.3	60
			Propane	3.4 – 8.3	45 – 65
Eldridge (1996)	Not specified	251 – 279	Propane	5.2 – 7.6	104
			Freon	5.2	121
Saintpere and Morillon-Jeanmaire (2000)	Not specified	200 – 6000	CO_2	6 – 12	35 – 45
Odusanya (2003)	Diesel	10	CO_2	8.3 – 17.2	35 – 60
Tunnicliffe and Joy (2007)	Not specified	1	CO_2	6.9 – 24.1	ambient – 43
Lopez-Gomez (2004)	Diesel	100	CO_2	8.9 – 15.2	40 – 60
Seaton and Hall (2005)	Diesel, Mineral oil, Synthetic	Not stated	Butane	3.4	ambient
			Propane	3.4	ambient
Massetti et al. (2006)	Not specified	Not stated	CO_2	6.8	20
Goodarznia and Esmaeilzadeh (2006)	Not specified	< 6	CO_2	16 – 22	55 – 79.5
Esmaeilzadeh et al. (2008)	Not specified	< 6	CO_2	20	55 – 79.5
Street (2008)	Synthetic	50 – 150	CO_2	14.5	40
Ma et al. (2019)	Mineral oil	5 – 20	CO_2	12 – 25	21 – 60

The results from all the studies suggest the effectiveness of supercritical carbon dioxide (SC CO_2) to extract hydrocarbon from cuttings. Eppig et al. (1984) investigated the use of supercritical propane, Freon, and CO_2 for the treatment of a variety of drilling wastes. The performance of the extraction was not quantified, but the treated cuttings appeared dry and free-flowing.

Eldridge (1996) investigated an SFE system using propane and Freon for the removal of hydrocarbon from drilling cuttings from North Sea oil platforms. The system achieved 98 % removal of the hydrocarbon contamination and determined that SFE for offshore treatment of drilling cuttings less expensive than a 20 well reinjection program, onshore processing, or substituting the oil-based drilling mud with water or synthetic-based muds.

Saintpere and Morillon-Jeanmaire (2000) investigated the treatment of hydrocarbon-contaminated drill cuttings from offshore in the North Sea using SC CO_2 and found that the extraction system could reduce the hydrocarbon content on the cuttings to below 1 %. Saintpere and Morillon-Jeanmaire (2000) also concluded that the range of carbon numbers in the base fluid hydrocarbon was unaltered by supercritical processing.

In the first of three lab-scale, batch SFE studies undertaken in the Department of Civil and Environmental Engineering at the University of Alberta, Odusanya (2003) determined that the hydrocarbon content of diesel contaminated cuttings could be reduced from 17 % to 0.6 %. As in Saintpere and Morillon-Jeanmaire (2000), the study also concluded that the hydrocarbon carbon number range was not altered in the extraction process, leading to the potential for reuse of recovered hydrocarbon base fluid in future drilling operations. The study recommended mixing to improve contact between the SC CO_2 and the waste.

The second study from the University of Alberta, completed by Lopez Gomez (2004), built upon the results of the first by designing and adding a mixer to the extraction vessel. The best process parameters tested were 14.5 MPa, 40°C, and 800 rpm, resulting in a reduction in cuttings hydrocarbon content from 19.4 % to 0.3 % by mass.

Seaton and Hall (2005) tested near supercritical propane and butane extraction as a treatment for diesel, mineral oil and synthetic contaminated drill cuttings. The tests were performed at ambient temperature due to the safety risk in using propane and butane. Mixing was incorporated after uneven flow of the supercritical fluid through the cuttings, resulting in a residual hydrocarbon content in the cuttings of 0.53 % by mass. Seaton and

Hall (2005) also tested a scaled-up version of their SFE equipment, capable of handling 10 kg of cuttings. Unfortunately, processing an increased mass of cuttings lead to failure of the equipment when fine particles from the cuttings clogged the flow lines.

Massetti et al. (2006) describe a liquid CO_2 extraction system for the "removal and recovery of the oily component from drill cuttings". Although experimental results given in the patent are limited, the system was able to achieve 1.0 % by weight hydrocarbon content residue on the cuttings.

Goodarznia and Esmaeilzadeh (2006) and Esmaeilzadeh et al. (2008) established good removal of hydrocarbons from small masses of cuttings using SC CO_2 but did not provide quantitative results on extraction efficiency or final hydrocarbon on solids.

A patent by Tunnicliffe and Joy (2007) described a bench-scale system for the removal of hydrocarbons from cuttings using near-critical CO_2. No quantitative results on extraction efficiency were given, but qualitative observations of the treated solids indicated an optimum process condition of 24.1 MPa and ambient temperature. Tests on the recovered hydrocarbon showed a lower flash point, lower viscosity, and higher API gravity, which indicates a preferential extraction of hydrocarbon components with lower carbon numbers.

The third University of Alberta study by Street (2008) demonstrated excellent hydrocarbon removal from fine-grained cuttings using SC CO_2, with extraction efficiencies up to 99 % and final hydrocarbon on solids of 0.1 % by weight. Like the results from Seaton and Hall (2005), the nature of the cuttings texture caused significant clogging of the flow lines downstream of the batch vessel, requiring the vessel outlet to be re-designed.

More recently, Ma et al. (2019) confirmed the extraction of hydrocarbons from cuttings using SC CO_2 by showing extraction efficiencies up to 98 %. The study also details the results of a carbon number analysis on the hydrocarbon in the cuttings before and after extraction. Ma et al. (2019) conclude that the range of hydrocarbon numbers is consistent before and after extraction, which confirms the previous results of others in the literature. The carbon

number analysis showed preferential extraction of hydrocarbons with carbon numbers less than 15 and n-alkanes, compared with higher carbon number hydrocarbon and iso-alkanes.

Despite years of excellent results at a lab-scale, SFE for the treatment of hydrocarbon contaminated cuttings has yet to be commercialized. Full-scale semi-continuous systems with two batch extraction vessels operating in parallel have been proposed, but never realized (Eldridge, 1996; Eppig et al. 1984; Saintpere and Morillon-Jeanmaire 2000; Masetti et al. 2006; Tunnicliffe and Joy 2007). The primary issue is batch or semi-continuous systems are not suitable for processing materials with high throughputs, like cuttings, because of the materials handling challenges in loading and unloading the vessel(s) (Akgerman and Yeo, 1993; Montero et al. 1996).

A continuous, counter-current SFE system would solve the materials handling problem and has been shown, on the basis of total material throughput, to reduce processing and capital costs (Brunner 2005; Laitenen et al. 2004). The challenge with such a system is in how to introduce and remove a contaminated solid matrix from ambient into a pressurized vessel. To meet that challenge, a lab-scale, fully-continuous SFE system was designed and built at the University of Guelph for the removal of polyaromatic hydrocarbons (naphthalene and phenanthrene) from soil. The system demonstrated successful counter-current flow of SC CO_2 and a soil/water slurry through a baffle tray column (Fortin 2003). The performance of the system was quantified by calculating overall volumetric mass transfer coefficients. A second study, by Forsyth (2006), improved upon the design of Fortin (2003) and improved the overall volumetric mass transfer coefficient by an order of magnitude.

The baffle tray column design by Fortin (2003) and Forsyth (2006) could be applied to drill cuttings but would require that the cuttings be slurried with water. It is known that the presence of water in a porous matrix can hinder SFE, primarily by preventing the contact between the supercritical fluid and the solute of interest (Saldana et al. 2005). As a step towards commercialization of the process, Jones (2010) conducted a study on a lab-scale batch reactor with SC CO_2 and cuttings slurried with varying amounts of water. The purpose of the study was to ascertain the impact of water on the extraction efficiency of the SFE

process. Jones (2010) initially found that the presence of water, ranging from a 1:1 to 5:1 water-to-cuttings ratio by mass, had a significant effect on the extraction efficiency, dropping the efficiency to as low as 35.4 %. However, Jones (2010) demonstrated that design changes to the vessel could overcome the mass transfer barrier presented by the water. By improving mixing with a new impeller design and introducing the supercritical fluid to the vessel to prevent short-circuiting of the flow, Jones (2010) was able to achieve 98 % efficiency on a 1:1 slurry. As an additional step towards commercialization, Jones (2010) also completed a preliminary study on the solubility of a pure base fluid in SC CO_2, as solubility is an important parameter in the design of a supercritical process.

In summary, toward a solution to the problem of cuttings waste, SFE has been shown to successfully remove hydrocarbon base fluids from cuttings and cuttings-water slurries, though only in batch systems. Batch systems are not the best option to meet the need for cuttings treatment primarily because of issues in handling large throughputs of materials, but a continuous process could fill the need. A continuous SFE process for water-soil slurries was shown to be successful at a lab-scale in terms of operation and in the extraction of polyaromatic hydrocarbons. In order to advance the technology toward commercialization, a pilot-scale continuous system, based on the design of Fortin (2003) and Forsyth (2006), is needed.

1.2 Research Objectives

Towards the commercialization of a continuous SFE process for the treatment of hydrocarbon contaminated cuttings, the specific objectives of this research are:

1. To design, build, commission, and operate a pilot-scale, continuous SFE process.
2. To measure the solubility of drilling fluid base hydrocarbons in SC CO_2.
3. To quantify the performance of the continuous SFE process by calculating extraction efficiencies and overall volumetric mass transfer coefficients.

Tasks involved in the first objective include completing the process design, building and commissioning the process, and using the process to conduct experiments. Success will be demonstrated by safe and reliable operation and the recovery of hydrocarbon. For the

second objective, solubility of a drilling fluid base hydrocarbon will be further investigated, following and improving upon the procedure developed by Jones (2010). A successful outcome will be reliable solubility data that can be used to help measure performance in Objective 3. For the third objective, tasks include sampling and analysing the hydrocarbon content of the slurry before and after treatment in the process. Success will be determined by the reliable measurement of slurry hydrocarbon content and the calculation of extraction efficiencies and overall volumetric mass transfer coefficients that are useful for future work.

1.3 Role of the Research in the Overall Project

This thesis is part of an overall project aimed at commercializing the use of SFE for the treatment of hydrocarbon contaminated cuttings. The overall project is a collaboration between the University of Alberta and the University of Guelph supported by an industrial partner (M-I SWACO) and the Natural Sciences and Engineering Research Council (NSERC) of Canada. Initial conceptual design work was completed by Dr. Selma Guigard at the University of Alberta, and Dr. Warren Stiver at the University of Guelph. Subsequent research contributions to the overall project have been completed under their supervision, including the piping and instrumentation (P&ID) diagrams and process pipe and flow diagrams (PFD) that were drafted and completed by Angelique Rosenthal at the University of Guelph (Rosenthal 2012). The diagrams were based on design elements from the lab-scale cuttings studies at the University of Alberta (Odusanya, 2003; Lopez Gomez, 2004; Street, 2008; Jones, 2010) and the lab-scale continuous soil slurry treatment studies at the University of Guelph (Fortin 2003; Forsyth 2006). The P&ID and PFD were updated by the author, Christianne Street, and Maedeh Roodpeyma (both University of Alberta).

Construction of the SFE process for this research was initiated in 2010 by Christianne Street. From 2011 to 2016, Christianne Street and Maedeh Roodpeyma were involved in completing the design, building and commissioning, and operating the process. The SFE system was built in the Innovative Process Laboratory in the Department of Civil and Environmental Engineering at the University of Alberta by Christianne Street and Maedeh Roodpeyma, with assistance from department technicians Perry Fedun and Todd Kinnee. The control system of the SFE process was built and programmed based on the control philosophy as proposed

by Rosenthal (2012) with the assistance of Les Dean (technician from the Department of Chemical and Materials Engineering, University of Alberta). The control philosophy was also initiated by Rosenthal (2012) and implemented by Maedeh Roodpeyma.

Commissioning and operating (running experiments) were completed by Christianne Street and Maedeh Roodpeyma. Once reliable operation with slurry had been established, it was the primary role of Christianne Street to implement a slurry sampling and analysis procedure as well as quantify the performance of the process by calculating the extraction efficiency and mass transfer coefficients as described in this thesis.

1.4 Thesis Structure

The body of this thesis is divided into four main chapters. These are:

- *Chapter 1 – Thesis Introduction & Background Information*. Chapter 1 reviews the problem of cuttings, reviews the previous research on supercritical fluids for cuttings treatment, and provides the overall objectives of the thesis.
- *Chapter 2 – Design, Build, Commission, and Experimental Runs*. Chapter 2 describes the results related to the first overall objective of the thesis that is the construction and operation of the pilot-scale SFE process.
- *Chapter 3 – Solubility of Distillate 822 in Supercritical Carbon Dioxide*. Chapter 3 provides the results related to the second overall objective of this thesis, which is to provide a measure of a drilling fluid solubility in SC CO_2. The solubility measurement will ultimately help define the current performance through the overall mass transfer coefficient.
- *Chapter 4 – Continuous SFE Process Performance in the Removal of Hydrocarbons from Drill Cuttings*. Chapter 4 provides a measure of the pilot-scale, continuous SFE process performance through the calculation of extraction efficiency and overall volumetric mass transfer coefficient.
- *Chapter 5 – Conclusions and Recommendations.* Chapter 5 summarizes the main research outcomes considering the study objectives and provides recommendations for future work.

A reference list and appendices are included at the end of the thesis.

Chapter 2: Design, Build, Commission, and Experimental Runs[1]

2.1 Introduction

If a continuous SFE process is the solution for the problem of drill cuttings treatment, then first the process must exist. Second, the process must function with the primary goal of removing hydrocarbons from the cuttings. As mentioned previously, a bench scale continuous SFE process was developed to treat contaminated solids (Fortin 2003; Forsyth 2006), however a larger, pilot-scale process, for the treatment of drill cuttings does not exist. Therefore, this Chapter details the development of such a process in the Innovative Process Lab in the Department of Civil and Environmental Engineering at the University of Alberta. The process that is described in this Chapter is unique - in both its size and function. To the authors' knowledge, it is the first pilot-scale SFE process that can continuously provide countercurrent flow of both a supercritical solvent and slurried solids through the extraction vessel.

The aim of Chapter 2 is to present this unique process and prove its functionality through experiments that demonstrate:

1. The process can operate at supercritical conditions of pressure and temperature (above 7.4 MPa and 31°C for CO_2).
2. The process can operate in a continuous, countercurrent flow regime with both SC CO_2 and slurry (containing water and cuttings or cuttings-like solids at varying solids: water ratios).
3. The process can be operated for a period of time, not dictated by deviations from normal operations that require emergency shutdowns.

[1] Chapter 2 of this thesis is a joint effort between M. Roopdeyma and C. Street and it is available in both theses of the authors. Chapter 2 is associated with the continued design, build and commission/operation of the continuous pilot-scale SFE process for treatment of drill cuttings. The three stated stages were conducted and completed as a collaboration between M. Roodpeyma and C. Street. Department technicians (Civil & Environmental and Chemical & Materials Engineering) P. Fedun, T. Kinnee and L. Dean contributed to the build stage of the process.

Additionally, in meeting the three objectives stated above, it will be shown that the process can operate safely and extract hydrocarbon from the slurry.

The preliminary design for the process is documented in the thesis of Rosenthal (2012), and is based upon the bench scale process developed at the University of Guelph (Fortin 2003; Forsyth 2006). Chapter 2 lays out the steps that were undertaken to complete the process design, procure its parts, build it, commission it and conduct safe operation. The development of the continuous pilot-scale SFE process is categorized into three main phases: design, build and commission/operation. Although the activities in each phase are distinct, implementation of the phases overlapped. The design of the SFE process was initiated in early 2009 and is available in Rosenthal (2012). Improvements to the design of the process were continuous and triggered by troubleshooting required in the building and commissioning phases but the majority of the process was built between late 2009 and mid-2014. The build phase specifically consisted of sourcing, purchasing and assembling the different components and programming the control system. Commissioning began in December 2012 as specific sub-systems were completed and is also currently ongoing. The commission/operation phase includes both proving basic functionality and studying the impacts of process parameters on mass transfer and process control.

In Chapter 2, Section 2.2 provides an overview of the SFE process that was developed. Section 2.3 describes the changes made to the preliminary process design proposed by Rosenthal (2012). In Section 2.4, the completed commissioning experiments are summarized. Important modifications made to the process as a result of certain experimental runs are also provided. The summary outlining the claims of the chapter is presented in Section 2.5.

2.2 SFE Process Overview

A schematic diagram of the pilot-scale continuous SFE process under investigation in this thesis is presented in Figure 2.1.

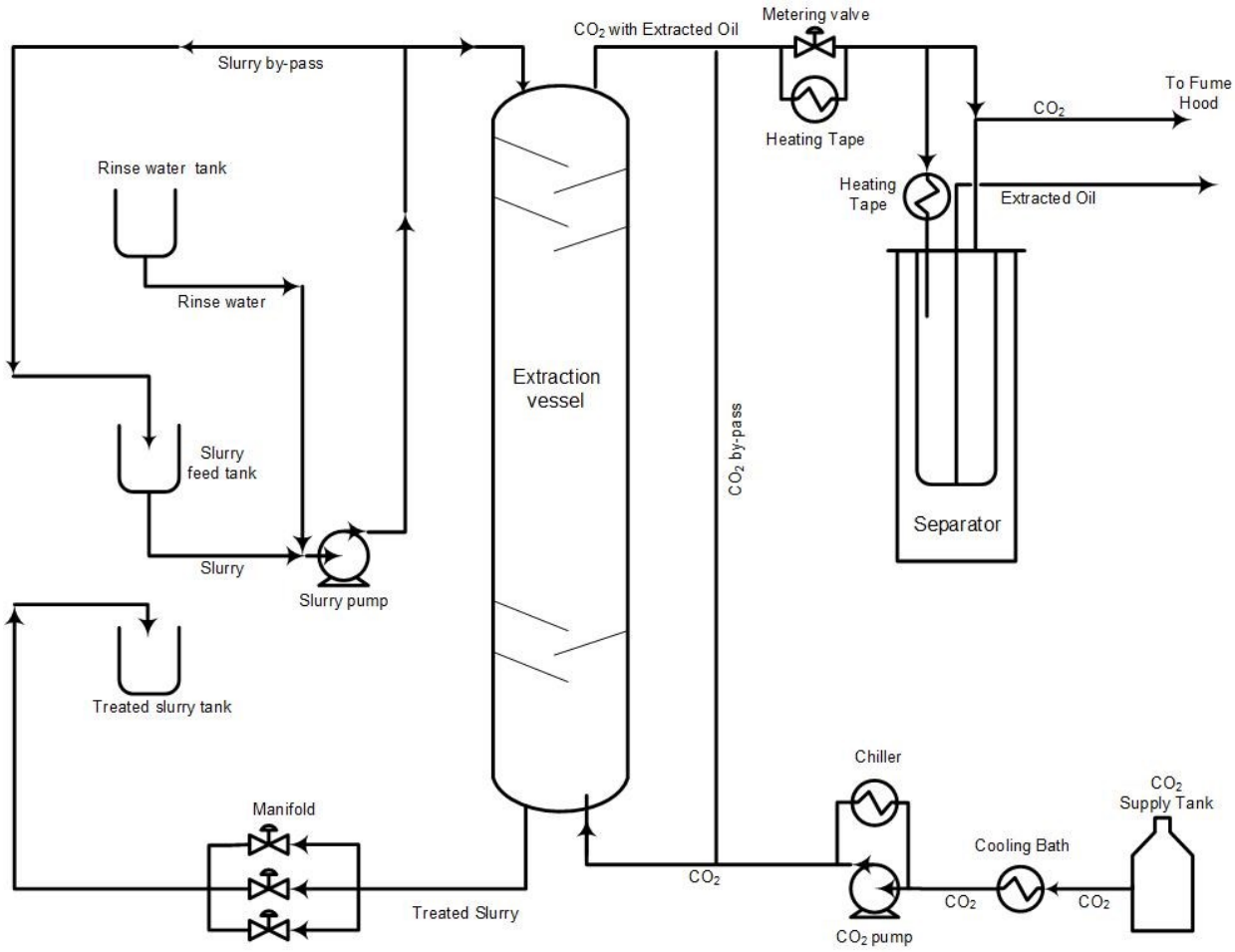

Figure 2.1: Schematic of the pilot-scale SFE process

The main unit operation in this process is an extraction vessel with a height of approximately 2.5 m. The CO_2 is pumped via a positive displacement pump from the CO_2 supply tank into the bottom of the extraction vessel. The pump head is cooled with a chiller. During the CO_2 pressurization stage, supercritical pressures for CO_2 are obtained. The slurry (drill cuttings mixed with water) is pumped via a positive displacement pump from the slurry feed tank to the top of the extraction vessel.

The slurry and CO_2 flows are brought into contact inside the extraction vessel countercurrently. The interior of the extraction vessel holds a structure consisting of 62 inclined baffles. The baffles provide mixing between the two phases. Upon entrance to the extraction vessel, the slurry feed cascades down the baffles, while the CO_2 moves from the

bottom to the top. As a result of this continuous contact, the CO_2 extracts the hydrocarbons present in the slurry.

The treated slurry exits from the bottom of the vessel, where it goes through a manifold to depressurize before entering the treated slurry tank. The manifold consists of three branches, only one of which is used based on the operating pressure of the process. CO_2 along with the extracted hydrocarbons and some extracted water exits from the top of the extraction vessel and flows through a heated metering valve, where it is depressurized through a metering valve prior to entering the separator. The separator has a height of approximately 1.5 m and allows for the CO_2 and extracted hydrocarbons to be separated. The depressurized CO_2 exits the separator and is vented into the fume hood. The hydrocarbons are collected inside the separator and are removed from the separator after the process has been depressurized. The built pilot-scale SFE process is presented in Figure 2.2.

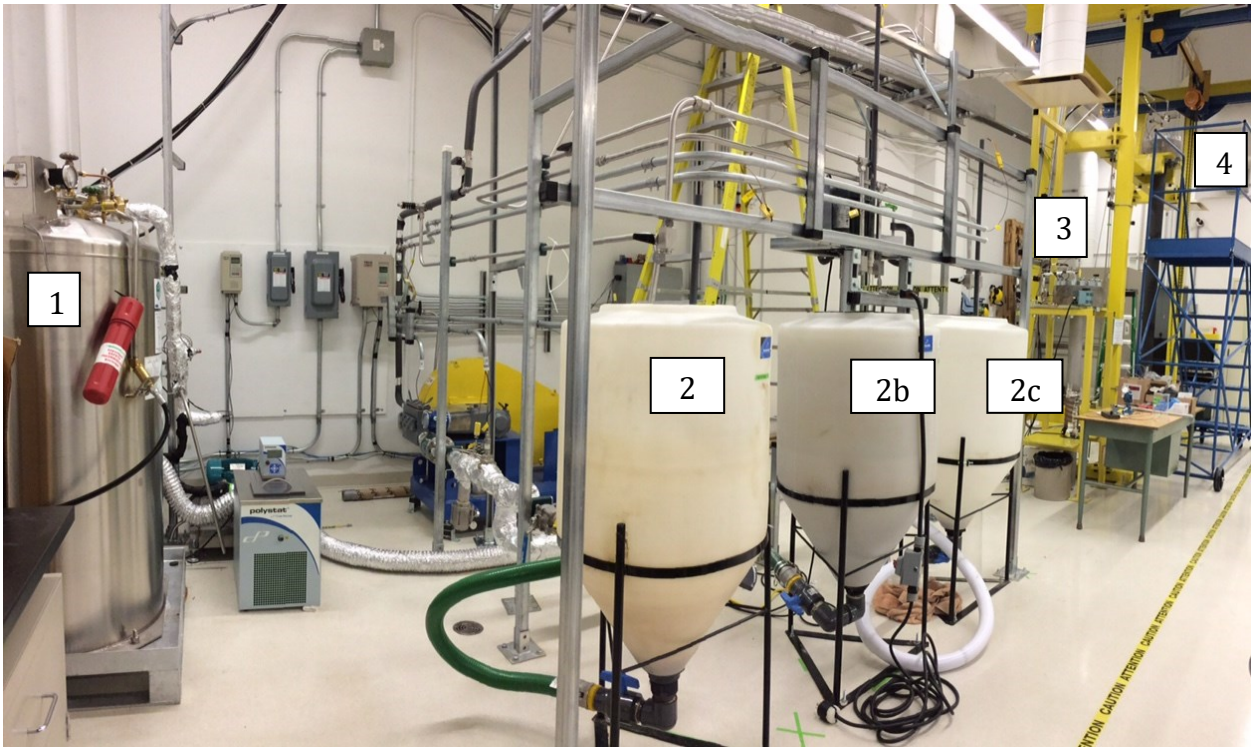

Figure 2.2: The pilot-scale SFE process for treatment of drill cuttings (1) CO_2 tank, (2a) rinse water tank, (2b) slurry feed tank, (2c) treated slurry tank, (3) separator and (4) extraction vessel

As seen in Figure 2.2, the scale of the process is much larger than a bench scale extraction process. Figure 2.3 and Figure 2.4 present a closer view of the extraction vessel and separator.

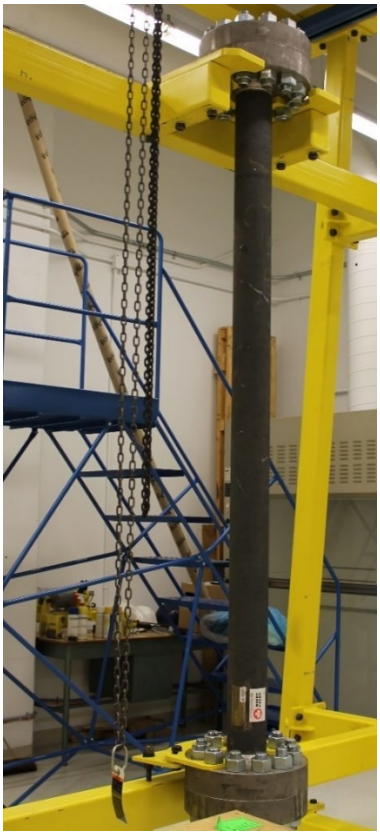

Figure 2.3: The extraction vessel of the SFE process (Length: 2.45 m, Inner diameter: 0.0833 m)

Figure 2.4: The separator of the SFE process (Length: 1.52 m, Inner diameter: 0.0833 m)

This process is the first of its kind to the best of the author's knowledge. The unique attributes of this process are two-fold:

1. A fully continuous SFE process designed to extract hydrocarbon from slurried solids.
2. A pilot-scale process that is beyond the size of a bench scale and a step closer to a commercial scale process.

Successful operation of this continuous pilot-scale SFE process paves the way to industrializing it for this drill cuttings application and other applications in the oil and gas industry.

2.3 Design Components

In building and commissioning the process, major modifications were made to the preliminary design of the process described in Rosenthal (2012). The following sections will outline these changes and will demonstrate how the process was built and commissioned.

The important design components of the SFE process are broken down into six main sections: (i) flow through the process, (ii) lab layout, (iii) P&ID (piping and instrumentation diagram), (iv) control philosophy, (v) operation manual and (vi) HAZOP (hazard and operability study). In each section, modifications to what was presented in Rosenthal (2012), are explained in detail. These details will include the stage in which the modification was made (build vs. commission) and the reason why the modification was made.

2.3.1 Flow Through the Process

In this section, the flow of CO_2, slurry and rinse water through the SFE process as built are described for a typical experiment.

CO_2

Liquid CO_2 is supplied to the process from a CO_2 feed tank. It is supplied through a 19.1 mm (¾″) insulated stainless steel pipe (consisting of flexible and rigid sections) at a pressure of approximately 2.8 – 3.1 MPa (400 – 450 psi). It should be noted that the CO_2 tank has a pressure building circuit which prevents large pressure drops in the CO_2 supply. Before entering the pump, the CO_2 supply line goes through a cauldron filled with a mixture of water and anti-freeze that is cooled to -15 °C with dry ice. The cauldron will maintain the cold temperature of the liquid CO_2 and prevent flashing in the lines. After going through the pump head (which is also cooled to -25 °C with the aid of a chiller), the pressurized CO_2 is pumped into the extraction vessel through a 6.4 mm (¼″) stainless steel line. At the entry of the vessel, the line size changes to 3.2 mm (1/8″) (due to the size of the fittings on the extraction vessel) and the CO_2 is introduced into the extraction vessel just below the lowest baffle. Introducing the CO_2 at this point causes better distribution of CO_2 flow up through the vessel and reduces channelling. SC CO_2 conditions of temperature and pressure are reached in the extraction vessel. As CO_2 flows upward in the vessel, it contacts the slurry, which is cascading down on the baffles, and the SC CO_2 extracts the hydrocarbon from the slurry. The SC CO_2 along with the dissolved hydrocarbons exit from the top of the extraction vessel through a 6.4 mm (¼″) stainless steel line and enters a heated metering valve where it is depressurized. This multiphase stream enters the separator through a 6.4 mm (¼″) stainless steel line where the CO_2 and hydrocarbons are separated. This line extends towards the wall

of the separator (inside the separator) to promote deposition of the hydrocarbons onto the wall to minimize entrainment. CO_2 which is in a gaseous state at this stage exits through a 6.4 mm (¼″) stainless steel line and goes to the fume hood.

Slurry

Slurry feed is stored in the slurry feed tank. From the feed tank, slurry flows through a 50.8 mm (2″) stainless steel pipe, goes through a flow meter before entering the slurry pump. A heater is installed in the slurry feed tank and is turned on prior to a run to heat the slurry to 40 – 45 °C. Therefore, the slurry entering the pump will be at atmospheric pressure and approximately 40 °C. The slurry is then pumped by the slurry pump and through a 19.1 mm (¾″) stainless steel line to the top of the pressurized extraction vessel, where the line reduces to 6.4 mm (¼”). The slurry cascades down the baffles and is exposed to the SC CO_2 flowing upwards in the extraction vessel. As a result, mass transfer occurs between the two phases and hydrocarbon is transferred from the slurry to the SC CO_2. The pressure within the vessel, forces the slurry to exit through the 6.4 mm (¼”) slurry outlet line at the bottom of the extraction vessel. Soon after exiting the extraction vessel, the slurry flows through the manifold. The manifold to be used for a given experiment is chosen before the experiment, based on the operating pressure in the extraction vessel. The manifold is designed to provide resistance in the slurry outlet line and cause pressure drop after slurry exits the extraction vessel. Slurry then flows through a 19.1 mm (¾″) stainless steel line and is directed towards the slurry receiving tank.

Rinse Water

Rinse water is used to create a water plug at the bottom of the extraction vessel prior to process pressurization. It is also used to clean the slurry lines and extraction vessel at the end of an experiment. The rinse water follows the same path as the slurry but it is supplied from the rinse water tank which is for storing rinse water only.

2.3.2 Lab Layout

During the design process, major equipment (the extraction vessel and its frame, the separator and its frame, the CO_2 pump, the slurry pump and CO_2 tank) were purchased and

placed in the lab based on the preliminary layout. However, due to the large components and their mass, Facilities and Operations at the University of Alberta requested an engineering analysis of the standard load that these components would place on the lab floor. The lab layout was independently evaluated by an engineering firm (DIALOG) in terms of structural load. The final approved lab layout is provided in Figure 2.5 and Figure 2.6. Figure 2.5 depicts dimension and Figure 2.6 depicts position of the main SFE process components.

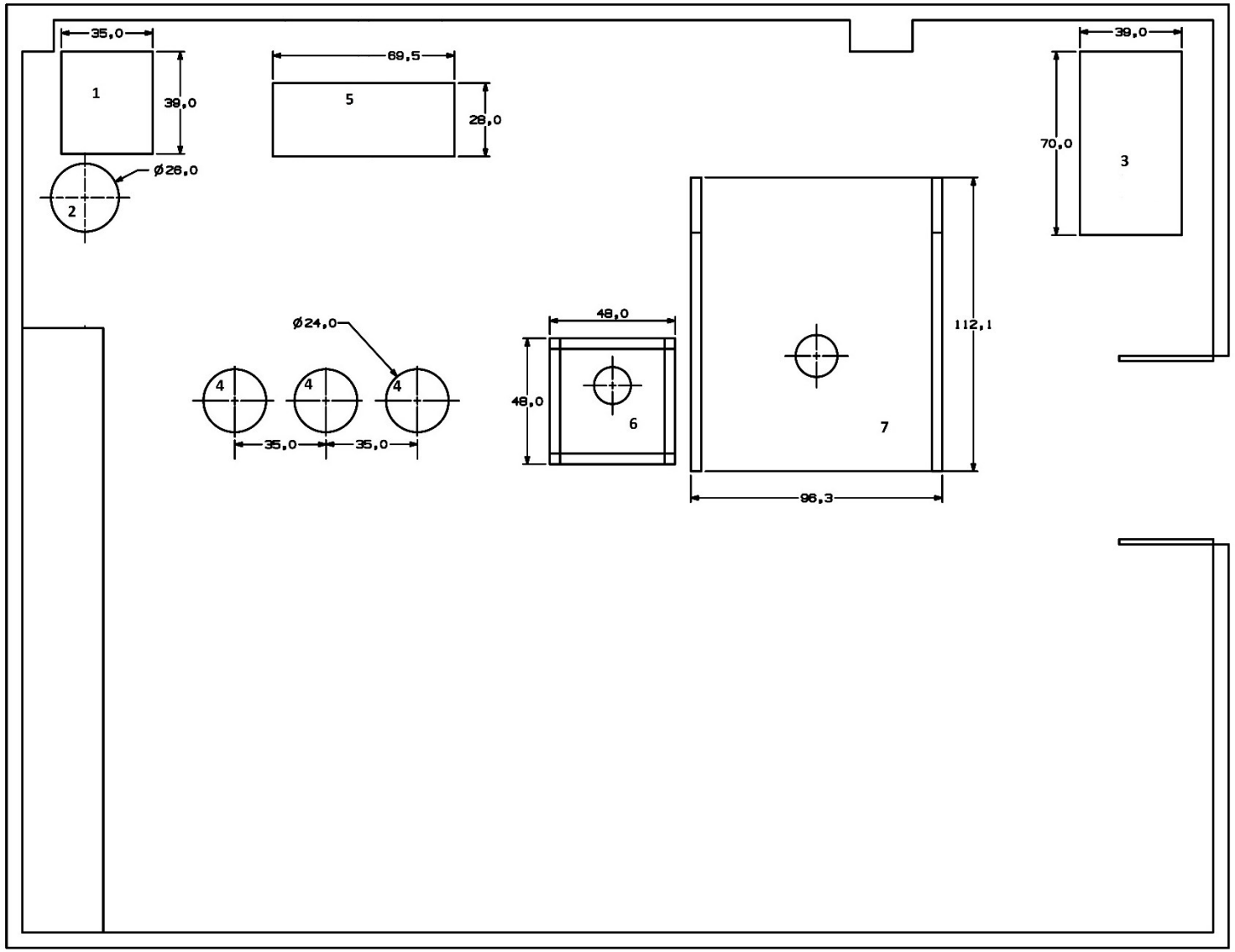

Figure 2.5: Lab layout containing dimension of the main SFE process components: (1) CO_2 pump, (2) CO_2 feed tank, (3) fume hood, (4) slurry and rinse water tanks, (5) slurry pump, (6) separator frame and (7) extraction vessel frame (all dimensions in inches)

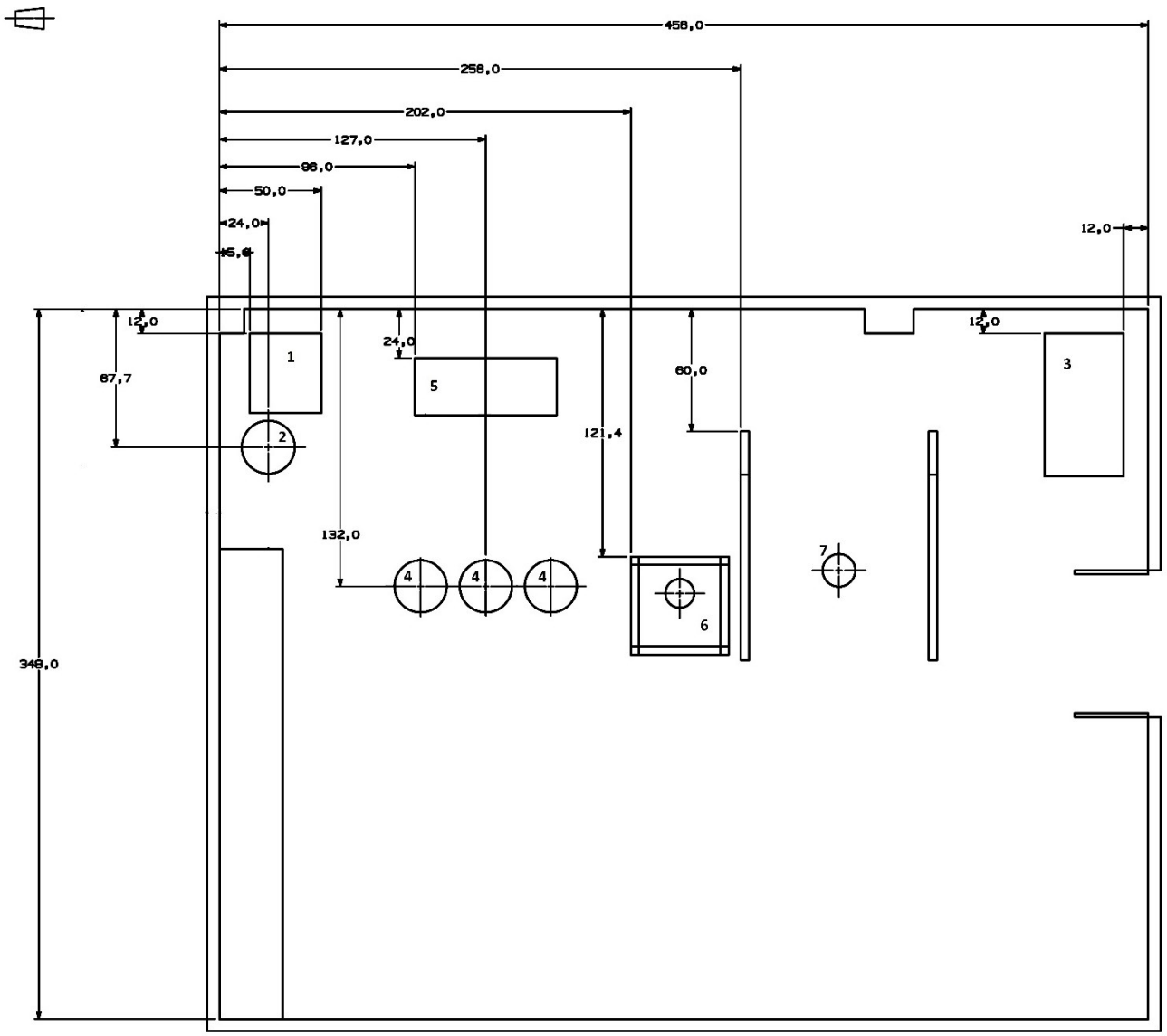

Figure 2.6: Lab layout containing position of the main SFE process components: (1) CO_2 pump, (2) CO_2 feed tank, (3) fume hood, (4) slurry and rinse water tanks, (5) slurry pump, (6) separator frame and (7) extraction vessel frame (all dimensions in inches)

2.3.3 Piping and Instrumentation Diagram

In this section, piping and instrumentation diagram (P&ID) is presented. Also included in this section is a description of the major equipment, lines, valves and instrumentation in the SFE process. Modifications to the preliminary design are also outlined.

Major Equipment

The major equipment currently in use in the pilot-scale continuous SFE process includes the CO_2 tank, rinse water tank, slurry tanks, CO_2 pump, slurry pump, extraction vessel and separator. The specifications of the major equipment are listed in Table 2.1.

Table 2.1: Specification of major equipment used in the SFE process

Tanks							
ID	Description	Volume (m^3)	Dimensions (m)	Material of Construction	Pressure Rating (MPa)	Temperature Rating (°C)	Supplier
N/A	CO_2 Supply Tank	0.42 (liquid)	0.762 (ID) 1.557 (h)	SS (grade not specified)	3.1	N/A	Praxair, Alberta, Canada
FT-3603, FT-3601 & FT-3602	Rinse Water and Slurry Tanks	0.227	0.61 (ID) 0.99 (h)	Seamless Polyethylene	N/A	N/A	Blaze Plastics Inc., Alberta, Canada
Pumps							
ID	Description	Type	Capacity (L/s)	Power Supply	Suction (S) + Discharge (D) Pressure (MPa)	Pumping Temperature (normal, max) (°C)	Supplier
P-2201	CO_2 Pump	Positive displacement	0.108	208 V, 3Ph, 8.4 A	2.758 (S) 34.474 (D)	20 & 71	Pelco, Ontario, Canada
P-3201	Slurry Pump	Positive displacement	0.282	208 V, 3Ph, 38 A	0.1 (S) 34.474 (D)	N/A	North Fringe, Alberta, Canada
Vessels							
ID	Description	Volume (m^3)	Dimensions (m)	Material of Construction	Pressure Rating (MPa)	Temperature Rating (°C)	Supplier
EC-1101	Extraction Vessel with 62 baffles	0.0126 (empty bed)	0.0833 (ID) 2.45 (h)	316 SS	40	200	Price-Schonstrom, Ontario, Canada
SC-4101	Separator	0.0076 (empty bed)	0.0833 (ID) 1.52 (h)	316 SS	30	200	Price-Schonstrom, Ontario, Canada

ID=inner diameter; h=height; N/A = not available

The CO_2 tank originally installed in the process was the Carbomax750. During the commissioning stage, however, it was not possible to consistently pressurize lines downstream of the CO_2 pump. Working with both the CO_2 pump supplier (Pelco) and CO_2 tank supplier (Praxair), a number of steps were taken to try to remedy this problem. These are as follows:

1. Initially, it was thought that the pump valves might be damaged so the pump was opened and its low pressure seals were replaced. The issue was not resolved.
2. It was believed that perhaps gaseous CO_2 and not liquid CO_2 was reaching the CO_2 pump, due to "flashing" in the pump head. A chiller was purchased to cool the pump head and ensure that any liquid CO_2 reaching the pump head remained as liquid CO_2 in the pump head. Improvements were observed but consistency was not obtained.
3. Because the chiller was set to very low temperatures (-45 °C), it was thought that perhaps the high pressure seals in the pump were damaged (because they were not rated to very low temperatures). So the pump was opened again to look for possible damages. No sign of damage was observed.
4. The maximum allowable pressure on the CO_2 tank was 2.1 MPa (300 psi) but during operations it was even lower and normally around 2.0 MPa (285 psi). Based on the CO_2 phase diagram, there was a very small operating window to have liquid CO_2 enter the pump. The safest scenario was to be at 2.1 MPa (300 psi) and -30 °C which was hard to achieve. Therefore, it was concluded that in addition to the pump head, the CO_2 line itself had to be cooled to low temperatures and that was when a cauldron was introduced into the process. The cauldron is a large bucket containing water and anti-freeze solution. Before starting a run, this solution has to be cooled to around -15 °C by adding dry ice to it. After this modification, a few consistent experimental runs were achieved.
5. After a long SFE run, the CO_2 tank pressure did not recover to 2.0 MPa (285 psi) and the tank did not function anymore. Therefore, it was confirmed that this CO_2 tank would not work for the SFE process and that a tank is required with a higher pressure rating and also the capability of maintaining pressure inside it when being used. Therefore, the Carbomax750 CO_2 tank was replaced by a Permacyl 450 VHP CO_2 tank

between August to October 2014. As a result, the pressure in the Permacyl450 CO_2 tank was maintained at approximately 3.1 MPa (450 psi) in experimental runs. The Permacyl 450 VHP CO_2 tank resolved issues created when using the previous CO_2 tank i.e., the Carbomax750 tank.

Lines, Valves, and Instrumentation

In the following subsections, applied modifications with regards to lines, valves and instrumentation are summarized. The reason behind each modification is outlined.

Lines

Table 2.2 summarizes the modifications applied to the lines of the continuous SFE process. As a result of these modifications, the current state of the process in terms of lines is depicted in Figure 2.7. Line specifications are summarized in Appendix A.

Table 2.2: Summary of the modifications to the lines in the SFE process

Description/ID	Preliminary design	Final design	Reason for modification	Modification stage
Inlet line to slurry pump (LN-3008)	63.5 mm (2½″) OD	50.8 mm (2″) OD	A 50.8 (2″) line size is more common for sourcing valves and instrumentation.	Build
Inlet line to CO_2 pump (LN-2002)	25.4 mm (1″) OD	19.1 mm (¾″) OD	A 19.1 mm (¾″) line size is more common for sourcing valves and instrumentation.	Build
CO_2 lines entering and exiting the extraction vessel and separator	3.2 mm (1/8″) OD	6.4 mm (¼″) OD	The fittings on the extraction vessel lid and separator lid are 6.4 mm (¼″) , so the line was upsized to match and to minimize pressure drops into and out of the extraction vessel and separator.	Build
Line exiting the separator (LN-4006)	12.8 mm (½″) OD	6.4 mm (¼″) OD	The fittings on the separator lid are 6.4 mm (¼″), so the line was downsized to match. 6.4 mm (¼″) lines are also less expensive and readily stocked with suppliers.	Build
Flexible line from CO_2 tank (LN-2001)	none	new	The line allowed for installation flexibility which was needed due to the layout of the CO_2 tank and pump.	Build
Brass cooling coil (LN-2003)	none	new	The coil was added to cool the CO_2 entering the pump to below the liquid-vapor equilibrium temperature at tank pressure (to ensure a liquid feed to the pump).	Commission
Separator bypass line (LN-4009)	none	new	The bypass was added to give operational flexibility during depressurization or in a scenario where it might be necessary to bypass the separator (e.g., freezing in the separator).	Build
Flexible slurry line (LN-3011)	none	new	The line provided installation flexibility and also acts as a pulsation dampener.	Build
¼″ slurry line entering the extraction vessel (LN-3012)	none	new	Because the fittings on the extraction vessel lid are 6.4 mm (¼″), the slurry line had to be down sized to 6.4 mm (¼″) after the flexible hose to enter the extraction vessel.	Build
Extended CO_2 line into extraction vessel (LN-2006)	none	new	The line was extended to ensure the CO_2 entering the extraction vessel hits a baffle.	Commission

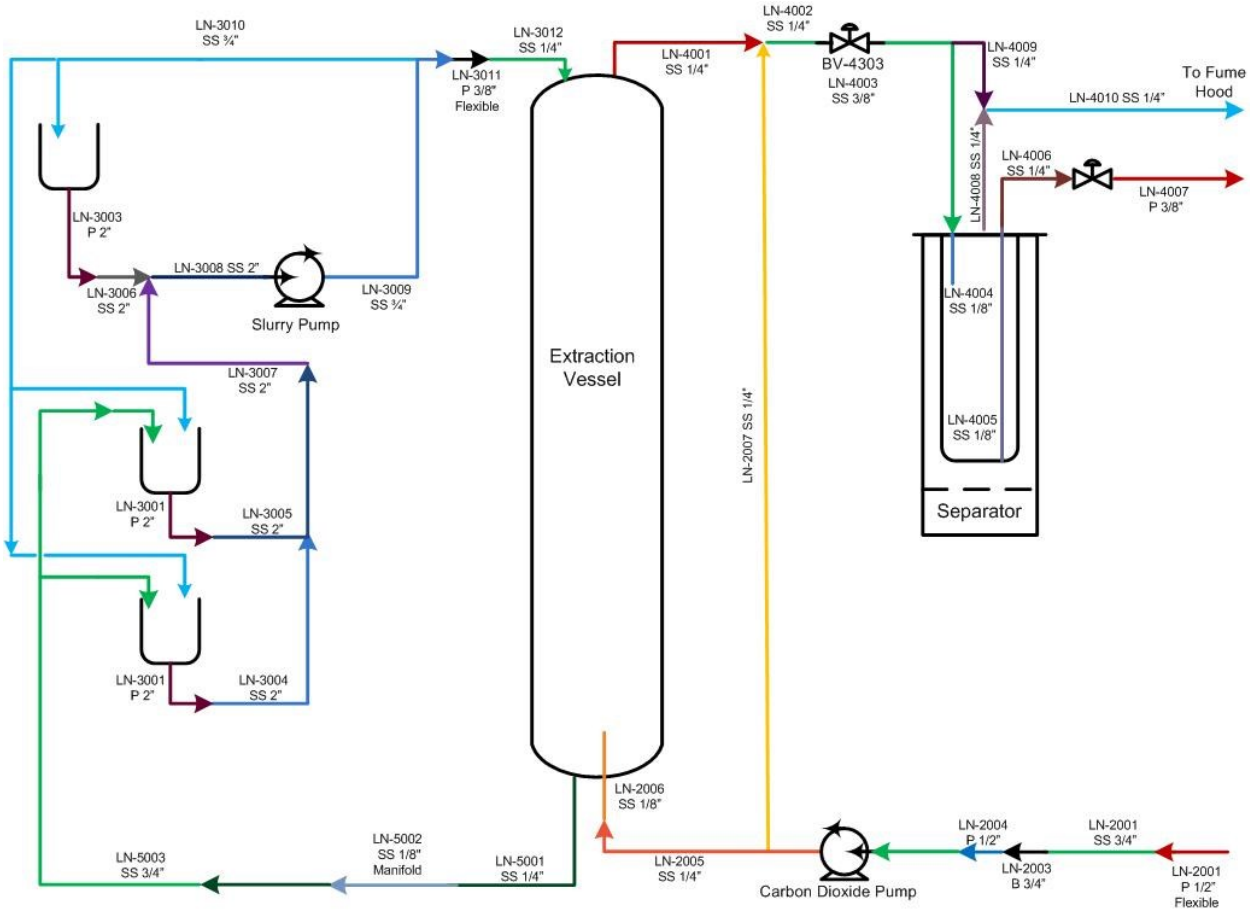

Figure 2.7: CO_2 and slurry line configuration in current state of the SFE process (line colours indicate a change in tag number, which corresponds to a change in line size and/or material)

Valves

Table 2.3 summarizes the modifications applied to the valves of the continuous SFE process. As a result of these modifications, the current state of the process in terms of valves is depicted in Figure 2.8. It should be noted that based on the modifications made to line sizes, related valves on those lines were accordingly upsized or downsized. These changes have not been reflected in Table 2.3. Valves specifications are summarized in Appendix B.

Two general modifications were made in terms of valve IDs i.e., ID of relief valves are changed from BV-XXXX to RV-XXXX. Similarly, metering valve ID is changed from BV-XXXX to MV-XXXX.

Table 2.3: Summary of the modifications in terms of valves used in the SFE process

Description/ID	Preliminary design	Final design	Reason for modification	Modification stage
Check/Relief valve (CV-2301)	One valve that served both as a check valve and relief valve	Addition of RV-2307 to LN-2001	It was decided to separate the two functions of this valve. Hence, CV-2301 acts as a check valve only and RV-2307 acts as a relief valve on that line.	Build
Relief valve (BV-3303)	Existed in P&ID	deleted	The valve was needed for the slurry grinding loop which was not installed in the current build.	Build
2″ plastic isolation valves (BV-3320, BV-3321, BV-3322)	none	new	The valves were added to isolate the slurry in the tanks from the 50.8 mm (2″) SS slurry supply lines.	Build
¼″ isolation valves (BV-4302, BV-4306, BV-4307)	none	new	The valves were added on as a result of adding the separator bypass line.	Build
Manifold (BV-5302a, BV-5302b, BV-5302c)	none	new	The manifold was installed to restrict the slurry flow exiting the extraction vessel.	Build
Drain valve on CO_2 pump outlet line (BV-2310)	BV-2310	BV-2310a and BV-2310b	BV-2310b is a three-way valve which was installed as an alternative to BV-2310a which would allow the pump to be turned off and drained without depressurizing the extraction vessel.	Commission
Isolation valve (BV-3317)	none	new	The isolation valve on the slurry line before going in to extraction vessel (BV-3306) was located too far from the extraction vessel. It was decided that it would be useful to add another isolation valve closer to the vessel.	Commission

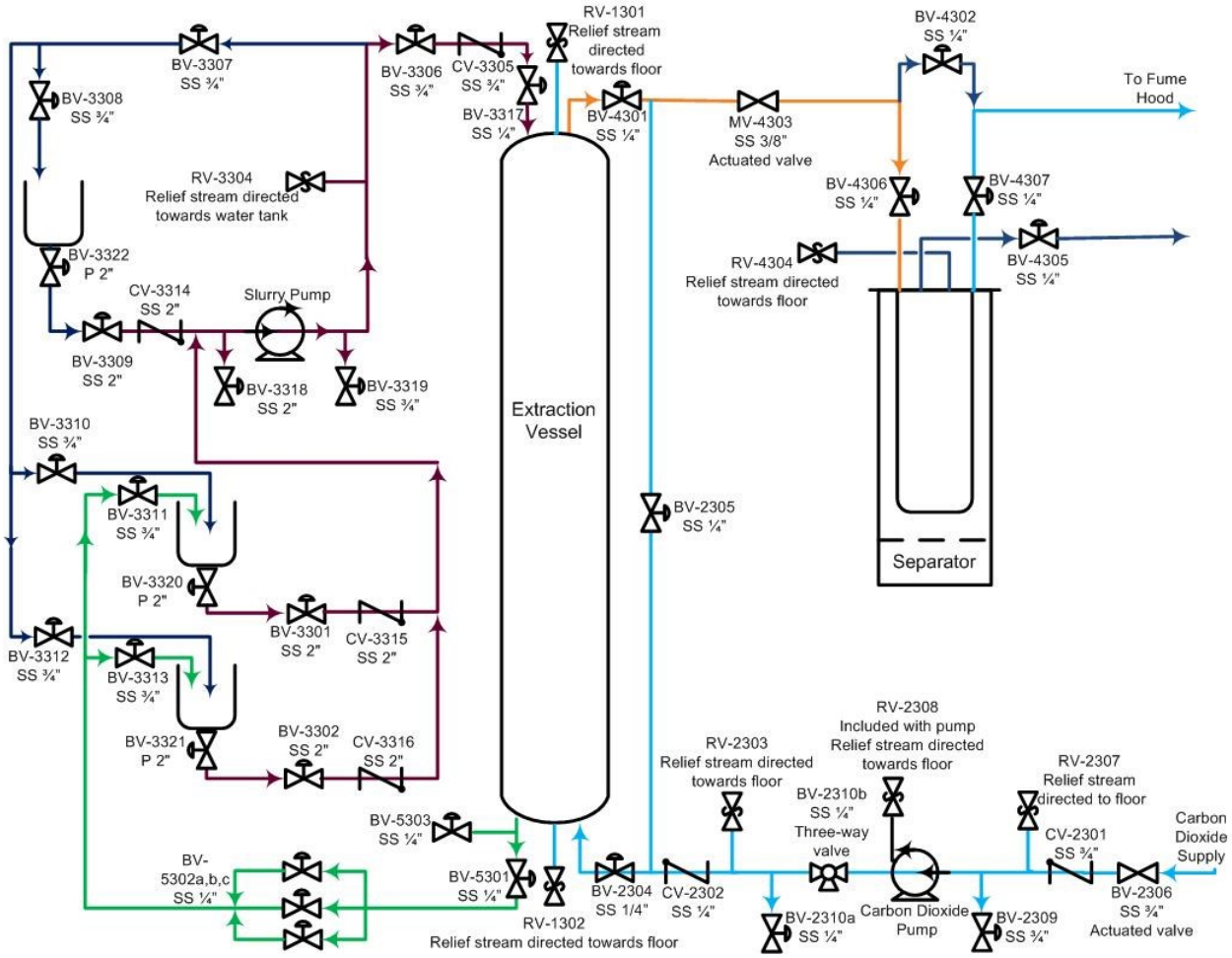

Figure 2.8: Valve configuration in current state of the SFE process

Instrumentation

Table 2.4 summarizes the modifications applied to the instrumentation of the continuous SFE process. As a result of these modifications, the current state of the process in terms of instrumentation is depicted in Figure 2.9. Instrumentation specifications are summarized in Appendix C.

Table 2.4: Summary of modifications to the instrumentation used in the SFE process

Description/ID	Preliminary design	Final design	Reason for modification	Modification stage
Pressure indicator (PI-1404)	In field display only	Data collection and control	The pressure sensor was added to allow for logging the data and controlling the CO_2 pump.	Build
Temperature sensor (TI-1410)	none	new	Adding a temperature sensor at the bottom of the extraction vessel allowed for better understanding of the temperature profile in the extraction vessel.	Commission
Heating tape (HX-1411)	none	new	In order to have SC CO_2, its temperature should be above 32 °C. Therefore, it was decided to heat the extraction vessel bottom, where CO_2 is expanding inside the vessel.	Commission
Temperature sensor (TI-2404)	Initially clamp-on and eventually an adhesive type	Inline temperature sensor	It is important to know the exact temperature of CO_2 entering the pump to ensure that the CO_2 is cooled adequately to provide a liquid feed to the pump.	Commission
Chiller (HX-2409)	none	new	In order to avoid flashing of the CO_2 in the pump, the pump head should be kept below the liquid-vapor equilibrium temperature at CO_2 tank pressure.	Commission
Cauldron-dry ice (HX-2410)	none	new	The cauldron cools the CO_2 supply to ensure a liquid feed to the pump.	Commission
Pressure indicator (PI-4406)	none	new	The indicator was installed to show pressure between extraction vessel and separator.	Commission
Heating tape (HX-4407)	none	new	The heating tape was installed to prevent CO_2 freezing in the automated metering valve due to CO_2 expansion.	Commission
Heating tape (HX-4408)	none	new	The heating tape was installed to prevent freezing of the ¼″ line going into the separator due to CO_2 expansion.	Commission
Pressure indicator (PI-5404)	none	new	The indicator was installed to monitor the pressure of the slurry outlet line from the manifold. The indicator helps with manually controlling the liquid level inside the extraction vessel.	Commission

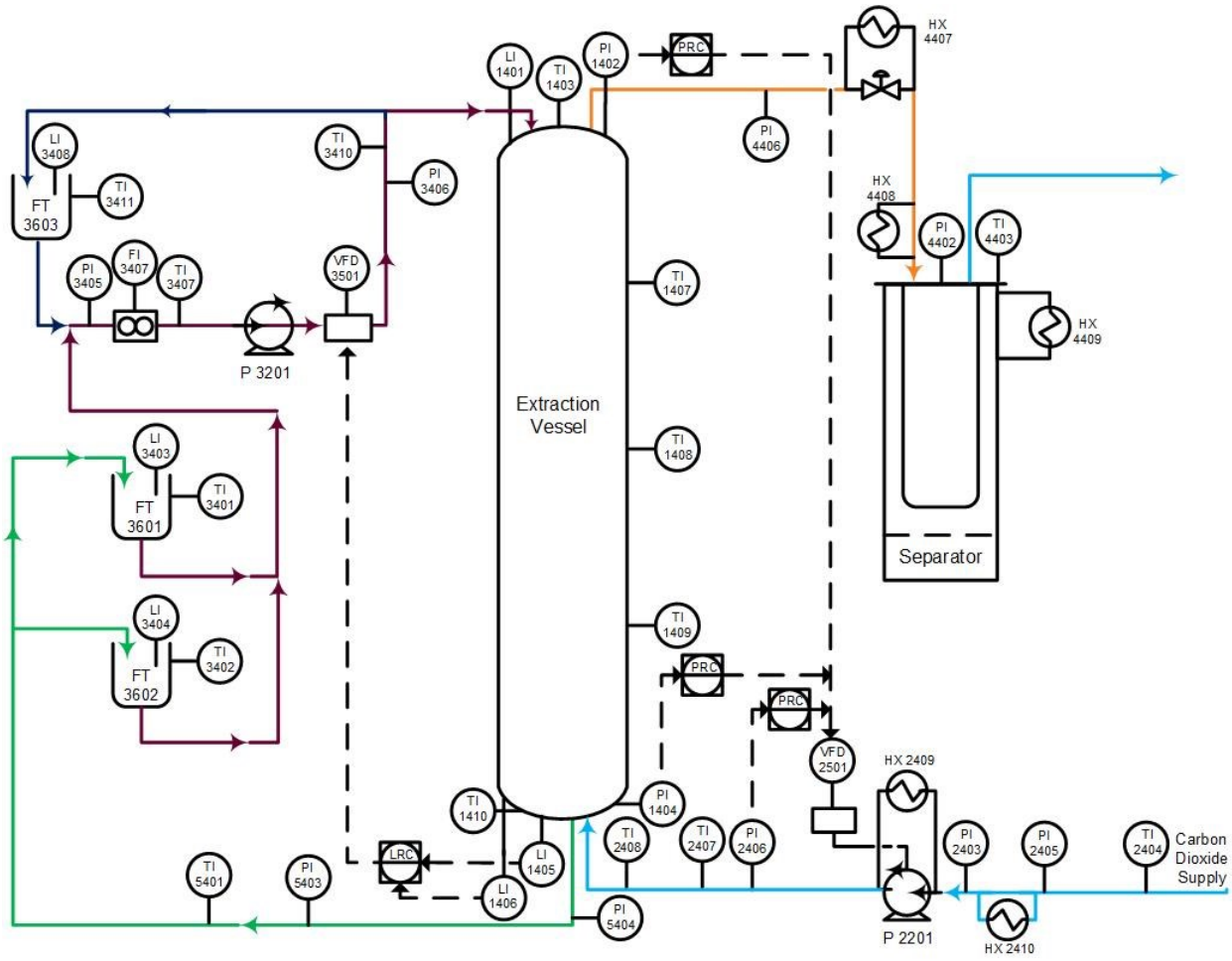

Figure 2.9: Instrumentation configuration in current state of the SFE process

As a result of the modifications applied to lines, valves and instrumentation, the final P&ID of the continuous pilot-scale SFE process is as shown in Figure 2.10.

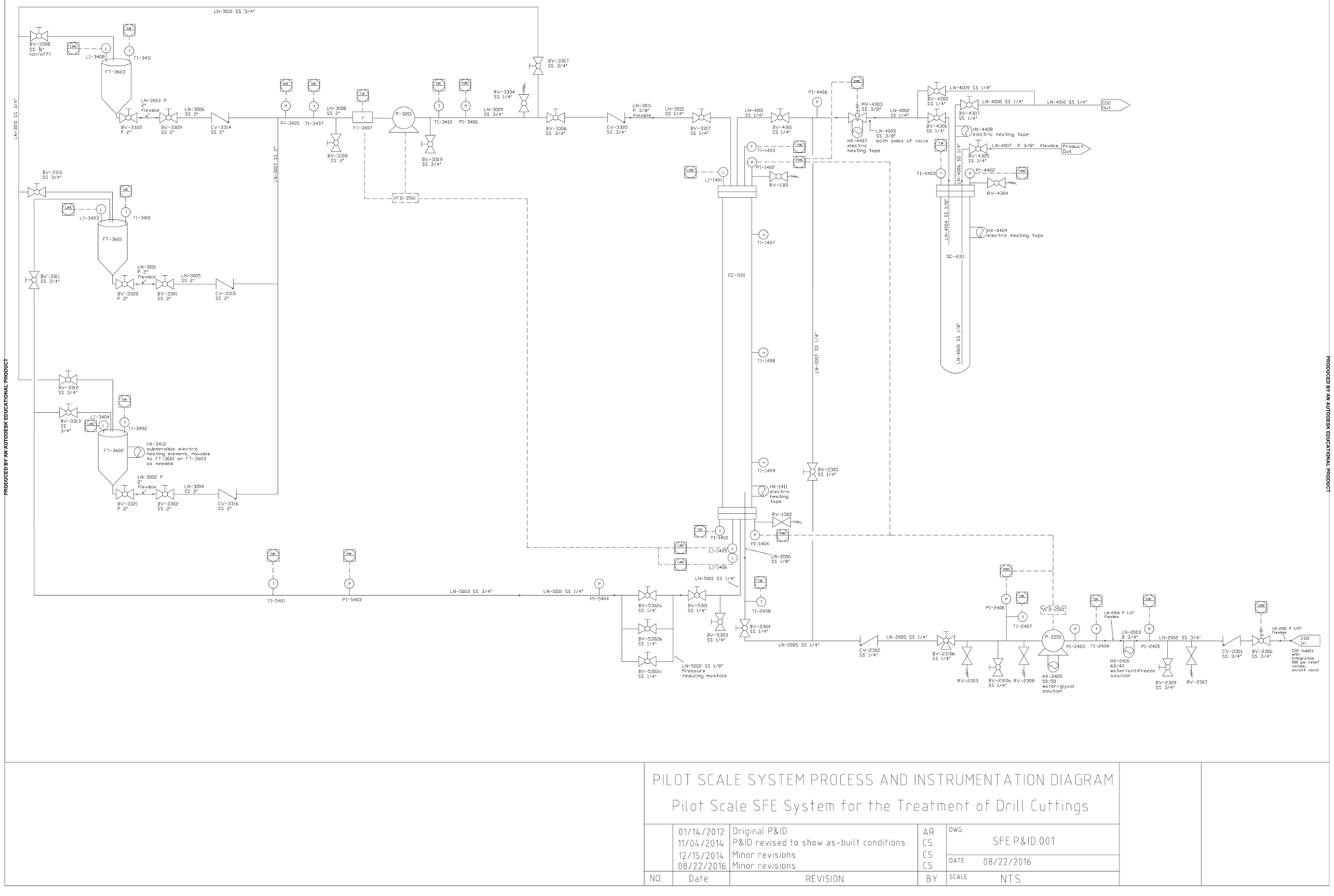

PILOT SCALE SYSTEM PROCESS AND INSTRUMENTATION DIAGRAM Pilot Scale SFE System for the Treatment of Drill Cuttings					
NO.	Date	REVISION	BY	DWG	SFE.P&ID.001
	01/14/2012	Original P&ID	AR	DATE	08/22/2016
	11/04/2014	P&ID revised to show as-built conditions	CS	SCALE	NTS
	12/15/2014	Minor revisions	CS		
	08/22/2016	Minor revisions	CS		

PRODUCED BY AN AUTODESK EDUCATIONAL PRODUCT

Figure 2.10: P&ID of continuous SFE process

2.3.4 Control Philosophy

A control philosophy for the pilot-scale continuous SFE process was proposed by Rosenthal (2012). Based on this control philosophy, the control system was built. For this purpose, National Instrument's CompactRIO, a programmable automation controller (PAC), has been chosen to provide communication between the system elements (i.e., instrumentation, automated valves, VFDs and computer). This real-time controller provides high performance control as well as reliability and serves as a bridge between the data coming from instruments/valves/VFDs and the computer. The programming software applied is National Instrument's LabVIEW™. LabVIEW™ also provides a graphical user interface (GUI) for controlling the SFE process from the computer. It should be noted that LabVIEW™ files have the extension .vi; therefore, files created in LabVIEW™ are also referred to as VI's.

The control program generally consists of two main VI's. One is the RT (Real Time) VI which is considered as the core program for control and it is loaded into the CompactRIO. The RT VI should be considered as a piece of hardware because it is the source of actions in the CompactRIO. The HMI (Human Machine Interface) VI on the other hand basically provides the interface for running the process but operational-wise is controlled by the RT. In other words, if for any reason the HMI VI is closed or if the computer crashes, after re-opening the HMI file, it will continue from the state it was closed and it will not restart from its initial mode.

Two monitors are connected to the computer in the SFE lab. When the HMI file is opened, monitor-1 displays the P&ID of the SFE process and the control panel, while monitor-2 displays SFE process modes, the alarms and interlocks. A view of the GUI is presented in Figure 2.11.

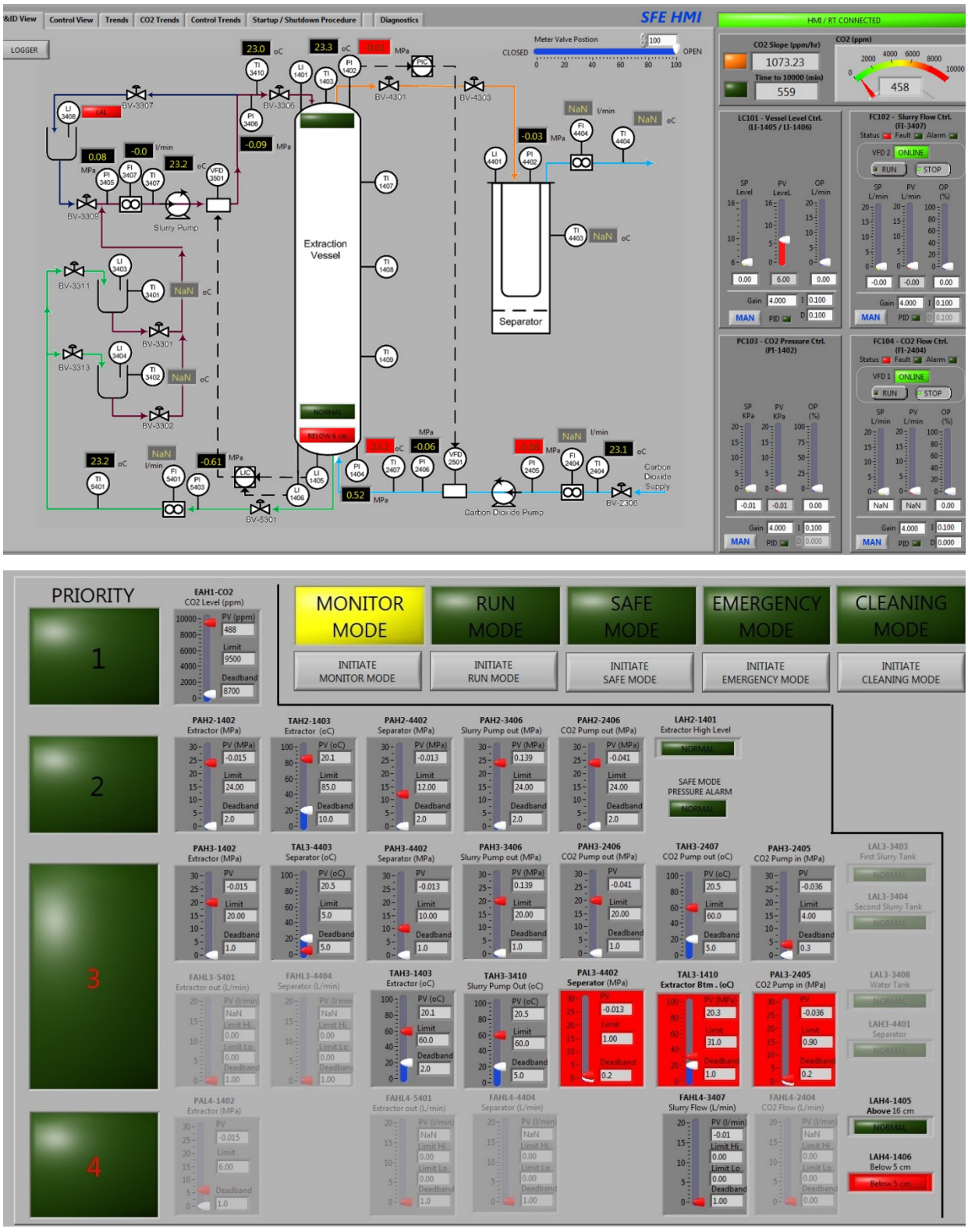

Figure 2.11: Display of the SFE process GUI (top: monitor-1, bottom: monitor-2)

A manual has been prepared to explain how the control system/GUI of the SFE process works. It is the responsibility of future operators to read and fully understand this document before conducting any runs on the process.

The following sections describe process modes, alarms and process control.

Process Modes

The SFE process can operate in five different modes. These modes are as follows:

1. *Monitor Mode*: This mode is mainly for testing and troubleshooting. Process control can be done manually or automatically when in this mode. The process automatically enters *Monitor Mode* when the HMI VI is started.

2. *Run Mode*: The main application of this mode is operating the process in an automated approach. In other words, when process enters this mode, process control is done automatically. This mode is to be used after testing and troubleshooting of the process is completed and all controllers have been designed and tested on the process. As built, the system has not been operated in *Run Mode*.

3. *Emergency Mode*: The process can enter this mode either automatically through the safety interlocks defined for the process or by manually clicking the *Emergency Mode* button on the interface. When the process enters this mode, the pumps are automatically stopped, the automated metering valve (MV-4303) is fully opened and the CO_2 feed tank actuated valve (BV-2306) is fully closed.

4. *Safe Mode*: This mode acts as an intermediate mode between *Emergency Mode* and *Monitor Mode*. A safety checklist should be completed before entering *Safe Mode* from *Emergency Mode*. Similarly, an emergency shutdown checklist should be completed before entering *Monitor Mode* from *Safe Mode*. Some operational restrictions apply when process is in *Safe Mode*. These restrictions are as follows:
    - System pressure limited to 3 MPa.
    - CO_2 pump flowrate limited to 1 L/min (equivalent to 15 % CO_2 pump speed).

- Slurry pump flowrate limited to 3 L/min (equivalent to 18 % slurry pump speed).

5. *Cleaning Mode*: This mode is designed specifically for cleaning and rinsing the extraction vessel. Because activation of the level sensor located at the top of the vessel (LI-1401) is an indication of a full vessel, this level sensor (LI-1401) is applied for stopping the slurry pump when filling the extraction vessel for cleaning purposes. However, activation of this sensor initiates emergency mode. To prevent confusion, *Cleaning Mode* was programmed to use when rinsing the extraction vessel and prevent any unnecessary false alarms.

Modifications made with regards to process modes are as follows:

- *Cleaning Mode* was added to process modes.
- Only *Emergency Mode* was programmed into the process modes. The preliminary design identified both an *Emergency Shutdown* and an *Emergency Mode*. It could not be understood whether the *Emergency Mode* was a result of an *Emergency Shutdown* or if they are two independent modes. However, it seemed that both modes perform the same actions. Thus, only an *Emergency Mode* has been programmed which can be activated by alarms or interlocks or by pressing the corresponding button.
- *Safe Mode* is a required mode before entering *Monitor Mode* from *Emergency Mode,* for both priority 1 and 2 alarms. The preliminary design required only priority 1 alarms to use *Safe Mode* (with the associated emergency shutdown checklist and supervisor authorization), but it is safer to also have priority 2 alarms, which are mostly related to high pressures in the process, go through *Safe Mode* also. Having both priority 1 and 2 alarms go through *Safe Mode* makes the procedure safer and less complicated.
- To enter *Safe Mode* from *Emergency Mode* a supervisor authorization password has been added as one of the requirements of the safety checklist.

Process Alarms

Alarms are prioritized into four groups:

- Priority 1 alarms: These alarms are a critical safety alarm because the alarmed conditions pose an immediate health threat to the operators and lab occupants. The process is interlocked to shut down. As a result, the process enters *Emergency Mode*.
- Priority 2 alarms: These alarms specify process instability due to a failure in the process itself or in the process control system. Similar to priority 1 alarms, the process is interlocked to shut down when a priority 2 alarm is activated and the process will enter *Emergency Mode*.
- Priority 3 alarms: These alarms indicate abnormal process conditions which might lead to process instability if not handled properly. Therefore, troubleshooting the process is required when a priority 3 alarm is activated. There is no change in mode associated with Priority 3 alarms.
- Priority 4 alarms: These alarms inform the operator of abnormal process conditions, which should be monitored. There is no change in mode associated with Priority 4 alarms.

A complete list of the alarms available in the process is provided in Appendix D. After initial testing of the process, some modifications were made to the alarms. These changes are summarized in Table 2.5.

Table 2.5: Summary of modifications applied to the SFE alarm system

Alarm ID	Alarm Priority	Preliminary design	Final design	Logic
PAH2-2406 PAH2-3406 PAH2-4402	2	none	Added to Priority 2 alarms	These high alarms were added for extra safety regarding process pressure. The system will shut down if alarm is activated.
LAH2-1401	2	Had not been specifically prioritized	Added to Priority 2 alarms	Because we do not have continuous reading of the slurry level inside the extraction vessel, this alarm will shut down the process if the extraction vessel fills with slurry.
PAH3-1402 PAH3-2406 PAH3-3406	3	22 < P < 27 MPa	22 MPa < P	The ranges of the alarms were changed because pressure exceeding 27 MPa will automatically result in a Priority 2 alarm.

Table 2.5: Summary of modifications applied to SFE alarm system, continued

Alarm ID	Alarm Priority	Preliminary design	Final design	Logic
PAH3-2405	3	2.1 < P < 2.4 MPa	2.75 MPa < P	The original alarm range is redundant and was modified based on the maximum allowable inlet pressure of the CO_2 pump.
PAL3-2405	3	0.9 > P > 1.0 MPa	P < 3.1 MPa	The original alarm values were mathematically incorrect. The modified value is based on the specifications of the CO_2 tank.
TAH3-2407	3	T > 85 °C	T > 60 °C	It was decided to decrease the limit of this alarm. The alarm relates to the temperature in LN-2005 (CO_2 line exiting the pump). This line is typically very cold and an increase in temperature represents a system upset that would need to be investigated quickly.
TAH3-3410	3	T > 85 °C	T > 60 °C	This alarm relates to the temperature of the slurry leaving the slurry pump (in LN-3009). As the slurry is not actively heated during the extraction phase, an increase in slurry temperature is an indication of a system upset that would need to be investigated quickly.
PAH3-4402	3	4 < P < 4.5 MPa	8 MPa < P	Based on initial testing, it was decided that the separator pressure should not exceed 8 MPa during normal operation.
LAL3-3408	3	none	Added to Priority 3 alarms	The alarm is triggered when the water level is low in water tank to prevent the slurry pump from running dry or to indicate a leak in the tank.
TAL3-1410	3	none	Added to Priority 3 alarms	A thermocouple, TI-1410, was installed at the bottom of the extraction vessel. The alarm alerts the Operator when the temperature drops below supercritical (32ºC).
PAL3-4402	3	none	Added to Priority 3 alarms	During normal operation, the separator pressure is above 1 MPa. If the pressure drops to below 1 MPa, it is an indication of freezing.
TAL3-4403	3	T < 16 °C	T < 0 °C	This temperature should be closely monitored. If the temperature in the separator drops below 0 °C, freezing might occur.

Table 2.5: Summary of modifications applied to SFE alarm system, continued

Alarm ID	Alarm Priority	Preliminary design	Final design	Logic
TAH3-1403	3	Priority 4 alarm	Changed to Priority 3	It was decided that the increase of this temperature could cause problems in the vessel and so it should be a Priority 3 alarm.
TAH3-1403	4	60 < T < 85 °C	60 °C < T	There is no need to have upper limit. Going over 85°C will automatically trigger a Priority 2 alarm.
PAL4-1402	4	4 < P < 6 MPa	P < 6 MPa	Because this is a low level alarm, the upper limit is sufficient.

Process Control

Two main control objectives for the pilot-scale continuous SFE process are (i) controlling the pressure and (ii) controlling the slurry level inside the extraction vessel. These two process variables must be controlled during a run to have efficient and safe operation of the process. Based on these objectives, three control loops have been programmed and exist on the control panel of the GUI. These control loops are as follows:

1. Control of slurry level inside the extraction vessel via slurry pump VFD: In this control structure, the slurry level in the extraction vessel is controlled by the speed of the slurry pump through a feedback control loop. Two modes exist for controlling slurry level: “man” and “auto”. In “man” mode, the slurry pump speed can be changed manually. In “auto” mode, control logic applies and the slurry level will be controlled via a feedback control loop. It should be noted that currently, due to lack of continuous level sensors in the extraction vessel, automatic level control is not fully functional and this control loop is mostly operated in manual mode (i.e., “man” mode). The manual approach that is conducted is based on visual observations of the system and adjusting slurry flow based on these observations. A pressure gauge located on the slurry outlet line from the extraction vessel is the main indicator used during manual mode. During normal operation i.e., when only slurry is flowing through this line, the pressure gauge on the slurry outlet line typically reads 0.7 MPa (100 psi). However, as the slurry level decreases, CO_2 starts exiting the slurry outlet line along with the slurry. The pressure gauge readings start to fluctuate and the slurry outlet line

becomes cold (as a result of CO_2 flowing through it). In some cases, the CO_2 exiting with the slurry goes into the receiving tank and into the lab, triggering an increase in the CO_2 levels in the lab as measured by the CO_2 sensors. To counteract this scenario, the slurry level inside the extraction vessel is increased by increasing the slurry pump flow in increments of 0.5 % until conditions are back to normal i.e., pressure gauge fluctuation stops and CO_2 sensors measurements are back to normal. Normal conditions indicate that slurry level is high enough to prevent the bulk CO_2 flow from exiting the slurry outlet line. Overfilling of the vessel is also not desirable and level should be kept as low as possible. For this purpose, the slurry flow is decreased in increments of 0.5 % until CO_2 is again observed in the slurry outlet line. This procedure is repeated throughout an experiment in order to manually maintain level within an acceptable range near the bottom of the extraction vessel.

2. Control of pressure inside the extraction vessel via CO_2 pump VFD: In this control structure, the extraction vessel pressure is controlled by the CO_2 pump speed through a feedback control loop. One of three pressure sensors (PI-2406, PI-1404 or PI-1402) can be chosen as the process variable for this purpose (i.e., to provide feedback in the control loop). Based on the desired set-point and the pressure readings recorded from the chosen pressure sensor, the CO_2 pump speed is manipulated. This control structure can also be set to “man” and “auto” mode. In “man” mode, the pressure can be adjusted by manually changing the CO_2 pump speed. In “auto” mode, the control logic applies. In using this feedback loop for controlling the extraction vessel pressure during the pressurization stage for a typical run, PI-2406 (the pressure sensor located on the CO_2 inlet line to the extraction vessel) is chosen as the desired process variable. The reason for this selection is that, during testing, it was observed that this pressure sensor responds much faster to changes in CO_2 flow in comparison to PI-1402 or PI-1404 pressure sensors, which are located at the top and bottom of the extraction vessel, respectively. But, the pressure measured at PI-2406 is slightly higher than the extraction vessel pressure and it is not an accurate representation of the pressure inside the extraction vessel. Hence, when the desired pressure set-point is reached at

PI-2406 (e.g., 14 MPa), the control system then uses PI-1404, the pressure sensor at the bottom of the extraction vessel, for the rest of the operation of the SFE process.

3. Control of pressure inside the extraction vessel via the metering valve: In this control structure, the extraction vessel pressure is controlled by the metering valve (MV-4303) located on the CO_2 outlet line from the extraction vessel. This control loop gets feedback from pressure sensor PI-1402, which is located at the top of the extraction vessel and close to the metering valve. During initial testing of the process, it was observed that the pressure sensor at the top of the extraction vessel (PI-1402) did not respond as quickly as the sensor at the bottom (PI-1404). It was also observed that the opening of the metering valve quickly affects the pressure reading at this pressure sensor (PI-1402). Therefore, it was decided to program a feedback loop to control the pressure at the top of the vessel (PI-1402) by manipulating the metering valve opening. In later stages, it was decided that the metering valve opening should stay unchanged during a run (excluding pressurization and depressurization stages). Hence, this loop is no longer used.

2.3.5 Operation Manual

During this research, the preliminary operation manual was modified during the commissioning and troubleshooting of the SFE process. In this section, major changes made to the operation manual and the reasons behind each change is explained in detail.

Environmental Monitoring

Preliminary environmental monitoring included two CO_2 sensors and one O_2 sensor. Rosenthal (2012) proposed connecting one of the CO_2 sensors to the University of Alberta Central Control and connecting the other CO_2 sensor to the control system to trigger in-lab alarms and initiate emergency shutdown of the process. Connecting the O_2 sensor to the control system to trigger in-lab alarms and initiate emergency shutdown of the process had also been proposed.

The final environmental monitoring of the SFE process lab, which was designed during the "build" phase, consists of two O_2 monitors and two CO_2 monitors. The O_2 monitors are portable and are attached to a belt or lab coat pockets, to be worn by two operators as soon as they enter the lab and throughout their time spent in the lab. The two O_2 monitors have a low alarm setting of 19.50 % (volume) and a high alarm setting of 23.50 % (volume). If these levels are reached, the monitor will start beeping and vibrating to notify the user of the state of the O_2 concentration in the lab. It should be noted that these monitors are not connected to the DAQ system and their data is not being logged.

The CO_2 monitors, CO_2(1) and CO_2(2), are stationary and both probes are located inside the lab at a height of approximately 50 cm on the east wall of the lab. The display of CO_2(1) is located inside the lab, near the DAQ box and also connected to the DAQ system. Hence, the CO_2 concentration in the lab can be seen on the computer as well as on the CO_2(1) monitor display at all times. Data from the CO_2(1) monitor is being logged 24 hours a day and saved on the computer. The operating range of the CO_2(1) monitor is 0 -10,000 ppmv. When 5,000 ppmv is reached through this monitor, the orange light of a stack light, located above the monitor and connected to the monitor, will start to flash along with a beeping sound. When 10,000 ppmv is reached, the red light of the stack light will start flashing with a constant beep. The audible alarm and stack light serve to notify occupants to leave the lab. Also, if the system is in use and running, the emergency shutdown is activated through the programmed interlocks of the process.

The display of CO_2(2) is located just outside the lab (in the hallway) and its operating range is 0 – 5 %. This CO_2 sensor is connected to University's Central Control. As a result, if a CO_2 level of 1 % (equivalent to 10,000 ppmv) is recorded by this monitor, a critical alarm is activated in Central Control, which requires them to move building ventilation to 100 % fresh air, increase the air exchange rate of the lab, dispatch trades people and start calling the people on the emergency contact list, starting with the lab itself. It should be noted that the CO_2(2) monitor is connected to two stack lights: one inside the lab (above the computer) and the other outside the lab (above the CO_2 monitor in the hallway). The purpose of the

stack lights is to inform the lab occupants or others in the hallway of potentially unsafe conditions in the lab.

Start-up and Controlled Shutdown Procedures

After commissioning runs and troubleshooting the process, start-up and controlled shutdown procedures for the process were upgraded. These upgrades are outlined in the following subsections.

Start-up Procedure

The major changes made to the start-up procedure are as follows:

- In the preliminary procedure, the plan was to pressurize the vessel with CO_2 and then introduce the slurry. However, based on initial runs, it was difficult to create an initial plug of slurry at the bottom of the extraction vessel while the vessel was pressurized. As a result, it was decided to create a plug of water before the vessel was pressurized. This procedure also helped prevent fast temperature drops at the bottom of the vessel when initially introducing CO_2 into the empty extraction vessel. With the extraction vessel containing an initial volume of water at approximately 45 °C, the CO_2 is warmed as it enters the extraction vessel.
- Based on experiments, it was concluded that having the level slightly above 16 cm is a good level for the initial water plug inside the extraction vessel. In creating the water plug, due to splashing, the 16 cm level sensor is immediately activated and the actual level of water inside the vessel could not be determined. Since the level sensor could not be used to determine the level of slurry, the slurry pump has to be stopped once to stop splashing in the vessel and determine the approximate level of water (i.e., level above vs. below 16 cm). However, based on calculations, it was concluded that running the slurry pump for approximately 20 seconds at 15 % of maximum pump rpm would provide a 16 cm of water level inside the extraction vessel. Therefore, this approach was applied for creating a 16 cm plug of water in the extraction vessel at the beginning of an experiment.

- After initial testing, it was concluded that the slurry temperature has a dominant effect on the temperature inside the extraction vessel. Therefore, to reach a higher temperature inside the extraction vessel, the slurry feed needs to be heated.
- After initial testing, the procedure that ultimately worked best for introducing countercurrent flow of slurry and CO_2 (after creating a plug of water) was to first bring the extraction vessel to CO_2 tank pressure (~3 MPa) by opening the valve on the CO_2 feed tank. After the extraction vessel reached CO_2 tank pressure, the slurry pump and CO_2 pump are turned on simultaneously to initiate countercurrent flow. The starting flowrates for the two pumps are typically 13.8 % and 12.5 % respectively. When the pressure inside the extraction vessel reaches approximately 10 MPa, the pressure control loop is set to "auto" and the set point is increased step wise to reach the desired pressure inside the extraction vessel. In the presence of level sensor (or an alternative approach for measuring level inside the extraction vessel), the level control loop is set to "auto" after reaching the desired pressure in the extraction vessel.
- An "Operation Log" was prepared and placed in the lab. As part of the start-up procedure, operators are required to fill out this log at the beginning of each run.

Controlled Shutdown Procedure

The major change made to the controlled shutdown procedure is as follows:

- For cleaning the vessel at the end of an experiment, rinse water is used (slurry flow is switched to rinse water flow). Therefore, water and SC CO_2 are countercurrently flowing through the extraction vessel and the system is still pressurized. At this stage, samples will be taken from the receiving slurry tank to make sure that solids have mostly exited the process and then the pumps will be stopped. In addition, after the depressurization stage, the extraction vessel is completely filled and then rinsed from the drain valve at the bottom of the vessel to clean the extraction vessel from any remaining solids.

Checklists

The checklists proposed in the preliminary design (i.e., start-up checklist, shutdown checklist, operation checklist, safety checklist and emergency shutdown checklist) were developed before the process had been set up. As a result, these checklists were very general. Completing the process set up and conducting several experiments allowed more detailed checklists to be developed. These checklists are available on the computer in the lab (in the GUI). Important modifications are as follows:

- A complete valve checklist was prepared to be placed in lab and checked as part of the start-up procedure.

Slurry Level in Extraction Vessel

Three single point type level sensors exist in the extraction vessel (LI-1401, LI-1405 and LI-1406). LI-1401 is located at the top of the extraction vessel. LI-1405 and LI-1406 are located at the bottom of the extraction vessel. LI-1405 has a length of approximately 16 cm and LI-1406 has a length of approximately 5 cm.

The two level sensors located at the bottom of the extraction vessel are not giving reliable readings especially LI-1405 which is the 16 cm level sensor. The reason is that when the slurry pump is turned on and slurry flows through the vessel, splashing of water/slurry in the vessel causes this level sensor to activate even though the level is below 16 cm. Better solutions should be considered for this purpose. Hence, an automated response for level control does not exist at the moment and level control is done manually. The slurry pump speed is adjusted based on physical observations of the slurry outlet line and the pressure gauge located on that line.

Extraction Vessel and Separator Temperature

Temperature control in the extraction vessel and separator is not automated. However, the temperature can be kept within a certain range if the heating equipment is turned on, functioning correctly and adjusted to the correct set-point. Regarding the extraction vessel temperature, the slurry temperature plays a dominant role in controlling the temperature in

the extraction vessel; therefore, the slurry tank heater (HX-3412) is turned on before initiating a run. As a result, the slurry enters the extraction vessel at approximately 45°C.

Regarding the separator temperature, heating tape on the CO_2 line entering the separator (HX-4408), heating tape located on MV-4303 (HX-4407) and heating tape on the separator itself (HX-4409) are turned on during normal operations and set to their maximum value i.e., 204.4 °C (equivalent to 400 °F). These three heating devices play a significant role in determining the temperature inside the separator and preventing the lines from freezing and preventing the temperature in the separator to drop below 0 °C.

2.3.6 Hazard and Operability (HAZOP) Study

A HAZOP study was completed in November 2010 by some members of the SFE design team (A. Rosenthal and C. Street) and team members from M-I SWACO (industrial partner). Those HAZOP results are provided in Rosenthal (2012) and have been updated for this thesis. The primary changes are as follows:

- Equipment tag numbers were updated in the HAZOP document to reflect any system design changes (provided in Tables 3.3, 3.4 and 3.5).
- The original HAZOP (Rosenthal 2012) assumed that spill containment ("drip trays") would be installed; however, these have not been installed. Some slurries are dilute enough to be disposed of directly. For those slurries that cannot be disposed of directly, spills are contained, collected and disposed of according to protocols outlined by Environmental Health and Safety (EHS) of the University of Alberta.
- Flow meters have not been installed on CO_2 lines upstream or downstream of the CO_2 pump or downstream of the extraction vessel. Originally, the justification for installing these flow meters was to avoid pump damage or process upsets that would be caused by low or high flows in these locations. Due to issues of specifications and cost, the flowmeters were not installed. To prevent pump damage, the CO_2 pump cannot be started until the CO_2 supply valve is open (by both an automated valve programmed into the control system and a manual valve integrated on CO_2 tank). Process upsets in the vessel caused by CO_2 primarily affect pressure. Increases or decreases in pressure are monitored by pressure sensors at the top and bottom of the

extraction vessel.

- The original HAZOP specified the installation of a flow switch prior to the slurry pump to prevent cavitation in the slurry pump. There were issues in sourcing adequate flow switches. Operators currently ensure the feed tanks are full and valves are in the correct position to avoid running the pump dry.
- The grinding loop is not installed. Instead, a procedure regarding slurry preparation has been completed and added to the Operations Manual.

2.4 Summary of Runs

Table 2.6 summarizes the experimental runs conducted on the continuous pilot-scale SFE process. The summary includes the date of run, the component/fluid(s) that were used for conducting the SFE experimental runs, the objective of the run, and the main outcomes and observations of the run. Runs are presented in chronological order. Each experiment is identified with a run number which is used in following chapters for referencing purposes.

Experimental Runs 1 to 11 are associated with pressurizing the extraction vessel with CO_2 (via the CO_2 pump). Pressure control loops were also implemented, tested and modified in these runs. Experimental Runs 12 to 18 were aimed at establishing countercurrent flow of CO_2 and slurry (as water) inside the vessel for as long as possible. Experimental Runs 13 to 26 were also aimed at establishing countercurrent flow. However, from Run 13, the original CO_2 feed tank was replaced with the current CO_2 feed tank and troubleshooting was again required for pressurizing the extraction vessel. Experimental Runs 27 to 30 were conducted to obtain data for system identification (developing a model of the process based on data from the continuous pilot-scale process).

From Run 31, slurry was used in the countercurrent SFE process, instead of only water, as in previous runs. Experimental Runs 31 to 40 were mainly associated with adding solids to the slurry and troubleshooting to maintain continuous flow of slurry through the process. Experimental Runs 41 to 61 were associated with collecting data from the process for model validation purposes and performing mass transfer calculations. Experimental Runs 62 to 82

were conducted for various purposes, for example testing different operating conditions and different control strategies.

Table 2.6: Summary of runs conducted on the pilot-scale SFE process

Run	Date	Component(s)	Objective	Outcomes	Observations
Experiments to test system pressurization					
1	30/05/2014	CO_2 only	Have the CO_2 pump produce pressure.	The CO_2 pump produces pressure, as long as it is provided with a liquid CO_2 feed. This can be accomplished by venting CO_2 through the pump until the line temperature reaches -21°C, and maintaining the cauldron and chiller at approximately -25 °C.	None.
2	2/06/2014	CO_2 only	Pressurize vessel to 10 MPa and hold the pressure.	The vessel was successfully pressurized.	Re-pressurization of the system after a shutdown is achievable if cauldron temperature is maintained at around -20°C. A temperature gradient exists along the vessel. The bottom of the vessel (where the CO_2 enters) is much colder than the top where the thermocouple is placed. Thus, the CO_2 may exist in several states throughout the vessel.
3	3/06/2014	CO_2/water	Attempt to introduce water into the vessel when vessel is pressurized with CO_2 at 4 MPa.	Slurry was successfully introduced into the pressurized vessel.	The level sensors did not give reliable results. The reason might be that water froze on them because it is very cold at the bottom of the vessel where CO_2 enters.
4	4/06/2014	CO_2 only	Repeat Run 2	The vessel was successfully pressurized to 10 MPa.	A large temperature gradient exists along the vessel which should be resolved.
5	11/06/2014	CO_2 only	Introduce CO_2 first from top and then bottom to see if the temperature gradient along the vessel can be reduced.	The temperature gradient was not improved by this vessel pressurization method.	A pressure spike happens at around 8 MPa. The reason could be that the system is operating in the liquid region and a few additional grams of CO_2 increases pressure significantly.

Table 2.6: Summary of runs conducted on the pilot-scale SFE process, continued

Run	Date	Component(s)	Objective	Outcomes	Observations
6	13/06/2014	CO_2 only	Observe the effect of pump speed on pressure response.	The pressure did respond to changes in pump speed as expected.	A steady state pressure was not achieved. The reason could be that the temperature is changing inside the vessel which affects the pressure.
7	4/07/2014	CO_2 only	Test the pressure control loop (the pump speed is varied according to the pressure at the top of the vessel).	Steady state pressure was achieved, especially when the pump controller parameters were optimized.	There was a distinct pressure difference between the line, vessel bottom, and vessel top readings. The CO_2 line before the pump warms up if pump RPM decreases. A 5 % to 60 % limit should be put on CO_2 pump RPM (do not allow the pump to stop or to jump to high speed).
8	14/07/2014	CO_2 only	Test the effect of having a heating tape at the bottom of the vessel.	The heating tape did not have a large effect on the temperature at the bottom of the vessel. (Prior to this test, a thermocouple was installed in the bottom of the vessel). Overall, a 10 °C temperature profile exists along the vessel length.	When the pump speed increases, vessel bottom temperature starts to decrease.
9	17/07/2014 (a)	CO_2 only	Test the effect of slowly increasing the pressure to operating conditions to try to minimize the temperature gradient in the vessel.	Slowly increasing the pressure to operating conditions results in the same temperature gradient in the vessel.	Slowly increasing the pressure reduces rapid changes in temperature (which was previously observed).

Table 2.6: Summary of runs conducted on the pilot-scale SFE process, continued

Run	Date	Component(s)	Objective	Outcomes	Observations
10	17/07/2014 (b)	CO_2 only	Limit the pressure gradient in the vessel by testing a new control structure where the vessel bottom pressure is controlled with pump rpm and the vessel top pressure is controlled with metering valve position.	A smaller pressure gradient was observed in the vessel.	Controlling the pump RPM with the bottom pressure can result in very high pressures in the inlet line (as a result of flow restrictions and pump controller settings).
11	18/07/2014	CO_2 only	Limit the pressure gradient in the vessel by testing a new control structure where the CO_2 inlet line pressure is controlled with pump rpm and the vessel top pressure is controlled with metering valve position (limit on metering valve between 5 % and 50 %).	Uniform pressure between the inlet line and the vessel top can be observed; however, it takes some time to reach steady state.	None.

Table 2.6: Summary of runs conducted on the pilot-scale SFE process, continued

Run	Date	Component(s)	Objective	Outcomes	Observations
Experiments to establish countercurrent flow of CO_2 and slurry (as water) inside the extraction vessel as long as possible					
12	23/07/2014	CO_2/water	Attempt to pump slurry into a pressurized vessel at 10 MPa by first pressurizing with CO_2 while water is between 5 and 16 cm. Then, when the pressure is steady, turn the CO_2 pump off and turn slurry pump on.	Successfully introduced slurry into pressurized vessel of 10 MPa.	After turning on the slurry pump, the bottom temperature is the same and even more than the top temperature. So, the slurry brings in heat to the process. The level sensors not giving consistent results.
13	24/07/2014	CO_2/water	Attempt countercurrent flow.	Countercurrent flow achieved.	The manifold was set to 1 meter of 3.2mm (1/8″) tubing. This seems to be able to hold the pressure inside the vessel.
14	29/07/2014	CO_2/water	Attempt countercurrent flow.	Countercurrent flow achieved but run aborted due to freezing in the metering valve.	The separator was drained after this run and quite a lot of water came out.
15	31/07/2014	CO_2/water	Attempt countercurrent flow with new heating tape on the metering valve to prevent freezing.	The CO_2 tank was recently filled and the pressure wasn't high enough for a run (it was at 1.9 MPa (280 psi)). And it even dropped to 1.8 MPa (260 psi) when the run started. Countercurrent flow could not be achieved because CO_2 pump failed to pressurize; however, continuous flow of water was achieved through the vessel for quite some time with the pressure at around 5-6 MPa.	7 to 10 days is required to pressurize the CO_2 tank from fill pressure before a run because the pressure is dropped to accommodate the truck to fill it and it relies on temperature in the lab to pressurize. For the water flow part of the test, the manifold was set to the second most restricted line (3.2mm (1/8") ID and 0.5 m length), which seemed to be enough for the pressure the vessel was at.

Table 2.6: Summary of runs conducted on the pilot-scale SFE process, continued

Run	Date	Component(s)	Objective	Outcomes	Observations
16	7/08/2014	CO_2/water	Countercurrent run for as long as possible.	Ran for 23 min until the slurry receiving tank was overfilled and the run had to be terminated.	Restart of the CO_2 pump was not possible because CO_2 line had warmed up.
17	8/08/2014	CO_2/water	Repeat Run 16.	Ran for 22 min. The run was terminated because it sounded like freezing was happening somewhere in the lines and/or near the separator.	
18	20/08/2014	CO_2/water	Repeat Run 16.	Countercurrent run was achieved for one hour. No reason was observed to terminate run.	The CO_2 tank pressure had dropped significantly over the run and was far away from the necessary 2.0 MPa (290 psi). It was decided to change the CO_2 tank. This was the last run done with this CO_2 tank.
19	2/10/2014	CO_2 only	Test the new CO_2 tank.	Successfully pressurized the system to 8 MPa.	This run was initiated without venting to pre-cool the system to liquid CO_2 temperature (at tank pressure). Venting requirement removed from operation manual. A leak was observed on the pressure building circuit on the tank which has to be fixed.
20	7/10/2014	CO_2 only	Test the new CO_2 tank after the tank leak was fixed.	Successfully pressurized the system to 7 MPa.	The CO_2 pump stopped at the middle of the run and was successfully restarted (previously not possible due to venting requirement). The tank was able to maintain its pressure at around 3 MPa.
21	9/10/2014	CO_2/water	Run system countercurrently with the new CO_2 tank.	Countercurrent run was achieved for around 20 minutes before CO_2 pump stopped pressurizing.	None.

Table 2.6: Summary of runs conducted on the pilot-scale SFE process, continued

Run	Date	Component(s)	Objective	Outcomes	Observations
22	17/10/2014 (a)	CO_2/water (first part of the run)	Obtain data for system identification.	Unsuccessful due to CO_2 pump stopped pressurizing after 20 minutes of running.	None.
23	17/10/2014 (b)	CO_2 (second part of the run)	Solve issue in previous part of the run i.e., will the pump stop again with CO_2 only?	Unsuccessful at achieving pressure with CO_2 pump after 45 minutes of running.	None.
24	21/10/2014 (a)	CO_2 only	Test CO_2 pump with the pump head chiller at -25 °C.	CO_2 pump did not pressurize.	None.
25	21/10/2014 (b)	CO_2 only	Retry Run 24 with line cooling cauldron back into the process and cooling it to -15 °C.	Ran successfully for 1 hour, indicating that the cauldron is required and needs to be cooled to around -15 °C.	None.
26	23/10/2014	CO_2/water	Replicate Run 16.	Successfully ran for 1 hour.	Could not run beyond 1 hour because of freezing in the CO_2 line going to fume hood, likely because of water carry over. For next run, consider extending the separator inlet line to prevent carry over.
Experiments to obtain data for system identification					
27	30/10/2014	CO_2/water	Obtain system identification data at around 8 MPa.	Successfully obtained system identification data.	Process will stay relatively stable during "Manual Mode" at a constant CO_2 and slurry rpm.
28	4/11/2014	CO_2/water	Replicate of Run 27.	Successfully obtained system identification data.	None.
29	6/11/2014	CO_2/water	Obtain system identification data at around 12 MPa.	Successfully obtained system identification data.	Temperatures inside vessel slowly decreases over the run. Consider a heater for slurry tanks (as the slurry controls the system temperature). A lot of CO_2 is used. Consider closing metering valve to conserve CO_2.

Table 2.6: Summary of runs conducted on the pilot-scale SFE process, continued

Run	Date	Component(s)	Objective	Outcomes	Observations
30	12/11/2014	CO_2/water	Replicate of Run 29.	Successfully obtained system identification data.	None.
Experiments with slurry (both control system and mass transfer tests)					
31	18/11/2014	CO_2/slurry	Test the system with actual slurry (solids in the water).	Successfully ran countercurrent flow with solids in the water (actual slurry).	Solids separate out of the slurry in the tank. Consider a mixer for the tank. Separator shows signs of freezing. Consider another heating tape for around the separator body.
32	16/12/2014	CO_2/water	Test the new designed pressure controller to 14 MPa and observe the response of RBS signal to be used to identify the system again.	Test completed successfully but the new controller seemed to be very sluggish.	There was a high atmospheric CO_2 concentration during run (mainly around 14 MPa).
33	18/12/2014	CO_2/slurry	Test a countercurrent run with slurry, mixed with a hockey stick. Run includes new composition of solids in slurry. Tested sending the slurry to a receiving tank to prevent the temperature from dropping.	The test was completed successfully. The mixing allowed more solids to flow to the vessel. The longer manifold prevented the CO_2 concentration in the atmosphere from increasing. Because the feed tank was different from receiving tank this time, slurry temperature didn't drop as fast as before.	None.

Table 2.6: Summary of runs conducted on the pilot-scale SFE process, continued

Run	Date	Component(s)	Objective	Outcomes	Observations
34	20/01/2015	CO_2/slurry	Replicate of Run 33 but tested switching from pressure control on CO_2 inlet line to vessel bottom.	Successful run. After the pressure stabilized, the pressure sensor on the control loop was changed from the line pressure to vessel bottom pressure. This change keeps the vessel closer to the pressure set point.	None.
35	26/01/2015	CO_2/slurry	Replicate of previous Runs 33 and 34. However this run included a longer manifold, a heater, and a mixer.	Successful run. The longer manifold (3.2 mm (1/8") ID and 2m length) worked well with the higher pressure in vessel (14 MPa) to prevent CO_2 "burps". The heater was effective, increasing the vessel bottom temperature to 40 °C.	None.
36	13/02/2015	CO_2/slurry	Replicate of Run 35, but the heating tape was moved from the bottom of the extraction vessel to the CO_2 inlet line.	Successful run. The heating tape on the CO_2 inlet line did not seem to have any impact on the vessel temperature.	None.
37	18/02/2015	CO_2/slurry	Replicate of Run 36 but with increased solids content of the slurry.	Successful run. Increased solids did not cause any operational difficulties.	A blender was used to successfully create slurry. Took a long time just to create one pale of slurry.
38	24/02/2015	CO_2/slurry	Replicate of Run 37 but with additional solids mixed in using the tank mixer.	The tank mixer worked well to incorporate the additional solids and the increase in solids content did not cause operational difficulties.	Freezing occurred in the separator near the end of the run. The vessel seemed quite full.

Table 2.6: Summary of runs conducted on the pilot-scale SFE process, continued

Run	Date	Component(s)	Objective	Outcomes	Observations
39	3/03/2015	CO_2/slurry	This run was a flow test to make sure the vessel is not filling during the run by minimizing the slurry flow as much as possible (create burps).	Modestly successful run but complete burps could not be created because the CO_2 level would increase inside the lab. However, the run had a lower slurry pump rpm in comparison to previous runs.	At the end, only 125 mL of rinse water was collected from the vessel.
40	13/03/2015	CO_2/slurry	Replicate of Run 38 but with high solids concentration (approximately 5 %).	Unsuccessful run as the slurry pump could not be operated at low speeds (15 rpm).	None.
Experiments to validate hydrodynamic model and to determine mass transfer					
41	26/03/2015	CO_2/slurry	Get validation data at 10 MPa and 14 MPa but dilute the slurry because of Run 40 outcome.	Successfully obtained system data.	None.
42	1/04/2015	CO_2/slurry/water	Replicate Run 41 and test the new CO_2 coil (coil of tubing wrapped in heating tape).	Unsuccessful run because of the increased flow resistance of the CO_2 coil and also freezing occurring in the slurry outlet line when attempting to start countercurrent phase.	None.
43	8/04/2015	CO_2/water	Troubleshoot the CO_2 coil and decide whether to keep it.	The run start-up was very slow because of the coil. As configured, the coil does not seem to provide any temperature benefit at the bottom of the vessel.	Freezing occurred in the slurry line when attempting to start countercurrent, but was successful when slurry pump was started at 20 %.
44	15/04/2015	CO_2/water	Conduct a pulse test at 14 MPa without the CO_2 coil (based on Run 43).	Unsuccessful run because there was a blockage at the slurry outlet line. Blockage was not due to freezing as in Runs 42 and 43. There was a solid blockage at the exit of the vessel (of unknown origin).	None.

Table 2.6: Summary of runs conducted on the pilot-scale SFE process, continued

Run	Date	Component(s)	Objective	Outcomes	Observations
45	22/04/2015	CO_2/water	Do an hour uncontrolled CC run and compare results with modelling results. Burps of CO_2 were expected at certain times (based on modelling prediction).	First attempt was unsuccessful due to freezing and the incorrect manifold was used. Second attempt was successful as the same steady state pressure was reached as the model predicted (10 MPa). However, no burp was observed.	None.
46a	24/04/2015 (a)	CO_2/water		The run was successful as the same steady state pressure was reached as the model predicted (10 MPa). However, no burp was observed.	Mid-run pressure slightly increased.
46b	24/04/2015 (b)	CO_2/water		The run was successful as the same steady state pressure was reached as the model predicted (14 MPa). However, no burp was observed.	Mid-run pressure slightly increased.
47	29/04/2015	CO_2/water	Replicate Runs 45 and 46 but include a heating tape on the slurry outlet and fume hood lines to prevent freezing (that may be the cause of the mid-run pressure increase and no burps).	The same steady state pressure reached as the model predicted (10 MPa) with no pressure increase. However, still no burp was observed.	Noticed vessel filling procedure not the same between Runs 45, 46, 47. Need a consistent filling procedure in order to compare better between runs.
48	5/05/2015	CO_2/water	Measure the amount of time it takes to empty the vessel at 10 MPa.	Unsuccessful test as once the slurry outlet valve was opened a burp was observed which typically indicates that the vessel is empty. It was later realized that the CO_2 may be short circuiting because its density is quite high at the vessel conditions.	None.

Table 2.6: Summary of runs conducted on the pilot-scale SFE process, continued

Run	Date	Component(s)	Objective	Outcomes	Observations
49	7/05/2015 (a)	CO_2/water	Test the model prediction of the vessel emptying (observed as a CO_2 burp) after 10 minutes of an uncontrolled run.	The run was not successful as no burps were observed after 10 minutes.	None.
50	7/05/2015 (b)	CO_2/water	Replicate of Run 48 but with the CO_2 pump turned off after pressurizing to 10 MPa, and isolate the vessel before draining it.	The run was not successful because of an emergency alarm on the CO_2 line pressure between the pump and the vessel after isolating. The pressure reached 20 MPa.	It took approximately 4 minutes to drain the vessel.
51	7/05/2015 (c)	CO_2/water	Replicate of Run 50, but draining the CO_2 inlet line before isolating the vessel to avoid the emergency alarm.	Draining the line helped with the alarm initially but as soon as the drain valve was closed, the pressure increased again.	There were freezing issues of unknown origin at the beginning of the run.
52	12/05/2015 (a)	CO_2/water	Validate the model with an uncontrolled run to get to approximately 14 MPa.	Successfully reached 14 MPa and obtained validation data.	Towards the end of the run, the separator began to freeze even though the heating tapes were at their maximum.
53	12/05/2015 (b)	CO_2/water	Replicate of Run 50 but this time the CO_2 inlet valve was left open to prevent that line from pressurizing and activating the alarm.	Successfully emptied the vessel as expected. At approximately 3 min and 50 s CO_2 was observed to be leaving with the slurry. At 4 min and 10 s full CO_2 flow through the slurry line and into the receiving tank was observed (a “burp”).	None.
54	15/05/2015 (a)	CO_2/slurry	Get model validation and mass transfer data at 10 MPa and 14 MPa.	Unsuccessful run because the slurry flow was too high for the pressure and manifold settings (10MPa and longest manifold).	None.

Table 2.6: Summary of runs conducted on the pilot-scale SFE process, continued

Run	Date	Component(s)	Objective	Outcomes	Observations
55	15/05/2015 (b)	CO_2/slurry	Replicate of Run 54.	Successful run.	None.
56	20/05/2015	CO_2/slurry	Replicate of Run 54.	Successful run.	None.
57	26/05/2015	CO_2/water	Get model validation and mass transfer data at 18 MPa.	Unsuccessful run as atmospheric CO_2 concentration kept going up and down. There was a leak in the pressure relief on the CO_2 pump.	None.
58	2/06/2015	CO_2/water/slurry	Replicate of Run 57 but used a bucket in the fume hood to catch any oil leaving with the CO_2.	Successful run, but the atmospheric CO_2 was going up and because of the bucket in the fume hood.	None.
59	15/06/2015	CO_2/water/slurry	Replicate of Run 57 with no bucket.	Successful run.	The atmospheric CO_2 concentration was consistent with movement of gauge slurry outlet pressure gauge. When depressurizing, the separator was isolated to try to prevent oil from being pushed out into the fume hood.
60	17/06/2015	CO_2/water/slurry	Replicate of Run 57 but with the shorter manifold until 10 MPa is reached.	Unsuccessful run because as soon as the system was switched from water to slurry at 18 MPa the slurry outlet line froze. The reason could be that the shorter manifold was used while pressurizing to 10 MPa and so the vessel slurry level was quite low (not as high as when the longer manifold was used) causing more CO_2 to exit that line.	None.

Table 2.6: Summary of runs conducted on the pilot-scale SFE process, continued

Run	Date	Component(s)	Objective	Outcomes	Observations
61	24/06/2015	CO_2/water/slurry	Replicate of Run 57.	Successful, however towards the end of the run, the vessel started to lose pressure and seemed like the CO_2 pump was not pressurizing perhaps as a result of the pump head chiller leaking.	None.
Experiments for miscellaneous purposes					
62	30/06/2015	CO_2/water	Uncontrolled CO_2 run for model validation.	Unsuccessful run because there was a problem with pressurizing the system which could be a result of the pump, tank, or a line blockage. Eventually the system was depressurized and it was confirmed not to be a line blockage.	None.
63	6/07/2015 (a)	CO_2/water	Conduct a flow test to see how high the system can go in terms of slurry flow and CO_2 flow.	Unsuccessful test because of a high atmospheric CO_2 alarm.	Pressurizing still seemed to be a bit slow and was using more CO_2 than usual to maintain pressure.
64	6/07/2015 (b)	CO_2/water	Do an uncontrolled CO_2 flow for model validation.	Successful test as 10.3 MPa steady state was reached.	None.
65	9/07/2015 (a)	water only	Test pressure drop in slurry line by running slurry pump at 50 % going into the vessel.	Successful test as 10 MPa is observed on the pressure sensor of the slurry inlet line. This pressure is because of the restriction caused by the line change from 3.2 mm (¼″) to 6.4 mm (1/8″) going into the vessel.	None.
66	9/07/2015 (b)	CO_2 only	Do an uncontrolled run of CO_2 for model validation.	Successful run.	It was determined that when only CO_2 is going in and out of the vessel, the vessel is a bit slow in pressurizing.

Table 2.6: Summary of runs conducted on the pilot-scale SFE process, continued

Run	Date	Component(s)	Objective	Outcomes	Observations
67	15/07/2015	CO_2/water/slurry	Do a second pass of the slurry from Run 61 at 14 MPa	Successful run.	The CO_2 pump rpm was observed to be higher than usual.
N/A	07/2015	CO_2/REAL slurry	Attempt a run with real cuttings made into slurry.	Unsuccessful run because the slurry pump began pulsing (not providing flow) as a result of solids settling in the 50.8 mm (2″) SS pump supply line.	None.
68	10/08/2015	CO_2 only	Check to make sure that the slurry pump can withstand the back pressure from the CO_2.	Successful run.	None.
69	12/08/2015	Real slurry	Test the slurry pump on bypass with the real slurry to see if the pulsation problem can be replicated. The support ring was also removed from the top of the vessel baffle structure and removed the 3.2 mm (1/8″) slurry extension line into the vessel.	When using the real slurry, the slurry pump started pulsating if the pump was left running at low flows. However, when the pump speed was increased it recovered from the pulsating. It was concluded that higher flows should be used for this slurry type to make sure the solids in the slurry don't settle out and restrict supply to the pump.	None.
70	13/08/2015 (a)	CO_2/water	To test shorter manifolds and higher water flows to see how high the system can go before switching from water to slurry.	Successful as up to 27 % slurry flow was shown with the medium length manifold. However, as soon as the flow was switched to slurry, there was a high level emergency shutdown because of slurry splashing.	None.

Table 2.6: Summary of runs conducted on the pilot-scale SFE process, continued

Run	Date	Component(s)	Objective	Outcomes	Observations
71	13/08/2015 (b)	CO_2/water	Replicate of Run 70 to observe if splashing incident is repeatable.	Successful run as the same thing happened as in Run 70.	It was decided to extend the 3.2 mm (¼″) line into the vessel until it touches a baffle.
72	19/08/2015	CO_2/water	Conduct a pulse test with the slurry flow as a method to sense level.	Due to clogging issues, run was unsuccessful.	None.
73	20/08/2015	CO_2/water	Replicate of Run 72.	Pulse test program worked but there was a small programming issue. Also, there was an emergency shutdown because workers had disconnected our CO_2 sensor power in the hallway.	None.
74	25/08/2015	CO_2/water/slurry	Replicate of Run 72 with a new slurry.	The pulse test seemed to be calculating, but the results did not seem to be reliable. The system went on emergency shutdown when the flow was switched to slurry as a result of splashing (as in Run 71).	None.
75	31/08/2015	CO_2/water/slurry	Replicate of Run 74 with increased time between pulses and the angle of the slurry inlet line towards vessel wall to help with splashing issue.	The pulse test worked better by increasing time between pulses. Successfully switched the system to slurry without splashing and emergency shutdown. Unfortunately, there was an emergency shutdown for splashing when the flow was switched back to water.	None.

Table 2.6: Summary of runs conducted on the pilot-scale SFE process, continued

Run	Date	Component(s)	Objective	Outcomes	Observations
76	9/09/2015	CO_2/water/slurry	Conduct a controlled pulse test with the position of the level sensor at the top of the vessel opposite the slurry inlet (instead of being at the centre). The sensitivity of the level sensor at the top was also slightly changed. Take mass transfer samples.	Controlled pulse test did not work and it suddenly decreased slurry pump speed from 20 % to 1 %. After the pulse test was terminated, the system was switched to slurry (controlling level manually) to get mass transfer samples. However, after 10 min there was freezing in the separator and run had to be terminated.	Less than 1L of slurry was drained from the bottom of the vessel.
77	16/09/2015	CO_2/water/slurry	Conduct a controlled pulse test with a new separator inlet line was switched from 3.2 mm (1/8″) to 6.4 mm (¼″) to prevent freezing issues. Take mass transfer samples.	Controlled pulse test is still not working due to a programming bug. Run was terminated in the end because CO_2 pump could not pressurize due to the CO_2 tank getting near empty.	None.
78	3/11/2015	CO_2/water/slurry	Take mass transfer samples new slurry (with soap + heavy solids removed to prevent pulsing of pump).	The vessel high level alarm was activated due to splashing in first attempt, therefore run was terminated. The second attempt was good.	None.
79	10/11/2015	CO_2/water	Test level control with pulsing water flow.	The pulse level control is still not working, this time because of an issue with a controller parameter.	None.
80	17/11/2015	CO_2/water	Replicate Run 79.	Good run as the level measurements are consistent. However, the pump control part is still not working as expected.	None.

Table 2.6: Summary of runs conducted on the pilot-scale SFE process, continued

Run	Date	Component(s)	Objective	Outcomes	Observations
81	26/01/2016	CO_2/water	Test the model-based controller on the process and compare its performance with the previous manual based controller.	Successful run. Run had to be terminated at the end because of freezing near the separator.	None.
82	24/08/2016	CO_2/water	Test the level controller and compare the experimental result to the model prediction.	Unsuccessful run. The level controller was not calculating realistic levels and the pump control would shut off the slurry pump instead of lowering the speed in set increments.	None.

Based on Table 3.6, the general phased development of the process occurred from pressure testing with CO_2 only, to CO_2 with water, then to CO_2 with slurry. By Run 35, the process was operating as it is currently. That is, no major changes were made to the equipment or experimental procedures beyond Run 35.

From the 82 total runs completed on the process, the 12 runs summarized in Table 2.7 are the runs that meet the functionality objectives presented in Section 2.1, that is runs in which slurry (not water) was processed and they were not aborted due to process issues (e.g., emergency shutdowns, lines or valves freezing, major equipment malfunction, running out of CO_2).

From the remaining 70 runs, only 5 runs (i.e., Runs 15, 24, 40, 42 and 44) completely failed to initialize. The problem in Runs 15 and 24 was associated with the CO_2 feed tank - CO_2 pump incompatibility. The problem in Run 40 was associated with pumping a high solids concentration slurry (> ~3 wt%). Because of the configuration of the slurry pump upstream line and also the incapability of the mixer to provide a completely homogeneous mixture, a very thick slurry was delivered to the slurry pump. The thick slurry resulted in the slurry pump output pulsing, and therefore malfunctioning of the slurry pump. The problem in Runs 42 and 44 was associated with freezing/blockage (in the slurry outlet line from the extraction vessel) of unknown origin.

From the remaining 66 runs, 55 runs were partially or completely successful in reaching their proposed objective. The remaining 11 runs (i.e., Runs 48, 49, 50, 51, 54, 57, 60, 62, 63, 72 and 82) failed in reaching their objectives (as outlined in Table 2.6). The failures were due to different reasons such as activation of an emergency alarm, freezing in lines, CO_2 leak in the process, etc. The design evolved to address these factors.

Table 2.7: Summary of runs, with operating conditions, that meet the functionality objectives

Run	Pressure (MPa)	Temperature (°C)	CO_2 flow (L/min, at pump)	Slurry flow (L/min, at pump)	Slurry solids (% wt.)	Duration (s)	Duration (min)
35	13.5	41.3	0.96	2.7	0.24	2030	34
36	13.9	44.9	0.97	2.5	0.16	2493	42
37	13.8	41.0	1.0	2.5	1.1	2395	40
38	13.9	44.1	0.86	2.7	3.0	1923	32
39	13.3	37.7	1.5	2.0	2.8	414	7
41	10.3	38.8	1.1	2.5	2.5	2557	43
	14.0	45.4	0.64	2.1			
55	10.0	42.7	0.70	2.3	2.6	1700	28
	14.0	41.1	1.3	2.6			
56	14.0	32.6	1.5	2.4	2.5	428	7
58	17.9	42.2	1.9	3.1	2.3	1331	22
59	17.9	43.2	1.7	3.4	2.1	1755	29
67	13.9	40.6	2.0	2.6	1.7	1355	23
78	13.9	34.1	1.4	3.3	0.5	1530	26

The pressures and temperatures listed in Table 2.7 are the averages of measured values from both sensors (one of each located at the top and bottom of the extraction vessel) over the duration of the run. The flow rates are the average value of each pump speed, calculated as L/min (based on piston size and stroke length), also over the duration of the run. The duration is calculated as the time during the run where:

- the vessel has reached at least 7.4 MPa at the pressure sensors on the top and the bottom of the extraction vessel;
- the temperature is at least 31°C at the temperature sensors on the top and bottom of the extraction vessel; and
- the extraction vessel is being operated countercurrently with CO_2 and slurry.

For all the runs in Table 2.7, the duration start point occurred once the bottom temperature sensor reached 31°C. The duration end point was when the slurry feed was switched to the rinse water feed. As an example of the duration of a typical run, Figure 2.12 shows the pressure and temperature in the vessel at both the top and bottom sensors over the length of Run 38. In this case, the bottom temperature sensor reads 31°C at 2100 s. The feed was switched to rinse water at 4023 s, for a total duration of 1923 s.

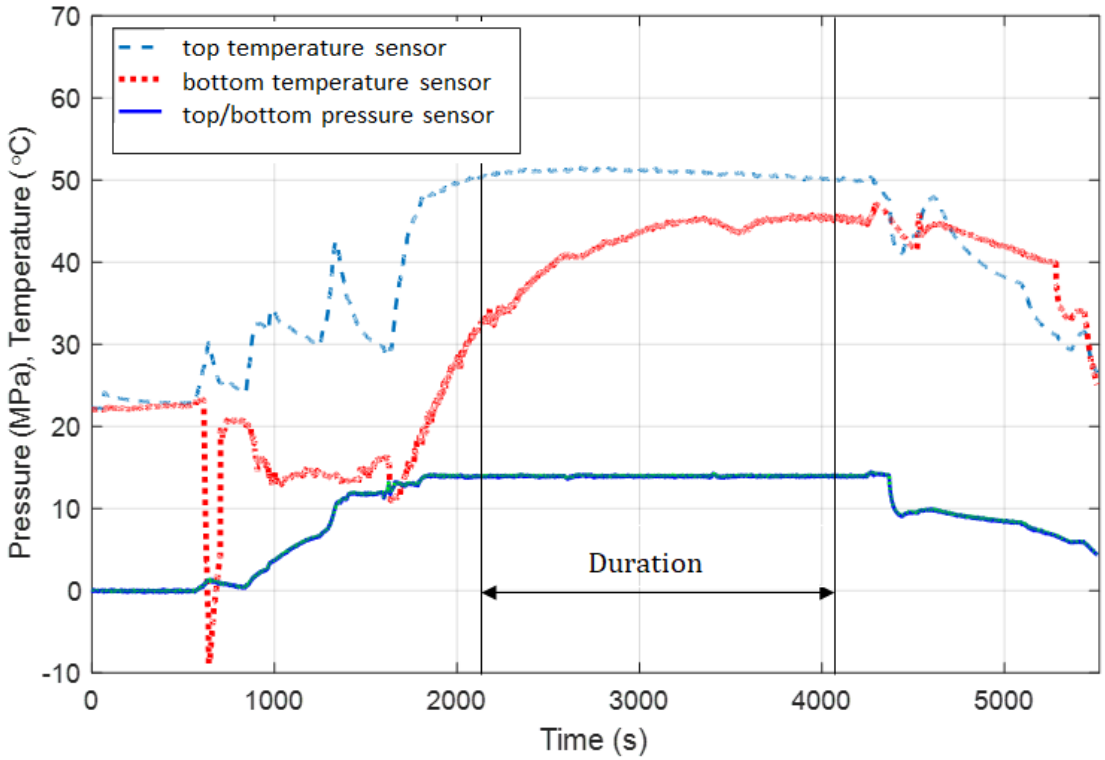

Figure 2.12: Pressure and temperature at top and bottom sensors over Run 38

Figure 2.12 also shows that the total typical run time was longer than the duration listed in Table 2.7, and as a matter of functionality, most of the extra time in a given run was also under SC CO_2 and countercurrent flow conditions using water instead of slurry (bringing the process up to pressure and rinsing under pressure at the end of the run). Although there has to be boundaries set to determine functionality of the process, the duration listed in Table 2.7 is shortened by considering both temperature sensors instead of an average. Because of its location near the incoming CO_2, which tends to be cold, the bottom sensor always dictated the start of the run duration. However, by that point in time, supercritical conditions would prevail in a majority of the extraction vessel length.

For Runs 41 and 55, where two pressure set points were tested without stopping and re-starting the process, the transition period was also counted in the duration. However, average pressure, temperature and flow rates (not including the transition period) were determined for each segment of the run.

Finally, for experiments in which hydrocarbon-contaminated slurry was processed, SC CO_2 successfully extracted hydrocarbon from the slurry phase. After select runs, once the process was depressurized, the accumulated oil in the separator was pumped out using a dip tube connected to a peristaltic pump. A sample of the collected hydrocarbon is presented in Figure 2.13.

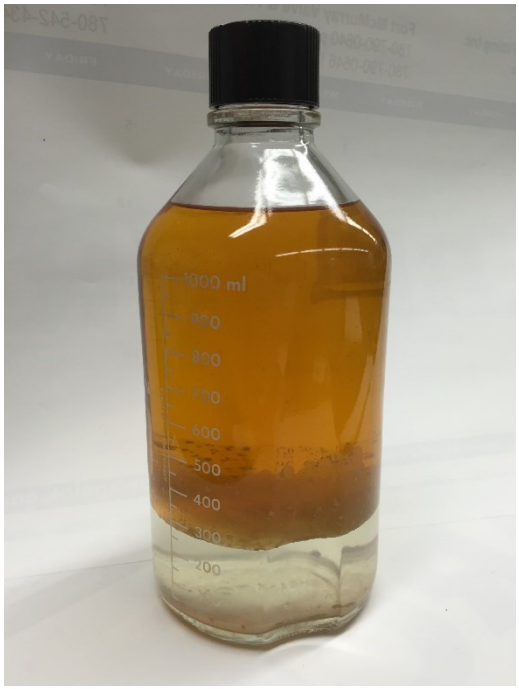

Figure 2.13: Hydrocarbon (top layer) and water (bottom layer) sample collected from the separator for Runs 39 and 41

2.5 Conclusion and Recommendations

To solve the problem of hydrocarbon-contaminated drill cuttings, a continuous pilot-scale SFE process, including both the physical equipment and a control system capable of maintaining process variables, has been successfully developed. This Chapter has detailed

the development from design, to construction, to commissioning and operation. The objective of the chapter is to demonstrate that the process can extract hydrocarbon from water-slurried cuttings under supercritical conditions (above 7.4 MPa and 31°C) using continuous, countercurrent flow.

From the basis of a previous preliminary design, modifications to flow specifications, lab layout, P&ID, control philosophy, operation manual and HAZOP were completed. Construction of the process was also successful, despite the challenges in procuring equipment for a novel SFE process of this scale.

For commissioning the process, 82 experimental runs were completed. The initial runs were mostly aimed at troubleshooting the process to ensure it was operating as expected. As necessary, equipment and procedural changes were made. Most of the remaining runs were aimed at gathering data for mass transfer and control studies.

Of the 82 experimental runs, 12 directly demonstrated the functionality of the process as solution to the drill cuttings problem. That is, the process extracted hydrocarbon from slurried cuttings while maintaining supercritical conditions in the extraction vessel (above 7.4 MPa and 31°C for CO_2); operating in a countercurrent, continuous flow scheme; and running for duration of time without process upsets or emergency shutdowns. Over the course of these runs, the process operated at pressures from 10.0 to 17.9 MPa; temperatures from 31.6 to 45.4°C; slurry flow rates from 2.0 to 3.4 L/min; CO_2 flow rates from 0.64 to 2.0 L/min and slurry solids concentration varied between 0.16 to 3 wt%. The experimental run durations varied from 7 to 43 minutes.

Safe process operation was integrated into all phases of the process development. The evidence is documented throughout this Chapter, including: an updated HAZOP on the as-built design; integration of the CO_2 alarms into Central Control of the University of Alberta; and updating the system process alarms/modes. The environmental monitoring and process alarm safety features activated appropriately in a number of the 82 runs completed.

The novel SFE process built for this project, which is the first of its kind, has been shown to be functional over a range of pressures, temperatures, solids concentrations, and flow rates. The process operates safely and can extract hydrocarbon from a slurried solid phase. As a solution to the drill cuttings problem, this is a major step towards a commercial process. Future work would expand the range of the process variables studied i.e., temperature, pressure, CO_2 flowrate, slurry flowrate, slurry solids concentration and it would include investigating the extraction of hydrocarbon from other types of solid slurries.

Chapter 3: Solubility of Distillate 822 in Supercritical Carbon Dioxide

3.1 Introduction

Mass transfer of drilling fluid hydrocarbons from cuttings into SC CO_2 during extraction is driven by the concentration gradient between the hydrocarbon-SC CO_2 interface and the bulk SC CO_2. The equilibrium concentration (or "solubility") of the drilling fluid hydrocarbon in SC CO_2 can be used to approximate the concentration at the interface. In Chapter 4, the driving force will be used to calculate mass transfer coefficients that quantify the performance of the pilot-scale cuttings treatment system developed in this thesis. Towards that objective, Chapter 3 investigates the solubility of a common, commercially available drilling fluid hydrocarbon, Distillate 822 (D822), in SC CO_2.

There is no single standard method for the measurement of solubility of any solute in supercritical fluids, owing largely to the wide range of solvent-solute systems studied, the type of data required (i.e., phase equilibria versus solubility only), and the methods used to ensure equilibrium is maintained during measurement. The significant challenges of making solubility measurements is captured well by Aim and Fermeglia (2003): "*…a long-term painstaking effort may be hidden behind a very simple statement describing a single step in an experimental procedure…work on high pressure fluid phase equilibria is not a simple task; some skill, experience, and even a good deal of sophistication are needed…modifications of experimental equipment, required according to the type of system to be studied, are by no means exceptions.*"

Gupta and Shim (2007) and Aim and Fermeglia (2003) provide summaries of the various experimental methods used for solubility measurements. Generally, the methods can be divided into either static or dynamic (Gupta and Shim 2007; Aim and Fermeglia 2003). "Static" implies that the contents of the experimental container are fixed and that the pressure and/or temperature are changed to investigate changes in phase composition (Aim

and Fermeglia 2003). Static measurement methods can be further sub-divided into analytic or synthetic (Aim and Fermeglia 2003).

View cells are a common type of static-synthetic apparatus (Gupta and Shim 2007). The vessel is equipped with a sapphire window through which phase changes can be observed when the volume of the cell is changed. Composition of equilibrium phases can be determined from the starting composition and calculations using known pressure-volume-temperature behavior (Aim and Fermeglia 2003).

The disadvantage of static-synthetic measurements is that pressure-volume-temperature data can be limited, necessitating the use of a static-analytic technique (Aim and Fermeglia 2003). Analytic methods involve sampling of the fluid phase(s) after equilibrium has been established, then analyzing the content of the phases through such techniques as gas chromatography, high performance liquid chromatography, or thin layer chromatography (Ran et al. 2019). Due to their smaller volume, static-analytic vessels are subject to equilibrium disruptions resulting from sampling of phases (Gupta and Shim 2007). In-line analysis techniques can eliminate issues due to sample withdrawals (Gupta and Shim 2007).

Dynamic methods involve measuring solubility while continuously flowing the solvent, solute, or both (Gupta and Shim 2007; Aim and Fermeglia 2003). Semi-flow methods, such as the one used in the current study, involve placing the solute in a high pressure, flow-through vessel. The solvent contacts the solute with no flow until equilibrium is achieved. Then, sampling begins where the solute-loaded solvent continuously exits the vessel. The concentration of solute can be determined directly by in-line sampling techniques (e.g., UV detection) or by collection in a cold trap for off-line analysis (Gupta and Shim 2007). Compared to static methods, the advantages of dynamic methods include: “off the shelf” apparatus; simple sampling procedures; and large amounts of data generated in a short time (Gupta and Shim 2007; Aim and Fermeglia 2003). However, care must be taken to ensure that equilibrium has been established in the vessel and that the flow rate during the sampling period is sufficiently low to prevent disruptions to equilibrium (Aim and Fermeglia 2003). High flow rates can also entrain solutes, resulting in over-estimations of solubility and/or

clogging of the outlet line (Gupta and Shim 2007; Aim and Fermeglia 2003). If the vessel has no window, phase changes and density inversions may not be detected, resulting in erroneous solubilities by sampling of the wrong phase (Gupta and Shim 2007; Aim and Fermeglia 2003).

Two studies have previously measured the solubility of drilling fluid hydrocarbons in SC CO_2. In a study using the similar semi-flow apparatus as used in this study, Lopez Gomez (2004) found the solubility of diesel in SC CO_2 at 14.5 MPa and 40 °C to be 0.09 $g \cdot g^{-1}$. Jones (2010) also used the same apparatus to measure the solubility of Distillate 822 (D822) in SC CO_2 at multiple pressures (10.3 MPa, 14.5 MPa and 17.2 MPa) and temperatures (35 °C, 40 °C and 50 °C). The solubility ranged from 0.002 $g \cdot g^{-1}$ to 0.1 $g \cdot g^{-1}$ and increased with pressure. However, the n-hexadecane (nC16) system validation completed by Jones (2010) showed a consistent, unexplained bias.

Several cuttings extractions experiments have included measurements of "apparent solubility", or the solubility of the hydrocarbon in SC CO_2 as measured from cuttings instead of the hydrocarbon alone (Lopez Gomez 2004; Esmaeilzadeh et al. 2008; Jones 2010). The general idea is that the solubility of the hydrocarbon can be estimated by the slope of the early part of the cuttings extraction curve (cumulative mass of hydrocarbon collected versus cumulative mass of CO_2). However, for drilling fluid hydrocarbons, apparent solubility is lower than actual solubility. At 14.5 MPa and 40 °C, Lopez Gomez (2004) found the apparent solubility of diesel to be 0.05 $g \cdot g^{-1}$ (pure diesel = 0.09 $g \cdot g^{-1}$), and Jones (2010) found the apparent solubility of D822 to be 0.06 $g \cdot g^{-1}$ (pure D822 = 0.09 $g \cdot g^{-1}$). The reduction in solubility can be attributed to a loss of equilibrium if the extraction flow rate of CO_2 is high (for example, in Lopez Gomez 2004). However, in Jones (2010) the flow rate was kept low and the rate of hydrocarbon extracted was constant. Jones (2010) suspected the reason for the reduction in solubility was that the presence of the cuttings solids resulted in decreased contact between the hydrocarbon and the SC CO_2, or as a result of increased interactions between the solids and the hydrocarbon.

Esmaeilzadeh et al. (2008) measured the apparent solubility of an unnamed drilling fluid hydrocarbon at 20 MPa from 55 °C to 79.5 °C. The apparent solubility ranged from approximately 0.008 $g \cdot g^{-1}$ to 0.015 $g \cdot g^{-1}$, with apparent solubility increasing with increasing temperature (the published data was converted from $g \cdot m^{-3}$ assuming 1 atm and 20 °C at the sample collection point). The study did not provide pure hydrocarbon solubility data with which to compare.

With the overall challenges of making solubility measurements and no real way to estimate experimentally (i.e., apparent solubility), there is benefit in finding a correlation that will allow equilibrium concentrations of drilling fluid hydrocarbon to be determined. For this work, the Chrastil equation will be used (Chrastil 1982). The Chrastil equation is widely applied for modeling the solubility of many compounds including organometallics, biologicals, pharmaceuticals, aromatics, and organics (Škerget et al. 2011). There has been no documented previous use of the Chrastil equation for modeling drilling fluid hydrocarbon solubility, but there is evidence the Chrastil model is suitable for individual n-alkanes in the drilling fluid hydrocarbon range (Reverchon et al. 1993; Shi et al. 2015). The Chrastil equation is also commonly used for multi-component natural oils for example, fish oil (Lopes et al. 2012) and *Moringa oleifera* oil (Zhao and Zhang 2014).

It is commonly observed that the log-solubility is linearly related to the density (or log-density) of the supercritical fluid, which is the basis of the Chrastil equation (Chrastil 1982). The Chrastil equation is:

$$\ln y = C \ln \rho + \left(\frac{A}{T} + B\right) \qquad \text{Eq. (3-1)}$$

where y is the solubility of solute ($g \cdot g^{-1}$), ρ is the density of the supercritical solvent ($kg \cdot m^{-3}$), T is the temperature (K), and A (K), B (unitless), and C (unitless) are constants. A is related to the heats of vaporization and solvation of the solute, B is related to C and the molecular weights of the solvent and solute, and C is an association number, related to the equilibrium between the solute and C molecules of the solvent (Chrastil 1982).

Although the Chrastil equation has a theoretical basis and the constants have physical meaning, the equation is largely used as an empirical correlation of solubility data (Škerget et al. 2011). The Chrastil equation is valid when the log solubility-(log) density relationship is linear, up to solubilities of 200 $g \cdot L^{-1}$, where the density of the solution is not different from the density of the solvent (ρ) (Chrastil 1982). The equation is more accurate over small temperature ranges where the heat of vaporization may be assumed constant with temperature (Chrastil 1982). Density-based models, including the Chrastil equation, typically give good results in the 10 MPa – 30 MPa range where most supercritical processes operate, and most solubility data is collected (Kautz et al. 2008).

Towards determining and modeling solubility of D822 in SC CO_2 for later use in mass transfer calculations, the objectives of Chapter 3 are to:

1. Develop a semi-flow solubility measurement method and validate the method using nC16 solubility in SC CO_2.
2. Measure the solubility of D822 in SC CO_2 between 35 °C – 50 °C and 10.4 MPa – 24.2 MPa.
3. Fit the collected D822 solubility data to the Chrastil equation for future use to estimate the interface concentration in mass transfer coefficient calculations.

3.2 Materials and Methods

This section will describe the materials and methods used to measure the solubility of nC16 and D822 in SC CO_2 on a lab-scale, batch extraction system.

3.2.1 Reagents

Table 3.1 lists the chemical reagents used in the solubility experiments.

Table 3.1: Reagents used in the nC16 system validation and drilling fluid hydrocarbon/SC CO_2 solubility experiments

Chemical	Specification	Experimental Use	Supplier
Carbon dioxide	Liquid, Grade 3.0, bone dry	Supercritical solvent	Praxair (Edmonton, AB)
n-Hexadecane	99 % purity	Solute	Sigma-Aldrich (Oakville, ON)
Distillate 822	Commercially available	Solute	Diversity Technologies Corp. (Edmonton, AB)
Acetone	Certified ACS grade	Sample collection bath	Fisher Scientific (Ottawa, ON)
Dry ice	>99% purity	Sample collection bath	Praxair (Edmonton, AB)

D822 drilling fluid is a hydrocarbon mixture containing primarily n-alkanes with carbon numbers from nC11 to nC20 and a maximum of 12 wt% aromatics. The approximate composition of D822 is 1.6 wt% nC12, 4.1 wt% nC13, 7.2 wt% nC14 and 84.7 wt% nC15+, with <0.1 wt% BTEX (benzene, toluene, ethylbenzene, and xylene) (Advantage Mud Systems Ltd., n.d.).

Twenty litres of D822 were purchased and then stored in a sealed container at 4 °C to minimize volatilization and microbial degradation. Sub-samples of approximately 2 L were taken from the 20 L pail as needed and stored at 4 °C in between solubility experiments.

3.2.2 Apparatus

The solubilities of D822 and nC16 in SC CO_2 were measured using the apparatus described in Jones (2010), with some notable differences that were needed to improve the solubility measurements. These improvements were made during the nC16 validation stage, over a total of 37 trials prior to actual data collection experiments, and they are detailed in the following paragraphs.

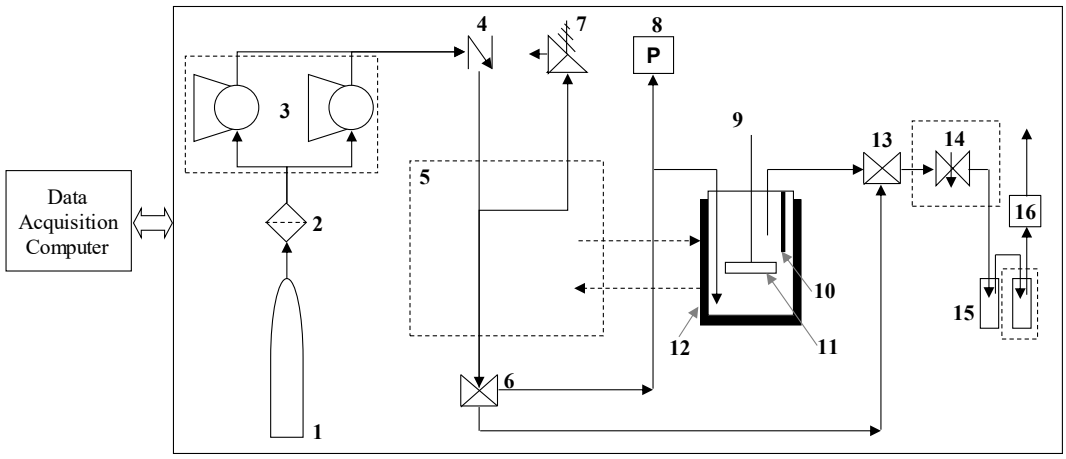

Legend:

1. Carbon dioxide feed cylinder
2. Filter
3. Syringe pumps, circulating water cooling system
4. Check valve
5. Hot water bath
6. 3-way valve
7. Pressure relief valve
8. Pressure transducer
9. Extraction vessel with custom sleeve
10. Thermistor probe
11. Ribbon mixer
12. Heating jacket
13. 3-way valve
14. Metering valve, hot water bath
15. Sample and carryover vials, acetone/dry ice bath
16. Carbon dioxide flowmeter

Figure 3.1: SFE system setup for solubility measurements, updated and adapted from Street (2008) and Jones (2010)

To prevent short circuiting of the CO_2 in the extraction vessel, the inlet line was extended to the vessel bottom. The extension of the line required a custom sleeve to prevent the inlet line from becoming tangled in the mixer.

To improve solute collection, a sample and a carry-over vial were used (as opposed to a sample vial only) with the carry-over vial in an acetone/dry ice bath (< -20 °C) to minimize volatilization and loss of solute in the vented CO_2. Also, a pre-weighed piece of Kimwipe (Fisher Scientific, Ottawa, ON) was used to wipe any excess solute off the end of the outlet line and was placed in the sample vial to be weighed.

To minimize freezing in the outlet line because of depressurization, the sample vial was kept at atmospheric temperature (approximately 20 °C) and the outlet line between the metering valve hot water bath and the sample vial was warmed with a piece of paper towel that was periodically soaked with water from the bath.

Due to the lower flow rate of CO_2 through the system for solubility measurements (to minimize disruptions to equilibrium) there is less force to move the solute through the outlet line to the sample vial. Therefore, the vessel outlet line was shortened. To improve control over the flow rate, the Swagelok metering valve was replaced with an Autoclave Engineers (Erie, PA) metering valve (Part No. 10V2082; pressure rating = 75.8 MPa).

3.2.3 Solubility Measurement Methodology

D822 solubility was measured at temperatures ranging from 35 °C to 50 °C and pressures ranging from 10.3 MPa to 24.2 MPa. The experimental apparatus and methodology were validated by measuring the solubility of nC16 at 35°C between 9.5 MPa and 12.3 MPa, and at 40 °C between 12.4 MPa and 15.5 MPa. The system set up and validation with nC16 was completed by both the author and E. Underwood. The D822 experiments were completed by E. Underwood.

A known mass of solute, typically ~65 to 100 g, was added to the extraction vessel (270 mL, empty bed). Pressurized and pre-heated CO_2 was introduced to the vessel. The contents of the extraction vessel were mixed slowly (50 rpm) for 60 min to allow the system to reach equilibrium. The mixer was then turned off and the metering valve was opened to allow the solute-laden SC CO_2 to flow out of the vessel. In order to maintain the pressure in the vessel, CO_2 is allowed to flow into the vessel (i.e., the pumps are operated in constant pressure mode). The vessel configuration was such that the outlet port was at the top of the vessel and therefore the least dense phase was sampled, typically the CO_2-rich phase. Following depressurization to atmospheric pressure at the metering valve, the solute was collected into a 40 mL glass collection vial containing glass wool, glass beads, and a Kimwipe. The vial was kept at room temperature (approximately 20 °C). A second 40 mL glass collection vial (the carry-over vial), submerged in an acetone-dry ice bath, was used to collect any residual hydrocarbon that carried over from the first vial. Each sample and carry-over vial pair was in place for 5 min (one measurement). Each solubility experiment consisted of 5 consecutive measurements. Then the flow was stopped, and the vessel was held at pressure for 1 hour (with 50 rpm) re-establish equilibrium before the start of the next experiment. Experiments

were repeated in this way at least three times. Therefore, a total of 15 measurements at each pressure and temperature combination were made unless individual measurements were excluded due to experimental errors. The vials were weighed before and after the experiment on an analytical balance (Model AX205, Mettler Toledo, Mississauga, Ontario, Canada). For each measurement, the solubility of nC16 (in mol fraction, $mol \cdot mol^{-1}$) or D822 (in mass fraction, $g \cdot g^{-1}$) was determined using the mass collected in the vials and the mass of CO_2 flowed through the system during the collection. The mass of CO_2 was measured in one of two ways: 1) using the digital flowmeter (Part No. 5067-0223, Agilent Technologies, Mississauga, ON; accuracy = ± (0.8 % of reading + 0.2 % of full scale)) for the nC16 experiments, or 2) using the syringe pump controller for the D822 experiments (500D, Teledyne ISCO, Lincoln, NE).

To prevent disruptions to equilibrium during sampling, CO_2 flow was kept low but high enough to minimize the loss of hydrocarbons that may have fallen out of solution in the metering valve by using the flow to push the hydrocarbons from the metering valve into the collection vials. Relative to nC16, D822 has a slightly higher viscosity and required a higher CO_2 flow rate to ensure the best collection. This higher flow rate exceeded the range for the digital flowmeter. Thus, the pump controller was used to measure CO_2 instead. The flow rate of CO_2 from the pump controller was converted to a mass flow rate using the density provided by the Fundamental Equation of State (Span and Wagner 1996). Typical flow rates were approximately 0.1 $g \cdot min^{-1}$ and 0.7 $g \cdot min^{-1}$ for the nC16 and D822 experiments, respectively. Relative to the mass in the vessel of approximately 209 g (using the lowest SC CO_2 density of the conditions tested, 0.698 $g \cdot mL^{-1}$), these flow rates are low enough it is assumed that equilibrium is maintained in the vessel during the sampling period. The 0.7 $g \cdot min^{-1}$ flow rate represents a worst case of an 8.3 % reduction in solubility over the 5 samples (25 minutes).

It should be noted that, in the range of temperatures studied in this work, there is evidence of a single-phase region for nC16 and CO_2 at approximately 17 MPa (de Haan 1991; D'Souza et al 1988; Kordikowski and Schneider 1993; Nieuwoudt and du Rand 2002). Because this study focused on the solubility in SC CO_2 (i.e., nC16 concentration in the CO_2-rich phase),

steps were taken to ensure measurements were not in this single-phase region. For each experiment, a bulk single-phase concentration was calculated based on the mass of solute added to the vessel and the mass of the SC CO_2 (vessel volume converted to mass using the Fundamental Equation of State (Span and Wagner 1996)). The experimental and theoretical results were then compared. If conditions were in the single-phase region, it would be expected that the experimental measurement would match the theoretical calculation. If this was the case, the experiment was conducted once more but with a significantly larger initial mass of solute. If the experimentally measured value did not change, it was concluded that the CO_2-rich phase was sampled and that the experiment yielded a valid measurement of solubility.

3.2.4 Chrastil Modeling Methodology

The solubility data for nC16 and D822 was fit to Eq. 4-1, based on minimization of the average absolute relative deviation (AARD), with AARD defined as:

$$AARD = \frac{1}{n}\sum_{i=1}^{n}\left|\frac{X_{exp}-X_{calc}}{X_{exp}}\right| \qquad \text{Eq. (4-2)}$$

where n is the number of measurements, X_{exp} is the experimentally measured solubility value, and X_{calc} is the solubility value calculated by the Chrastil model. The Chrastil fitting for this Chapter was completed by Dr. W. Stiver.

3.3 Results and Discussion

This section provides the results of the nC16 system validation and the D822 solubility study, including the Chrastil model results.

3.3.1 n-Hexadecane System Validation

The solubility results for nC16 are provided in Table 3.2.

Table 3.2: nC16 solubility at 35 °C from 9.5 MPa to 12.3 MPa and 40 °C from 11.6 MPa to 15.6 MPa

Measured Temperature (°C ± 0.3 °C)[a]	Measured Pressure (MPa ± 0.2 MPa)[b]	Solubility (mol·mol^{-1})[c]	n[d]
34.8	9.5	0.011 ± 0.001	5
34.3	9.5	0.013 ± 0.001	5
34.1	9.5	0.012 ± 0.001	5
33.8	11.2	0.014 ± 0.003	5
33.7	11.2	0.016 ± 0.009	5
33.7	11.2	0.017 ± 0.001	5
34.0	12.3	0.02 ± 0.02	3
33.9	12.3	0.019 ± 0.001	5
33.8	12.3	0.019 ± 0.001	5
39.7	11.6	0.0143 ± 0.0005	5
39.7	11.6	0.0146 ± 0.0007	5
39.7	11.6	0.015 ± 0.001	4
38.7	12.5	0.020 ± 0.004	5
38.7	12.5	0.019 ± 0.001	5
38.7	12.5	0.0183 ± 0.0007	5
39.6	14.3	0.018 ± 0.002	2
38.1	14.3	0.022 ± 0.002	5
38.1	14.3	0.017 ± 0.003	2
39.6	14.3	0.023 ± 0.003	5
38.1	14.3	0.021 ± 0.007	3
39.6	14.3	0.02 ± 0.01	5
40.0	14.3	0.025 ± 0.002	5
39.9	14.3	0.04 ± 0.02	5
39.9	14.3	0.02 ± 0.03	5
39.6	15.6	0.035 ± 0.005	4
39.6	15.6	0.039 ± 0.001	5
39.6	15.6	0.038 ± 0.003	5
39.7	15.6	0.037 ± 0.001	5
39.7	15.6	0.03 ± 0.02	5
39.6	15.6	0.039 ± 0.002	5

[a] mean temperature during sampling ± expanded uncertainty (95 % confidence)
[b] mean pressure during sampling ± expanded uncertainty (95 % confidence)
[c] mean solubility of measurements ± one standard deviation
[d] n = number of measurements

Experiments at 35 °C and 15.6 MPa were attempted. Under these conditions the system was unstable: significantly more nC16 was sampled, causing the flow rate of CO_2 to be erratic. There are two potential reasons for this occurrence. First, the density of the CO_2 at this condition is the highest of those tested (i.e., 822.5 kg·m^{-3} based on the Fundamental Equation

of State (Span and Wagner 1996)). Therefore, it is possible that the density of the CO_2-rich phase was greater than that of the nC16-rich phase, which would have been at the top of the vessel and sampled instead. Alternatively, as mentioned, there is evidence of a single-phase region at these conditions and it is possible that this region was measured. Due to operational difficulties regarding flow, additional tests to further understand the cause of the high amount of nC16 sampled were not undertaken.

During the sampling of one experimental run of nC16 at 40 °C and 15.6 MPa, a larger amount of nC16 was collected in the sample vials (data for this run is not included in Table 3.2). This data point was initially dismissed as an experimental error but, upon retrospect, there was no issue with the experimental conditions or measurements (in contrast to the flow instability caused by the large amount of nC16 sampled at 35 °C and 15.6 MPa). The data point was investigated as a possible measurement of the nC16-rich phase. Figure 3.2 shows the measured nC16 mol fraction in both the CO_2-rich and nC16-rich phases (mean solubility of set point in Table 3.2), in comparison with a literature study, both at 40 °C. The data point of interest is shown as a grey diamond in Figure 3.2.

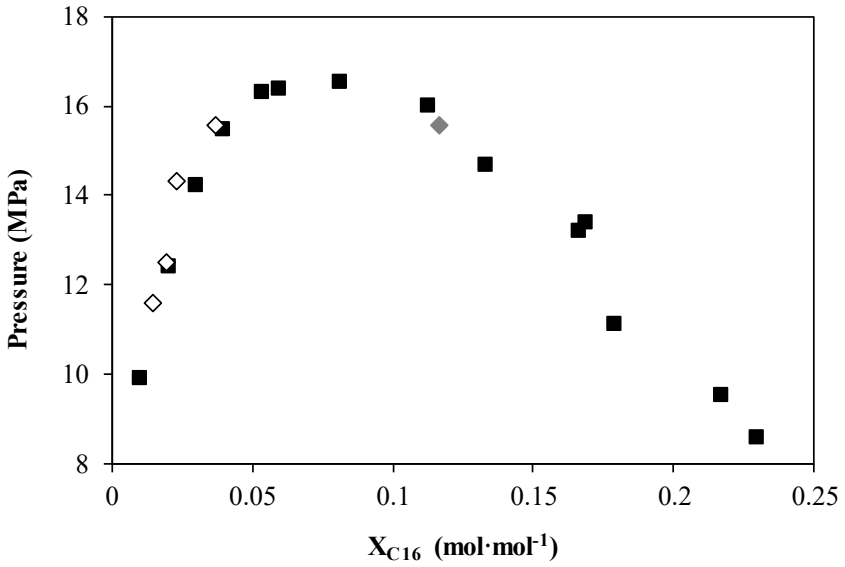

Figure 3.2: nC16 mol fraction in both CO_2-rich and nC16-rich phases as a function of pressure at 40 °C for: (◇) and (◆) current study; (■) Nieuwoudt and du Rand (2002).

The data point does not fit with the measured or literature data for the CO_2-rich phase, but it does appear to represent the nC16-rich phase. As the two phases approach the mixture critical point, a phase inversion may occur, allowing for the normally heavier nC16-rich phase to be sampled from the top of the vessel. At the process conditions, from the Fundamental Equation of State, pure CO_2 has a density of 0.789 g·mL^{-1} (Span and Wagner 1996), while liquid nC16 (at atmospheric conditions) has a density of 0.773 g·mL^{-1}. Depending on the resulting phase compositions, it is quite possible that the nC16-rich phase had a lower density. This measurement highlights the importance of being aware of the possibility of sampling other phases with a semi-flow apparatus.

Many studies have investigated the solubility and phase behavior of n-alkanes in SC CO_2 (binary and ternary systems). References to these studies can be found elsewhere (Gupta and Shim 2007; Škerget et al. 2011; Fonseca et al. 2011; Dohrn et al. 2010). Of interest for this study are the solubility data for nC16. Data sets were taken from the literature that included measurements of nC16 in the CO_2-rich phase, near the pressures and temperatures investigated in this study (data set temperatures ranging from 32 °C to 60 °C, and pressures ranging from 7.6 MPa to 20.0 MPa). Data provided exclusively in figures was excluded; therefore, the data of Holscher et al. (1989) and Venter et al. (2007) were not used. Three data sets stated the CO_2-rich phase nC16 concentration to be at or near zero (Charoensombut-Amon et al. 1986; King et al 1984; Lee and Sigmund 1979). Therefore, these data sets were also excluded.

To directly quantify the fit of the current nC16 data with that of others, the remaining literature data sets (Eustaquio-Rincón and Trejo 2001; de Haan 1991; D'Souza et al. 1988; Kordikowski and Schneider 1993; Nieuwoudt and du Rand 2002; Larson et al. 1989; Shi et al. 2105) were fit to the Chrastil equation resulting in A=-4197.64 K, B=-25.21, C=5.24, and an AARD of 30.7 %. This Chrastil model was used to calculate nC16 solubility values at the experimental conditions in this work. These calculated values were compared to the measured values in Table 3.2, resulting in an overall AARD of 10.1 %. This AARD indicates that the current data is well within the uncertainty present in the literature data.

The current and literature data sets were also individually fit to the Chrastil equation. The results are shown in Table 3.3. Note that parameter A was set to -5000 for datasets with only one temperature setting.

Table 3.3: Individual Chrastil equation fit of current and literature nC16 data

Reference	Chrastil Equation Constants			AARD (%)
	A (K)	B	C	
Eustaquio-Rincón and Trejo (2001)	-5000.00	-17.83	4.42	5.2
de Haan (1991)	-2923.12	-29.62	5.34	12.6
D'Souza et al. (1988)	-474.18	-15.48	1.98	18.0
Kordikowski and Schneider (1993)	-5000.00	-25.10	5.61	31.8
Nieuwoudt and du Rand (2002)	-4225.40	-34.76	6.78	18.3
Larson et al. (1989)	-5000.00	-39.58	7.78	15.0
Shi et al. (2015)	-4970.94	-34.45	7.02	6.5
ALL EXCEPT CURRENT STUDY	-4197.64	-25.21	5.24	30.7

Because of individualized fitting, the data set AARD's are lower than the overall AARD of 30.7 %. However, the differences in the Chrastil constants and AARD's between data sets speaks to the uncertainty in experimental solubility data, likely resulting from differences in measurement methods. Most measurements were made using view cell apparatus (Shi et al. 2015; Larson et al. 1989; Kordikowski and Schneider 1993; Nieuwoudt and du Rand 2002; D'Souza et al 1988) but there was also a packed stripping column (de Haan 1991) and a semi-flow apparatus like the system used in the current study (Eustachio-Rincón and Trejo 2001). Given the differences in measurement methods, it is highly unlikely that there is a common bias and it can be concluded that the current data is as accurate as the published data.

Figure 3.3 shows a comparison of the current nC16 solubility data (mean solubility of each set point in Table 3.2) to the literature data sets. The plot of ln solubility versus ln CO_2 density shows an approximately linear relationship for each data set as described by the Chrastil equation. Figure 3.3 also shows that the current data compares well qualitatively to the literature data.

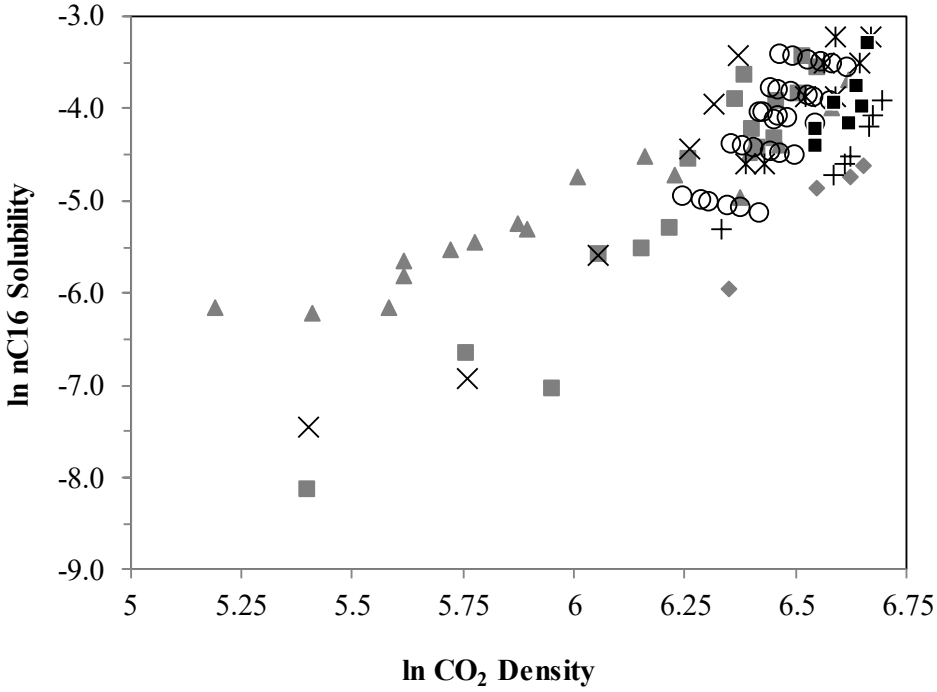

Figure 3.3: ln solubility of nC16 as a function of ln CO_2 density, comparing the current data to literature data: (■) current; (○) Shi et al. 2015; (◆) Eustaquio-Rincón and Trejo (2001); (✳) Nieuwoudt and du Rand (2002); (×) Kordikowski and Schneider (1993); (■) de Haan (1991); (+) Larson et al. (1989); and (▲) D'Souza et al. (1988).

Based on both the quantitative and qualitative comparisons with literature nC16 data, it is concluded that the apparatus and procedure developed in this study can produce solubility measurements consistent with literature values. The method is considered valid and can be used to measure the solubility of D822 and similar solutes in SC CO_2.

3.3.2 D822 Solubility

Table 3.4 provides the measured D822 solubility in SC CO_2. The solubility ranges from 0.002 $g \cdot g^{-1}$ at 10.4 MPa and 50 °C to a maximum value of 0.146 $g \cdot g^{-1}$ at 24.2 MPa for 40 °C. The D822 measurement at 35 °C and 24.2 MPa could not be obtained because of the same system instability observed for nC16 at 35 °C and 15.6 MPa.

Table 3.4: Solubility of D822 in SC CO_2 at 35 °C, 40 °C, and 50 °C from 10.4 MPa to 24.2 MPa

Set point Temp. (°C)	Set point Pressure (MPa)	Measured Temp. (°C ± 0.4 °C)[a]	Measured Pressure (MPa ± 0.1 MPa)[b]	Solubility ($g \cdot g^{-1}$)[c]	n[d]
35.0	10.4	35.5	10.4	0.04 ± 0.01	5
		35.8	10.4	0.046 ± 0.006	5
		35.8	10.4	0.04 ± 0.02	5
35.0	14.6	35.2	14.6	0.07 ± 0.02	5
		35.3	14.6	0.070 ± 0.007	4
		35.4	14.6	0.07 ± 0.01	4
35.0	17.3	34.0	17.3	0.08 ± 0.01	4
		34.7	17.3	0.097 ± 0.007	5
		34.9	17.3	0.097 ± 0.002	5
40.0	10.4	40.1	10.4	0.022 ± 0.006	5
		39.7	10.4	0.03 ± 0.02	5
		39.7	10.4	0.03 ± 0.02	4
40.0	14.6	40.2	14.6	0.069 ± 0.002	5
		40.3	14.6	0.066 ± 0.003	5
		40.3	14.6	0.068 ± 0.004	5
40.0	17.3	39.8	17.3	0.091 ± 0.009	5
		40.0	17.3	0.08 ± 0.01	5
		40.2	17.3	0.085 ± 0.004	5
40.0	24.2	39.3	24.2	0.146 ± 0.005	5
		39.4	24.2	0.14 ± 0.01	5
		39.4	24.2	0.140 ± 0.004	5
50.0	10.4	49.9	10.4	0.002 ± 0.002	5
		49.9	10.4	0.004 ± 0.001	5
		49.9	10.4	0.006 ± 0.001	5
50.0	14.6	49.5	14.6	0.056 ± 0.003	5
		49.5	14.6	0.054 ± 0.001	5
		49.8	14.6	0.052 ± 0.002	5
50.0	17.3	48.8	17.3	0.082 ± 0.005	5
		49.2	17.3	0.079 ± 0.004	5
		49.2	17.3	0.079 ± 0.002	5
50.0	24.2	49.8	24.2	0.144 ± 0.009	5
		50.4	24.2	0.14 ± 0.01	5
		50.6	24.2	0.143 ± 0.006	5

[a] mean temp. during sampling ± expanded uncertainty (95 % confidence)
[b] mean pressure during sampling ± expanded uncertainty (95 % confidence)
[c] mean solubility of measurements ± one st. dev.
[d] n = number of measurements

Figure 3.4 shows the D822 solubility as a function of pressure at the three temperatures. The symbols represent the mean solubility and the error bars represent one standard deviation for each set point in Table 3.4.

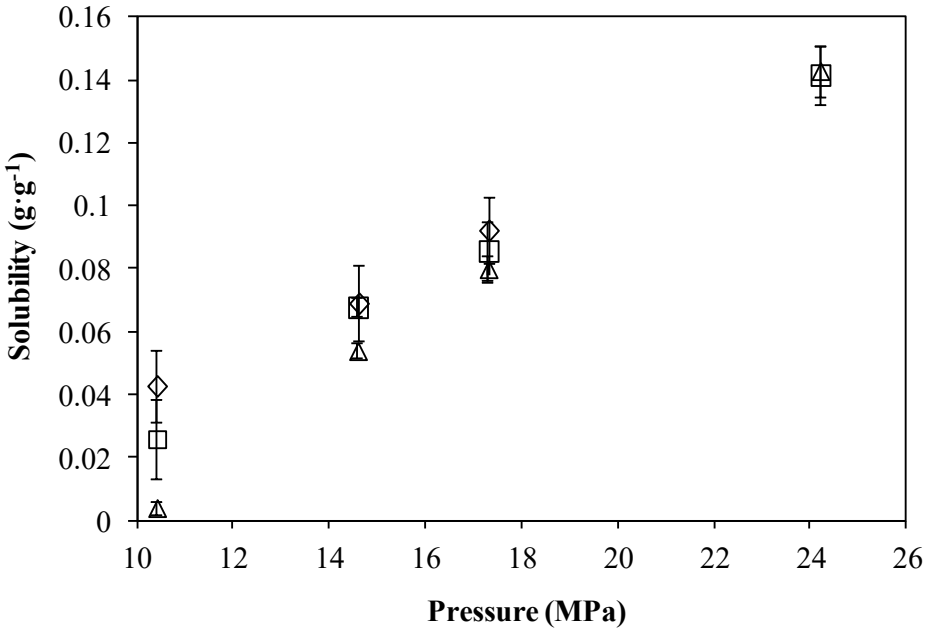

Figure 3.4: Solubility of D822 in SC CO_2 as a function of pressure (error bars indicate one standard deviation) at (◇) 35 °C, (□) 40 °C, and (△) 50 °C

For all temperatures studied, the solubility increases with increases in pressure. At constant temperature, increased pressure increases solvent density and therefore, increases solubility (Chrastil 1982; Kumar and Johnston 1988).

Unlike the nC16 data, a single-phase region for D822 and SC CO_2 was not directly observed. Nearing the single-phase region may be the reason that flow instability was observed at 24.2 MPa and 35 °C. Pressure limitations of the bench-scale, batch system prevented study beyond 24.2 MPa. Considering that previous drill cuttings-SC CO_2 extraction studies have shown good extraction of hydrocarbon from cuttings and cuttings slurries at 12 MPa to 24 MPa (Eppig et al. 1984; Odusanya 2003; Lopez Gomez 2004; Goodarznia and Esmaeilzadeh, 2006; Tunnicliffe and Joy 2007; Esmaeilzadeh et al. 2008; Street 2008, Jones, 2010; Saintpere and Morillon-Jeanmaire 2000), it seems unnecessary to pursue higher pressure.

The overlap of uncertainty in the data at the studied temperatures does not allow for any concrete conclusions regarding the effect of temperature on the solubility. However, solubility appears to be influenced by temperature, where higher temperatures at a given pressure result in lower solubilities. This temperature effect has been previously observed in solubility measurements of individual n-alkanes (Shi et al. 2015; de Haan 1991). Increasing temperature reduces the solvent density, but also increases the solute vapour pressure (Chimowitz 2005). In the range of conditions studied, the solvent density reduction appears to be the dominant of the two competing effects. The convergence of solubility data at higher pressure may indicate the presence of a crossover pressure near 24 MPa, after which the temperature would have a positive effect on the solubility (vapor pressure effect dominates).

Figure 3.5 shows the measured mean solubilities of D822 in SC CO_2 at 40°C compared to literature values for nC16 and n-octadecane (nC18). Typically, the solubility of n-alkanes decreases with increasing carbon number and increases with increasing pressure at a constant temperature (Nieuwoudt and du Rand 2002; Eustaquio-Rincón and Trejo 2001; Chandler et al. 1996; Schmitt and Reid 1988). As expected, the solubility of D822 is intermediate to the solubility of nC16 and nC18, which are mid-components in the D822 mixture.

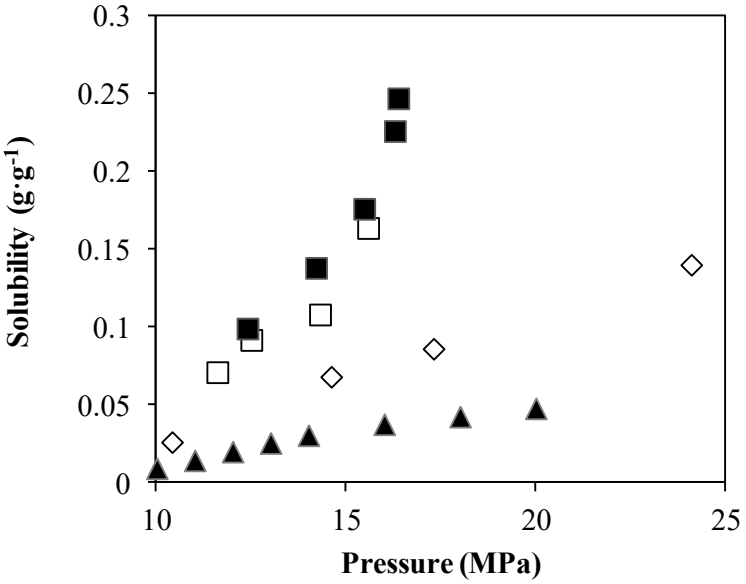

Figure 3.5: Comparison between D822 solubility in SC CO_2 at 40 °C with n-alkanes: (◇) D822 (current study; (■) n-hexadecane (Nieuwoudt and du Rand 2002); (□) n-hexadecane (current study); and (▲) n-octadecane (Eustaquio-Rincón and Trejo 2001)

The data in Table 3.4 was fit to the Chrastil equation, and the constants were found to be A=-3513.53 K, B=-28.61, and C=5.58 (AARD = 9.4 %). The low AARD value suggests that this model is suitable for the calculation of solubilities for D822 in the range of temperatures and pressures studied. Figure 3.6 shows the Chrastil model and the mean solubility for each set point in Table 3.4.

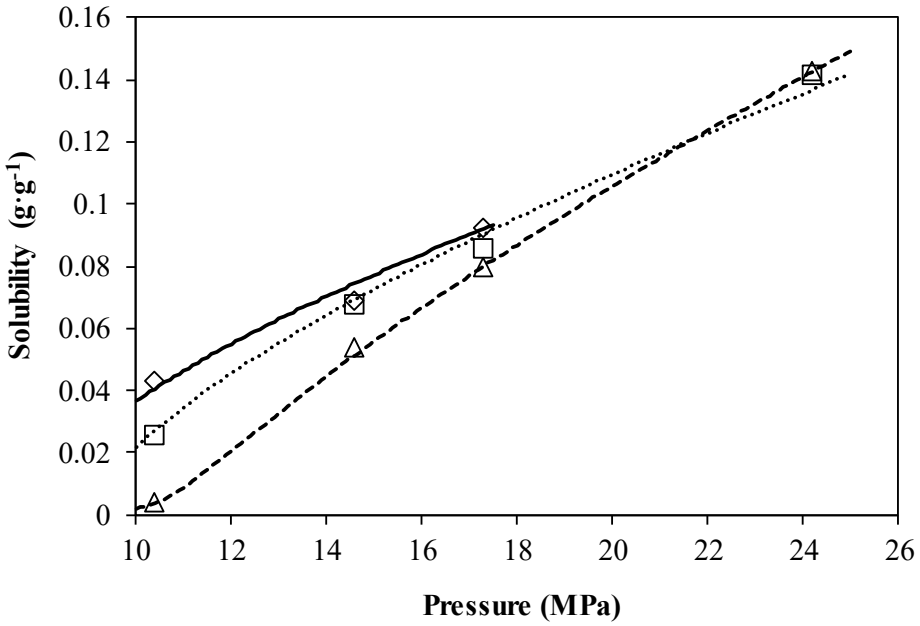

Figure 3.6: Chrastil model of solubility of D822 in SC CO_2 at (—) 35 °C, (·····) 40 °C, (- - -) 50 °C with experimental data at (◇) 35 °C, (□) 40 °C, and (△) 50 °C

No other studies could be found that use the Chrastil equation for modeling n-alkane mixtures like D822, or similar drilling fluid hydrocarbon mixtures. However, in the apparent solubility study by Esmaeilzadeh et al. (2008), three equations of state models were investigated. Esmaeilzadeh et al. (2008) found that the PC-SAFT equation performed the best, with an AARD of 9.73 %. The authors did not use binary mixing parameters (i.e., did not tune the model to experimental data), but did test two hydrocarbon number groupings as pseudo-components to improve the fit of the model. Given that the Chrastil model has equivalent performance and is simple to apply, the Chrastil model is recommended and will be used for the mass transfer calculations in Chapter 4.

3.4 Conclusion and Recommendations

In this Chapter, a semi-flow method for the measurement of drilling fluid hydrocarbon solubility in SC CO_2 has been developed. The method was validated by measuring solubility of nC16 at 35 °C and 40 °C from 9.5 MPa to 15.6 MPa. The nC16 solubility ranges from 0.011 mol·mol^{-1} to 0.039 mol·mol^{-1}. This experimental data was compared to solubility values calculated from a Chrastil model developed using nC16 literature data. The AARD between

the model calculated values and the experimental data was 10.1 %. In comparison, the AARD between the literature data and the calculated values from the model was 30.7 %, indicating that the solubility measurement method used in this work gives results within the uncertainty of the data present in the literature. It is concluded that the method used here is satisfactory for conducting solubility measurements.

The solubility of D822 in SC CO_2 was measured at 35 °C, 40 °C and 50 °C over 10.4 MPa to 24.2 MPa. The solubility of D822 increased with increasing pressure, to a maximum of 0.146 $g \cdot g^{-1}$ at 24.2 MPa at 40°C. The role of temperature was less clear, but appears to have a negative effect on solubility at pressures less than 24.2 MPa. The D822 solubility data were successfully modeled using the Chrastil equation, resulting in coefficients of A=-3513.53 K, B=-28.61, and C=5.58 with an AARD of 9.4 %. The Chrastil model developed in this Chapter is recommended for use in calculating solubilities of D822-like drilling fluid hydrocarbons in SC CO_2. The Chrastil model will be used to estimate the interfacial hydrocarbon concentration when calculating mass transfer coefficients of the pilot-scale treatment system developed in this thesis.

Chapter 4: Continuous SFE Process Performance in the Removal of Hydrocarbons from Drill Cuttings

4.1 Introduction

In Chapter 2, the pilot-scale, continuous SFE system was successfully constructed and operated in a counter-current flow scheme. Chapter 2 also confirms, qualitatively, that the system extracted oil from drill cuttings slurry. This Chapter will investigate the performance of the system in removing oil from drill cuttings slurries by calculating overall volumetric mass transfer coefficients and extraction efficiency for the baffle tray column.

Recall from Chapter 2 that the column has an internal baffle tray structure that can be visualized as Figure 4.1.

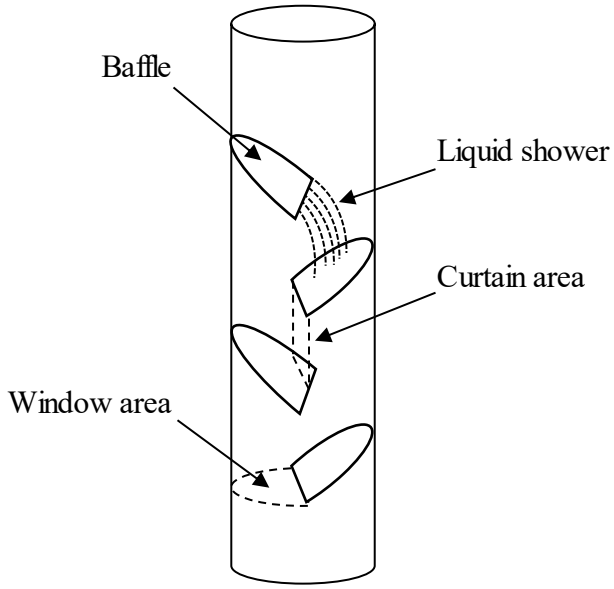

Figure 4.1: Representation of a section of the counter-current SFE column with inclined baffles adapted from Fair (1993)

In this type of baffle tray column, mass transfer occurs when the least dense phase flows upward through the window and curtain openings, contacting the denser phase, which cascades down from one baffle to the next. Most of the mass transfer occurs in the curtain

area which is typically not continuous of either phase (Fair 1993). Improved mass transfer occurs if the denser phase is broken up by the less dense phase, and broken up on contact of the column walls (Fair 1993). Normal operation results in a pressure drop across the column as the less dense phase imparts its momentum to the denser phase (Fair 1993). Generally, the pressure drop in a baffle tray column is lower than a conventional tray column and as good as a packed column with high-efficiency packing (Fair 1993). However, increased pressure drop, fluid buildup, and flooding may occur if the placement of the baffle trays causes a constriction in the window or curtain areas (Fair 1993).

Baffle tray columns have shown excellent service in industry processing when sedimentation-type fouling is a risk, including as refinery vacuum towers, ethylene quench towers, and saturator towers (Fair 1993; Kolmetz et al. 2004). Sedimentation fouling may occur in low velocity areas of contacting equipment and can include build-up of solids such as salts, metal oxides, catalyst fines, fermentation products, or coke fines (Kolmetz et al. 2004). However, the sacrifice for fouling reduction in baffle columns is a decrease in mass transfer efficiency compared with conventional packed or tray columns (Fair 1993; Kolmetz et al. 2004). For example, as a rule of thumb, a simple side-to-side baffle column (as Figure 4.1, but non-inclined baffles) has about half the mass transfer efficiency as a cross-flow sieve tray (Fair 1993).

Despite their comparatively simple geometry, low fouling potential, and pressure drop advantage, there is very little reported research on the design and mass transfer performance of baffle columns, and none for those in supercritical service. Fair (1993) provides correlations for capacity and mass transfer efficiency for baffle columns in liquid-gas service. The mass transfer correlation is based on heat transfer relationships. Fair (1993) cautions that, while the approach appears to provide a reasonable estimate of efficiency, the base data sets are small. Also, the approach has not been tested commercially according to Fair (1993) and a current literature search. Nevertheless, in the absence of any other method, the correlation provided by Fair (1993) can be used to calculate mass transfer coefficients and then to compare them to the experimentally obtained ones for the column described in Chapter 2.

The closest direct comparison to the current baffle tray column of Chapter 2 is the precursor design, which is a lab-scale, baffle tray column for the removal of polyaromatic hydrocarbons from contaminated soil slurries using SC CO_2 (Fortin 2003; Forsyth 2006). In these studies, the extraction column was 50 cm long with an internal volume of approximately 700 mL. In Fortin (2003), CO_2 flows ranged from 0.082 to 1.23 $g \cdot s^{-1}$ and the slurry flows were approximately 690 $mL \cdot min^{-1}$ (containing naphthalene contaminated solids at 0.0026 to 0.072 $g \cdot g^{-1}$). Overall volumetric mass transfer coefficients as high as 4.6×10^{-4} s^{-1} were determined (Fortin 2003). In Forsyth (2006), CO_2 flows ranged from 0.27 to 0.73 $g \cdot s^{-1}$ and slurry flows ranged from 210 to 820 $mL \cdot min^{-1}$ (containing naphthalene or phenanthrene contaminated solids at 0.014 $g \cdot g^{-1}$). Improvements to the column design from Fortin (2003), particularly in slurry level control, increased the overall volumetric mass transfer coefficient for naphthalene extraction to 5.1×10^{-3} s^{-1} (Forsyth 2006). The overall volumetric mass transfer coefficient for phenanthrene was determined to be as high as 4.9×10^{-4} s^{-1}.

Calculating overall volumetric mass transfer coefficients and extraction efficiencies requires collecting and comparing samples before and after the extraction. The analysis of drilling oil content in the slurries is performed using the *Reference Method Canada-wide Standard for Petroleum Hydrocarbons in Soil – Tier 1 Method* (CCME 2008). This method determines the F2 to F4 fractions (equivalent boiling points for normal straight chain hydrocarbons nC10 to nC50). As per CCME (2008), Soxhlet extraction with acetone/hexane is the preferred method for determining the oil content of soils; however, the use of the method for liquids or slurries has not been validated. Water present in the sample has been found to reduce the effectiveness of Soxhlet extraction (Hawari et al. 1995). Also, Soxhlet does not quantify the amount of water present in the sample. Thus, direct comparison of SFE efficiency of slurries containing different amounts of water is impossible without prior drying of the sample, which is impractical for high water content slurries. CCME (2008) allows for alternative extraction methods (such as Dean-Stark extraction, microwave, and SFE), if they are shown to meet or exceed the extraction efficiency of the standard Soxhlet method. Dean-Stark on cuttings and slurries has been proven to be as effective as Soxhlet in previous SFE/drill cuttings work (Jones 2010). However, the apparatus and consumables used in the Dean-

Stark method are expensive and the extraction itself takes 6 hours. Considering the increased number of samples from the pilot-scale system due to the continuous nature of the extraction, an alternative method is desired.

Liquid-solid solvent extractions (or, "cold shake" extractions) have previously been used to determine total petroleum hydrocarbon contents of cuttings and soils. On diesel contaminated cuttings, Odusanya (2003) used methylene chloride and a combination of ultrasonic/wrist-action shaking. The method was based on the proven work of Zytner et al. (2001) for analysis of diesel in contaminated soil, with additional guidance from "US EPA Method 3550B: Ultrasonic Extraction" (the current version is "Method 3550C: Ultrasonic Extraction" (US EPA 2007)). Schwab et al. (1999) demonstrated that a platform shaker using acetone and/or dichloromethane is equivalent to Soxhlet when extracting polyaromatic hydrocarbons from soils. In general, mechanical shaking-type extractions consume less solvent, require simpler equipment, and require less labour (Schwab et al. 1999).

4.2 Objectives

In order to quantify the performance of the current baffle tray column, the objectives of Chapter 4 are to:

1. Develop and validate a liquid cold shake method for hydrocarbon analysis of slurry samples before and after extraction in the column described in Chapter 2.
2. Using the slurry hydrocarbon analysis results, calculate an extraction efficiency for each extraction run.
3. Using the slurry hydrocarbon analysis results, calculate an overall volumetric mass transfer coefficient for each extraction run.
4. Investigate for potential trends in the results from Objectives 2 and 3 to find possible important extraction parameters and compare to any available literature values.

4.3 Materials and Methods

This section will describe the materials and methods used to measure the performance of the column in the removal of oil from cuttings-water slurries. Slurries were prepared and introduced into the column as described in Chapter 2. Oil content of the slurry before and

after extraction was determined by liquid-slurry extraction and gas chromatography (GC). Performance is quantified by calculating the extraction efficiency and the overall volumetric mass transfer coefficient.

4.3.1 Reagents

Table 4.1 provides the details of each of the reagents used in the extraction experiments, solvent extraction, and GC analysis.

Table 4.1: Reagent specifications, uses, and suppliers

Chemical	Specification	Experimental Use	Supplier
Carbon dioxide	Refrigerated liquid, beverage grade	Supercritical solvent	Praxair, Inc. (Edmonton, AB)
Diesel	Commercially available	Solute, test cuttings; GC standard	Petro Canada (Edmonton, AB)
Barite, BAROID 41	Commercially available	Solids, test cuttings	Rice Engineering & Operating Ltd. (Edmonton, AB)
ACROS Bentonite "Sample A"	Montmorillonite K-10	Solids, test cuttings	Fisher Scientific (Ottawa, ON)
Bentonite, BARIOD Aquagel "Sample B"	Commercially available	Solids, test cuttings	Rice Engineering & Operating Ltd. (Edmonton, AB)
Sparkleen Detergent	"1" for hand washing	Test cuttings	Fisher Scientific (Ottawa, ON)
Toluene	HPLC grade	Cold shake extraction	Fisher Scientific (Ottawa, ON)
Sodium sulphate	Anhydrous, 10/60 mesh	GC sample drying	Fisher Scientific (Ottawa, ON)
Hydrogen	Grade 5.0, UHP	GC gas	Praxair, Inc. (Edmonton, AB)
Nitrogen	Grade 5.0, UHP	GC gas	Praxair, Inc. (Edmonton, AB)
Air	Extra dry	GC gas	Praxair, Inc. (Edmonton, AB)
n-Decane	>99 % purity	GC standard	Sigma-Aldrich (Oakville, ON)

Table 4.1: Reagent specifications, uses, and suppliers, continued

Chemical	Specification	Experimental Use	Supplier
n-Hexadecane	99 % purity	GC standard	Sigma-Aldrich (Oakville, ON)
n-Tetratriacontane	98 % purity	GC standard	Sigma-Aldrich (Oakville, ON)
n-Pentacontane	>97 % purity	GC standard	Sigma-Aldrich (Oakville, ON)
D822	Commercially available	GC standard	Diversity Technologies Corp. (Edmonton, AB)
Motor oil	10W-30	GC standard	Canadian Tire (Edmonton, AB)

The drill cuttings used in this investigation were provided by Ramdar Resource Management Ltd. (Calgary, AB). The cuttings were sourced from a single drilling rig in Alberta (Nabors 53 rig, drilling in Red Rock, AB in July 2015). The cuttings were stored at 4°C until use in the experiments then the cuttings were well mixed and sub-sampled. The cuttings contained D822 base oil. The cuttings were non-cohesive and were of a coarse texture, as shown in Figure 4.2.

Figure 4.2: Drill cuttings

4.3.2 Slurry Preparation Method

The slurries used in the extraction experiments were of two sources: (i) simulated and (ii) drill cuttings from a drilling rig. The following procedure was used to create the simulated slurry:

1. Depending on the required concentration of solids in the slurry, a mass of bentonite and barite was weighed into a 20 L pail with a lid to minimize dust. The ratio of bentonite to barite was approximately 1:1 by weight. Bentonite sample A (ACROS Organics bentonite clay) was used first (already available in the lab, but only 1 kg), then later replaced by sample B (BAROID Aquagel).
2. The diesel was weighed and added to the pail containing the bentonite/barite mixture. Based on the oil content of typical cuttings, diesel was added to reach approximately 20 wt% (dry) oil on solids.
3. The diesel was mixed into the solids by hand with a large spoon for approximately 5 min, then water was added and mixed by the same manner until the resulting slurry was smooth (approximately another 5 min) to fill the pail approximately half full.
4. The solids/diesel mixture was poured into the slurry feed tank, which was then filled to the 55 gallon mark (208 L) with tap water.
5. The slurry was stirred continuously in the tank, initially manually (with a hockey stick) then later with a constant speed mixer (LEESON, ½ hp, 1725 rpm, McMaster-Carr, Aurora, OH).
6. The slurry was circulated through the column by-pass loop to further mix and to allow the slurry to be passed through a 40-mesh sieve (425 μm) positioned at the exit of the by-pass loop into the tank. The sieve size was selected based on a recommendation from the M-I SWACO team (during the HAZOP study of November 2010) to use a sieve that would remove particles larger than half the ID of the smallest flow line containing solids, i.e., the slurry manifold, ID = 0.055 in (1397 μm). 40-mesh was chosen because it was readily available from the Geotechnical Engineering Group in the Department of Civil & Environmental Engineering at the University of Alberta and was of a conservative size.

Subsequent simulated slurries were made directly in the slurry feed tank by amending the existing slurry with solids and/or diesel (i.e., no mixing in the 20 L pail), depending on the characteristics of slurry required. Most slurries tested on the system were of the simulated type.

Initial preparation of the slurry from drill cuttings involved blending the cuttings with water in a standard kitchen blender (Oster, 8 speed, Canadian Tire, Edmonton, AB), then passing the resulting slurry through the 40-mesh sieve into a 20 L pail. A sample of the slurry after blending is shown in Figure 4.3.

Figure 4.3: Drill cuttings slurry, after blending but prior to dilution

This slurry was further diluted with water to 208 L in the slurry feed tank to reach the desired solids concentration. However, even with blending followed by mixing in the feed tank, the cuttings did not remain in a stable suspension. The slurry settled in the slurry tank and pump supply line, creating a complete blockage (Figure 4.4).

Figure 4.4: Slurry blockage of the pump supply line

To better suspend the cuttings, Sparkleen 1 detergent was used at a rate of ~2 tsp per 500 mL of slurry and was added during blending. Sparkleen 1 contains common chemicals used during drilling: sodium carbonate is a clay de-flocculant (Bourgoyne Jr. et al. 1986); and sodium dodecylbenzenesulphonate is an anionic surfactant used as an emulsifier (Huntsman Corp. 2015). The resulting slurry behaved better in the system, but the more dense particles still settled, resulting in a flow restriction to the slurry pump. To remedy the situation, the portion of the slurry that remained in suspension was pumped to another tank to facilitate the removal of the settled solids from the feed tank and supply lines. Once the settled solids were removed, the slurry was pumped back to the feed tank for use. Because of the current design of the feed tank, mixer, and pump supply line, the solids content of the slurry was limited.

4.3.3 Continuous SFE of Cuttings Slurries

The extraction procedure used for slurry is provided in general in Chapter 2 (i.e., system start-up, shut down, etc.) The more detailed procedure is as follows:

1. The slurry was prepared as per Section 4.3.2. The mixer and heater in the slurry feed tank were turned on. The slurry pump was set to by-pass at a high motor speed (>50

%), to circulate the slurry to and from the tank. This circulation helped mix the slurry, warmed the lines and slurry pump head and primed the slurry lines.

2. Two samples of the slurry feed were taken (the initial, or untreated, slurry samples). One was taken from the tank and one was taken from the exit of the column by-pass.
3. Meanwhile, the clean water tank was filled with hot tap water (~ 50 °C), the cauldron for the CO_2 supply was cooled with dry ice to -20 °C, and the chiller for the CO_2 pump was turned on to -25 °C.
4. After approximately 2 hours, when chilling and heating were complete (slurry typically reached ~50 °C), the slurry pump supply was switched from slurry to water to clean the lines and pump.
5. Immediately once clear water was observed at the slurry feed tank, the motor speed was reduced and the flow was directed to the extraction column. The clean water represented no more than 1 L of water into the feed (less than 0.5 % error on the slurry feed solids content).
6. The system was brought to pressure with countercurrent water/CO_2 as per the procedure in Chapter 2. The water returning from the column was directed to the receiving tank.
7. Once the system had reached the set point pressure and supercritical temperature (i.e., >31 °C) at both top and bottom sensors, the slurry extraction portion of the run began.
8. The slurry heater was turned off before the slurry feed was directed to the column, as the heater could only operate with the element totally submerged.
9. The feed was switched from water to slurry by first opening the valve on the slurry feed tank to allow slurry to begin to flow to the pump. After ~30 seconds, the water tank valve was slowly closed. If the slurry lines were not properly primed as per Step 1, flow to the column would be lost, resulting in the total loss of water level in the column and total flow of CO_2 out the bottom.
10. The receiving tank was observed to ensure slurry returns/transition from water. Then, after another approximately 3 minutes, a slurry sample was taken from the return line. No samples were taken from the receiving tank due to dilution with water from start-up and cleaning.

The aim of each run was to obtain at least three extracted samples. Initially, samples were taken closer together in time due to the risk and probability of process upsets when switching to slurry. As the extraction continued, the timing between samples was increased from 3 minutes, to 5 minutes, to 10 minutes, approximately (as taking samples was a secondary task to operating the system).

4.3.4 Petroleum Hydrocarbon Analysis

In terms of hydrocarbon recovery, time, labour, and equipment availability, the following liquid-slurry solvent extraction method was determined to be the most suitable for determining the hydrocarbon content of the high water content slurries:

1. Approximately 20 mL toluene was measured into a volumetric flask, and the volume was recorded.
2. The toluene was added to 40 mL Teflon vials and weighed (scale: Mettler Toledo AX205, ±0.03 mg, Fisher Scientific, Ottawa, ON).
3. The slurry samples from the SFE system were shaken vigorously by hand to re-suspend the solid particles.
4. The shaken sample was quickly poured into the prepared 40 mL Teflon vial, to the level of the vial shoulder, weighed, and capped tightly.
5. The vials were placed on a wrist-action shaker (Burrell Scientific, Model 75, Pittsburg, PA). The samples were shaken at maximum deflection for 1 h.
6. The vials were moved to a centrifuge adapter, the adapters were balanced, and the samples were centrifuged at 2000 *g* for 10 minutes (Thermo Scientific Lynx Sorvall 4000, Fisher Scientific, Ottawa, ON). Centrifugation settled the sample solids and broke any solvent-water emulsions that were formed during shaking.
7. Most of the toluene layer was removed by glass syringe and dried through ~9 g of sodium sulphate in a glass funnel.
8. The toluene was filtered through a 0.45 µm Teflon syringe filter and a sub-sample was transferred to a 2 mL GC vial.

To validate the liquid-slurry solvent extraction method, spiked samples were analysed. These spiked samples were prepared by adding D822, in varying masses, to known masses of bentonite. The contaminated bentonite was then mixed into varying volumes of water. Subsamples were taken and placed in 40 mL Teflon vials with ~20 mL of toluene. First, as in Odusanya (2003), the samples were placed in an ultrasonic bath (FS26, Fisher Scientific, Ottawa, ON) for 30 minutes followed by wrist-action shaking for 1 hour at maximum deflection. Inspired by Schwab et al. (1999), only wrist-action shaking was also tested.

GC analysis was completed on a Varian CP-3800 (Agilent Technologies, Santa Clara, CA) equipped with a CP-8410 autoinjector and a CP-1177 split/splitless injector system. The GC was equipped with a flame ionization detector (FID). The FID voltage output was converted to area counts by the GC software *Star Chromatography Workstation (ver 5.5)*. The GC was equipped with a Restek 30m, poly(dimethylsiloxane), 0.32mm ID, low bleed column (minimum bleed temperature: 330°C; maximum operating temperature: 350°C) (Fisher Scientific, Edmonton, AB). The GC operating parameters were previously determined by Jones (2010) and are given in Table 4.2.

Table 4.2: GC operational parameters specifications

Parameter	Specification
Injection temperature	325 °C
Oven temperature	40 °C for 2 min, then ramp to 320 °C (20 °C·min^{-1}), then hold at 320 °C for 8 min
FID temperature	340 °C
Split/splitless	Split on (ratio 10), off at 0.01 s, on (ratio 50) at 0.75 s, on (ratio 10) at 2 min
Hydrogen	18 mL·min^{-1} carrier gas flow, 11 mL·min^{-1} detector flow
Nitrogen	12 mL·min^{-1} make-up flow
Air	487 mL·min^{-1} detector flow

CCME (2008) requires a minimum three-point calibration curve using standards containing approximately equal masses of n-decane (nC10), n-hexadecane (nC16), and n-tetratriacontane (nC34) in toluene. The detector response of each of the n-alkanes must be

within 10 % of the average response (as measured by the response factor, or the ratio of n-alkane area count to the known concentration) and demonstrate linearity within 10 %. An n-pentacontane (nC50) solution below 15 $mg \cdot L^{-1}$ must also be injected and its' response factor must be within 30 % of the average response factor of the other n-alkanes. The method also requires that the detector response show linearity within 15 % for a petroleum mixture (such as D822, as used in this case).

For this work, an approximate 500 $mg \cdot L^{-1}$ standard containing nC10, nC16, and nC34 was created and serially diluted to 100 $mg \cdot L^{-1}$ and 5 $mg \cdot L^{-1}$. The nC50 standard was 6.8 $mg \cdot L^{-1}$. Three standards of D822 at approximately 5000 $mg \cdot L^{-1}$, 15 000 $mg \cdot L^{-1}$, and 50 000 $mg \cdot L^{-1}$ were also prepared. The standards were placed in the ultrasonic bath to aid in dissolution of the solutes, especially nC34 and nC50 which are solids at room temperature. They were sonicated until no visible solids were present (approximately 20 min). They were stored at 4 °C to minimize volatilization until they were analysed on the GC in duplicate.

The CCME (2008) method requires that the lowest and mid-point calibration standard of nC10, nC16 and nC34 be run daily to confirm the stability of the calibration curve (area counts must be within 15 % and 20 % for the mid-point and low concentration standards, respectively). As the GC was not run daily, these standards were instead added to the end of each sample run. Other quality control items used in this procedure and as recommended by CCME (2008) include method blanks and duplicate sample analysis. Typically, for each set of samples collected during a SFE run, at least one sample, randomly selected, was run in duplicate. Later, this was increased to triplicate to get a better understanding of the variance. Glassware blanks were run every second analysis.

The GC output is an overall area count of the FID response curve. This area count is converted to a concentration of hydrocarbon in the toluene solvent using the previously determined GC calibration curve, adjusted by the area count of the method blanks. The primary assumption of the liquid-slurry solvent extraction and subsequent GC analysis is that all the hydrocarbon has been extracted from the slurry to the toluene. As the volume of toluene

added to the slurry for the liquid-slurry extraction is known, the mass of hydrocarbon that was present in the slurry sample can be determined.

4.3.5 Slurry Solids Content Analysis

The solids content of the slurry was determined before and after extraction. This analysis serves two purposes: first, to calculate the oil on solids in order to quantify the column performance considering regulations on ultimate solids disposal and second, to ascertain if any solids are being held up in the column during processing. The solids content analysis was completed on the slurry samples after the petroleum hydrocarbon analysis to avoid hydrocarbon interference in the results (i.e., the solids content analysis also assumes that all the hydrocarbons are removed from the slurry to the toluene). All samples from the slurry feed tank and column by-pass exit (the "initial" samples) were analysed in duplicate at a minimum. For the extracted slurry, initially three samples per extraction were analysed, in duplicate, to understand the change in solids content through the extractor. Those results ultimately allowed the number of samples to be reduced to one per run (analysed in duplicate) to represent the solids content of all the extracted samples in the run. As with the petroleum hydrocarbon analysis, there were a comparatively large number of samples to analyse. Selected triplicates were performed on both initial and extracted samples to understand the variance on the analysis method.

The procedure to determine the solids content of the slurry is as follows:

1. Following centrifugation and removal of the toluene sample for GC analysis (see Section 4.3.4), the remaining toluene and slurry were poured from the Teflon vial into a separatory funnel.
2. The slurry layer was added to a clean beaker and weighed. The beaker had been dried overnight (8 h minimum) in a 110 °C oven and cooled in a dessicator.
3. The beaker containing the slurry sample was returned to the oven and dried overnight. The sample was cooled in the dessicator and weighed again.
4. The solids content of the slurry samples ($g_{solids} \cdot 100\ g_{slurry}^{-1}$) can be determined by dividing the mass of solids in Step 4 by the initial total mass of slurry in the Teflon vial (Section 4.3.4, Step 4) and multiplying by 100.

5. Similarly, the oil on solids ($g_{oil} \cdot 100\ g_{solids}^{-1}$) can be calculated by dividing the mass of hydrocarbon in the Teflon vial (determined in Section 4.3.4) by the mass of solids in Step 4 plus the mass of hydrocarbon and multiplying by 100.

4.3.6 Extraction Efficiency Calculation

The overall objective of Chapter 4 is to quantify the column performance. Toward this objective, Section 4.3.6 will detail the method used for determining the extraction efficiency, which is a simple measure of the percentage of the original hydrocarbon in the slurry that is removed in the extraction.

The extraction efficiency (η, in %) of oil from cuttings slurries is calculated as in Eq. (4-1):

$$\eta = \frac{C_{sl,in} - C_{sl,out}}{C_{sl,in}} \times 100 \qquad \textbf{(4-1)}$$

where $C_{sl,in}$ is the mass fraction of oil in the slurry entering the column ($g_{oil} \cdot g_{sl}^{-1}$), and $C_{sl,out}$ is the mass fraction of oil in the slurry leaving the column ($g_{oil} \cdot g_{sl}^{-1}$). The mass fractions are determined through the petroleum hydrocarbon analysis in Section 4.3.4.

4.3.7 Overall Volumetric Mass Transfer Coefficient Calculation

As a measure of column efficiency, quantification of the overall volumetric mass transfer coefficient, ka (s^{-1}), is an important objective of Chapter 4. This section will present the derivation of the equation to calculate ka. The basic equations presented here are standard definitions of mass transfer and mass balance.

Assuming: 1) steady state flow of oil, and 2) that the water and solids in the slurry are inert, then the flows, mass flux, and concentrations of an infinitesimal slice, dz, of the column can be envisioned as in Figure 4.5.

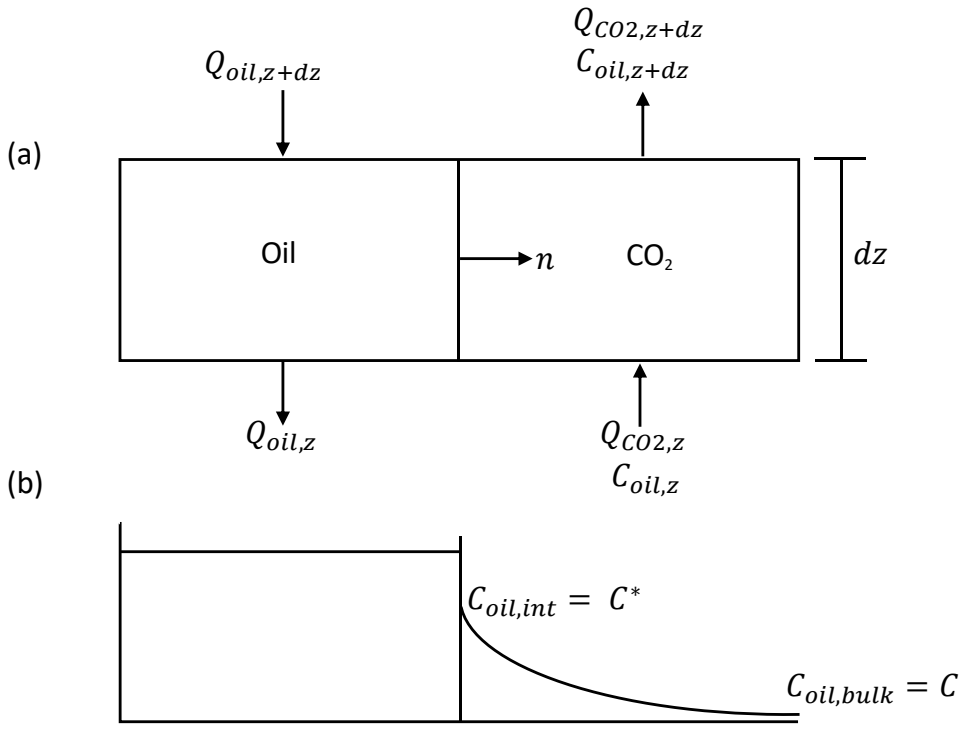

Figure 4.5: (a) Slice of column, *dz*, showing flows, *Q*, and mass flux, *n*, of oil into SC CO_2; and (b) oil concentrations in the slice.

Referring to Figure 4.5: (a) Slice of column, *dz*, showing flows, *Q*, and mass flux, *n*, of oil into SC CO_2; and (b) oil concentrations in the slice.Figure 4.5 (a), the mass balance of the oil in the slice may expressed as in Eq. (4-2):

$$Q_{oil,z+dz} - Q_{oil,z} = \left(Q_{CO_2,z+dz}\right)\left(C_{oil,z+dz}\right) - \left(Q_{CO_2,z}\right)\left(C_{oil,z}\right) \quad \textbf{(4-2)}$$

where $Q_{oil,z+dz}$ is the mass flow of oil into the slice ($g_{oil}\cdot s^{-1}$) in the slurry phase, $Q_{oil,z}$ is the mass flow of oil out of the slice ($g_{oil}\cdot s^{-1}$), $Q_{CO2,z+dz}$ is the mass flow of CO_2 out of the slice ($g_{CO2}\cdot s^{-1}$), $C_{oil,z+dz}$ is the mass fraction of oil in the CO_2 exiting the slice ($g_{oil}\cdot g_{CO2}^{-1}$), $Q_{CO2,z}$ is the mass flow of CO_2 entering the slice ($g_{CO2}\cdot s^{-1}$), and $C_{oil,z}$ is the mass fraction of oil in the CO_2 entering the slice ($g_{oil}\cdot g_{CO2}^{-1}$).

The rate of mass transfer in the slice may be described by Eq. (4-3) and is a function of the mass transfer coefficient, dimensions of the column, CO_2 density, and the concentration driving force:

$$n = -ka\ A_x\ dz\ \rho(C - C^*) \quad \textbf{(4-3)}$$

where n is the rate of mass transfer of oil from the slurry phase to the CO_2 phase ($g_{oil} \cdot s^{-1}$), ka is the overall volumetric mass transfer coefficient (s^{-1}), A_x is the cross-sectional area of the column (m^2), ρ is the density of the CO_2 at the average conditions of pressure and temperature in the column, calculated from the Fundamental Equation of State (Span and Wagner 1996), C is the concentration of oil in the bulk CO_2 in the slice, and C^* is the concentration of oil in the CO_2 at the interface and is assumed to be represented by the equilibrium solubility of the oil in CO_2 at the average conditions of pressure and temperature along the length of the column. C^* is calculated using the Chrastil correlation determined in Chapter 3. Using a single value for C^* assumes that the composition of the oil does not change along the length of the column (i.e., that the oil behaves as a single component).

Considering the change in oil concentration of the CO_2 phase in dz, the following is true from Eq. (4-2) and Eq. (4-3):

$$\left(Q_{CO_2,z+dz}\right)\left(C_{oil,z+dz}\right) - \left(Q_{CO_2,z}\right)\left(C_{oil,z}\right) = -ka\ A_x\ dz\ \rho(C - C^*) \quad \textbf{(4-4)}$$

Assuming steady state flow of CO_2, $Q_{CO2,z} = Q_{CO2,z+dz} = Q$ and Eq. (4-4) can be written as:

$$Q\left(C_{oil,z+dz} - C_{oil,z}\right) = -ka\ A_x\ dz\ \rho(C - C^*) \quad \textbf{(4-5)}$$

Rearranging Eq. (4-5) and setting up the integral over the height of the column from 0 → H, and for the oil concentration in the CO_2 from 0 at the column entrance → C at the exit:

$$Q \int_0^C \frac{dC}{(C - C^*)} = -ka\, A_x\, \rho \int_0^H dz \qquad \textbf{(4-6)}$$

Integrating Eq. (4-6) and solving for *ka:*

$$ka = \frac{-Q \ln\left(\frac{C^* - C}{C^*}\right)}{A_x H\, \rho} \qquad \textbf{(4-7)}$$

The values in Eq. (4-7) are determined from the experimental set up and extraction. Q is calculated by converting the motor speed of the CO_2 pump to a mass flow rate using the volume of the pistons and the CO_2 density at the pumping conditions, provided by the Fundamental Equation of State (Span and Wagner 1996). As mentioned, C^* was determined from the Chrastil correlation determined in Chapter 3. A_x was taken from the engineering drawings provided for the column as 0.0055 m^2. H was taken to be 2.2 m, which was determined from the drawings minus a small adjustment for the slurry and CO_2 inlet depths.

C is the concentration of oil in the exiting CO_2 flow. It is assumed that the oil removed from the slurry is fully transferred to the CO_2 and C can be calculated as:

$$C = \frac{Q_{sl}\left(C_{sl,in} - C_{sl,out}\right)}{Q} \qquad \textbf{(4-8)}$$

where Q_{sl} is the mass flow of slurry through the column ($g_{sl} \cdot s^{-1}$), $C_{sl,in}$ is the mass fraction of oil in the slurry entering the column ($g_{oil} \cdot g_{sl}^{-1}$), and $C_{sl,out}$ is the mass fraction of oil in the slurry leaving the column ($g_{oil} \cdot g_{sl}^{-1}$). The slurry flow rate is calculated by converting the motor speed of the slurry pump to a mass flow rate using the volume of the pistons and assuming a slurry density of 1 $g \cdot mL^{-1}$. The mass fractions of oil in the slurry before and after extraction are determined from the petroleum hydrocarbon analysis in Section 4.3.4.

4.4 Results and Discussion

This section provides the results of the GC calibration, the cold shake method, and pilot SFE performance in terms of efficiency and overall volumetric mass transfer coefficient.

4.4.1 GC Calibration Results

The GC calibration was carried out according to the method described in Section 4.3.4. Table 4.3 shows the results from the GC calibration completed in January 2015. The n-alkane standards were injected in duplicate.

Table 4.3: n-Alkane calibration of January 2015

n-Alkane	Average Response Factor ($L \cdot mg^{-1}$)	Difference from Overall Average (%)
n-Decane	7095	6.4
n-Hexadecane	6902	3.5
n-Tetratriacontane	6003	9.8
Overall Average	**6666**	-

The average n-alkane response factors are within 10 % of the overall average response factor, as specified in CCME (2008). The difference between the average nC50 response factor and the overall response factors was 89 %. This does not meet the CCME (2008) requirement of 30 %. For this analysis, the GC autosampler was unable to inject samples at the regular speed of 1 second without becoming stuck and/or bending the syringe. The injection time was increased to 5 seconds and, while that solved the problem with the autosampler, it resulted in molecular weight bias via needle discrimination (Restek Corp. 2002). The bias is also observed in the nC10 to nC34 standards in Table 4.3 where the response factor decreases with increasing carbon number. Having the syringe needle in the heated injector for longer increases the volatility of the lighter hydrocarbons, while simultaneously causing the heavier hydrocarbons to condense in the needle (Restek Corp. 2002). Needle discrimination is a reproducible error and can be ignored if the sensitivity in higher weight compounds is not needed (Restek Corp. 2002). For drilling oil, such as D822, the molecular weight of the heavier components is typically much lower than nC50. Figure 4.6 shows the typical GC response for D822 in relation to the n-alkane retention times.

Because drilling oil is eluted from the GC column before nC34, it is considered acceptable that the nC50 standard did not meet the CCME specification.

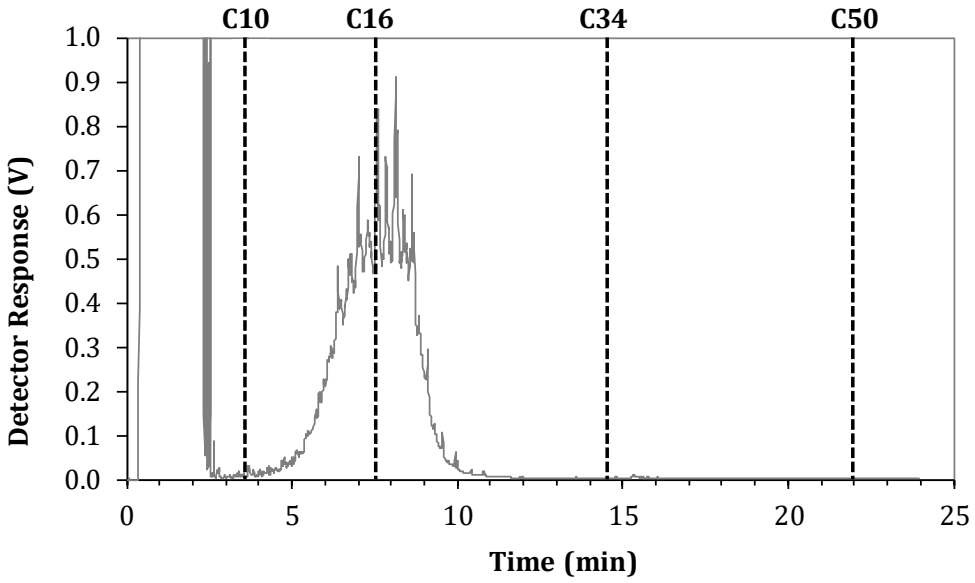

Figure 4.6: D822 GC elution in relation to n-alkane standards

Figure 4.7 shows the linearity checks for the nC10/nC16/nC34 and D882 standards. The data points are fit with a linear trend line (with y-intercept set to zero) using MS Excel, with R^2 values shown on the graphs. Based on Figure 4.7, the GC shows linearity within the values required by CCME (2008).

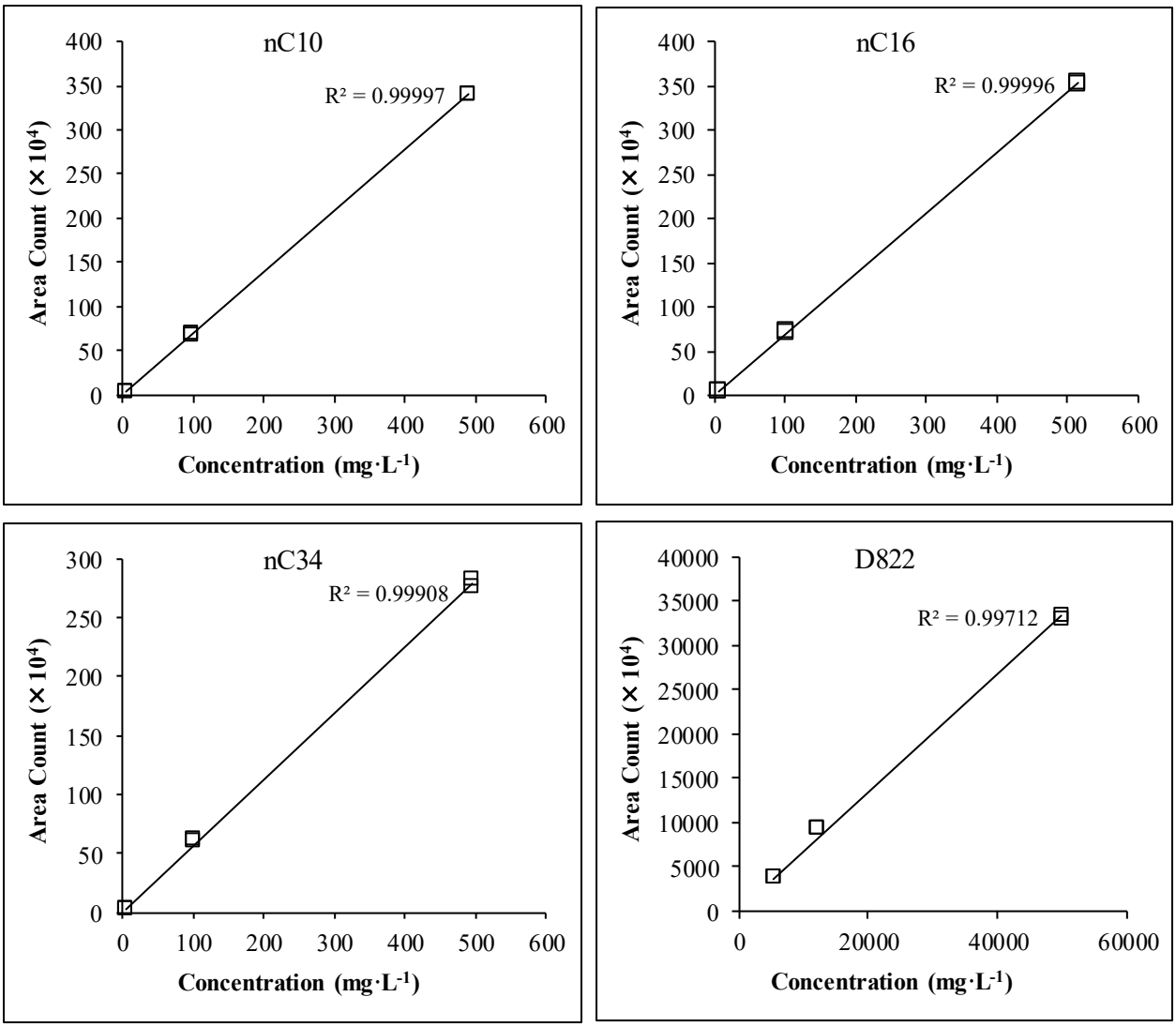

Figure 4.7: n-Alkane and D822 linearity check for January 2015 calibration

4.4.2 Cold Shake Method Selection

This section describes the results for two methods of cold shake, used to determine the hydrocarbon content of the slurry samples: the ultrasonic plus wrist action shaking and wrist-action shaking only. The results are shown in Table 4.4. Variability on the stated average recovery is plus or minus one standard deviation.

Table 4.4: Comparison of shake methods on recovery of D822 from bentonite

Shake method	No. of samples	Solids Content (wt%, wet)	D822 Content (mg/kg, wet)		D822 Recovery (%)
Ultrasonic + wrist-action	1	2.830	3731		77.0
	1	3.906	4008		96.9
	2	4.974	272.6		132, 103
	1	10.77	1371		101
	1	11.40	19020		104
				average	103 ± 15.0
Wrist-action	1	1.090	136.0		98.8
	3	5.964	663.4		95.6 ± 2.61
				average	96.4 ± 2.7

Based on CCME (2008) requirements, complete method recovery of spiked performance samples must be >80 %. Except for one recovery of 132 % for ultrasonic + wrist-action, both shake methods have good recoveries. However, the ultrasonic + wrist-action shake recovery has a higher variability. Considering both variability and time to complete the analysis, the wrist-action shake only was chosen for analysis of slurry samples from the column.

4.4.3 Column Performance: Extraction Efficiency and Mass Transfer Coefficient

The primary objective of Chapter 4 is to calculate the column performance by determining the extraction efficiency and overall volumetric mass transfer coefficient for the baffle tray column. Towards achieving this objective, fifteen successful extraction runs were completed. These runs are summarized in Table 4.5, which provides the average extraction conditions for each experimental run, and the calculated average extraction efficiency and average overall volumetric mass transfer coefficient, *ka*. A sample calculation for *ka* is provided in Appendix E.

Table 4.5: Summary of extraction experiments (experimental conditions and results)

Run No.*	Pressure (MPa)	Temp. (°C)	ρ CO_2 ($g \cdot mL^{-1}$)**	CO_2 flow ($g \cdot s^{-1}$)	Slurry flow ($g \cdot s^{-1}$)	Slurry solids content ($g_s \cdot 100g_{sl}^{-1}$)	Initial oil on solids ($g_{oil} \cdot 100g_{s,dry}^{-1}$)	Extraction efficiency (%)***	$ka \times 10^{-5}$ (s^{-1})***
Simulated cuttings – initial experiments									
35	13.5	41.3	0.7429	17	45	0.3	17.0	65.5 ± 3.97	3.12 ± 3.85
36	13.9	45.0	0.7178	17	42	0.2	14.9	43.9 ± 13.9	1.21 ± 14.0
37	13.8	41.0	0.7521	17	44	1.1	8.3	43.1 ± 55.7	3.64 ± 56.0
38	13.9	44.1	0.7260	15	44	3.0	10.6	88.8 ± 10.0	33.5 ± 10.7
Simulated cuttings – pressure data points									
41a	10.2	38.8	0.6678	19	41	2.5	21.1	70.8 ± 9.46	96.9 ± 12.1
41b	14.0	45.4	0.7161	11	34	2.5	21.1	88.9 ± 2.58	48.8 ± 3.28
55a	10.0	42.8	0.5613	12	38	2.6	9.1	43.9 ± 38.2	61.5 ± 45.8
55b	14.0	41.1	0.7534	22	43	2.6	9.1	75.5 ± 21.5	16.5 ± 24.8
56a	10.0	37.5	0.6750	9	37	2.5	7.6	75.3 ± 14.3	28.8 ± 16.3
56b	14.0	39.2	0.7691	25	39	2.5	7.6	61.1 ± 54.1	9.05 ± 54.8
58	17.9	42.2	0.8056	33	52	2.3	12.9	79.8 ± 13.9	17.4 ± 14.4
59	17.9	43.2	0.7991	29	56	2.1	14.7	81.9 ± 5.62	20.6 ± 2.43
61	17.9	39.7	0.8201	32	54	1.9	18.0	92.3 ± 3.90	23.8 ± 3.36
Real cuttings									
67	13.9	40.6	0.7566	35	44	1.7	13.7	80.8 ± 19.4	18.8 ± 20.7
75	13.9	40.9	0.7535	15	67	0.2	31.5	74.8 ± 23.5	5.20 ± 24.0
76	13.9	40.5	0.7569	19	54	0.2	21.1	36.6, 63.6	1.56, 2.72
77	13.9	36.3	0.7900	25	51	0.2	22.1	73.1 ± 23.8	2.75 ± 24.0
78a	13.9	34.1	0.8069	24	55	0.5	44.8	95.8 ± 3.24	33.9 ± 3.24
78b	13.9	39.9	0.7623	19	53	0.5	44.8	89.5 ± 10.1	35.6 ± 11.0

* from Chapter 2, Table 2.6

** from the Fundamental Equation of State (Span and Wagner 1996)

*** average value ± relative standard deviation (RSD, as % of mean); or single measurements if only two samples

4.4.4 Extraction Efficiency

From Table 4.5, the extraction efficiency of the column ranges from 36.6 to 95.8 %. These extraction efficiency results are consistent with extraction efficiencies obtained on a smaller, batch SFE system at the University of Alberta (Odusanya 2003; Lopez Gomez 2004; Street 2008, Jones 2010) and batch studies performed elsewhere (Saintpere and Morillon Jeanmaire 2000; Ma et al. 2019), as shown in Table 4.6.

Table 4.6: Extraction efficiency ranges of previous studies on supercritical carbon dioxide treatment of drill cuttings and drill cuttings/water slurries

Ref.	Feed Material	Operating Pressure (MPa)	Operating Temperature (°C)	Extraction Efficiency Range (%)
Saintpere and Morillon Jeamaire (2000)	Cuttings only and cuttings/water slurry up to 1:0.3	6 – 12	35 – 45	up to 95
Odusanya (2003)	Cuttings only	8.3 – 17.2	35 – 60	33 – 97
Lopez Gomez (2004)	Cuttings only	9.0 – 15.2	40 – 60	69.0 – 98.6
Street (2008)	Cuttings only	14.5	40	52.1 – 99.1
Jones (2010)	Cuttings/water slurry up to 1:1	14.5	40	35.4 – 91.5
Ma et al. (2019)	Cuttings only	12 – 25	21 – 60	31 – 75

In order to ascertain which process variables might be important to improving the extraction efficiency of the column in the future, regression of the data was undertaken. Initially, all the measured process variables from Table 4.5 (i.e., pressure, temperature, mass flow rates, slurry solids content, and initial oil content) and the natural log of the CO_2 density were input as variables to the linear regression function of MS Excel (a least squares regression), with α=0.05. The natural log of the density was included (over just density) because of its known effect on solubility (such as the Chrastil correlation described in Chapter 3). The initial regression results showed that the slurry solids concentration and the oil concentration of the solids were the significant variables, with an adjusted R^2 of 0.58 for the equation. To improve the equation, the regression was re-run with one variable removed, beginning with the variable which was the least statistically significant. This procedure was continued in the

stepwise fashion until the R^2 did not show further improvement or all the remaining variables were shown to be statistically significant. The resulting equation is shown in Eq. (4-9):

$$\eta = 71.5 + 102.8\,(\ln \rho) + 1185.3\,\left(C_{s,sl}\right) + 0.5\,\left(C_{oil,s}\right) \qquad \textbf{(4-9)}$$

where $C_{s,\,sl}$ is the slurry solids content ($g_s \cdot 100g_{sl}^{-1}$) and $C_{oil,s}$ is the initial oil on solids ($g_{oil} \cdot 100g_s^{-1}$). The adjusted R^2 of the equation is 0.68. Figure 4.8 shows the parity plot of the extraction efficiency calculated from Eq. (4-9) and the experimental extraction efficiency.

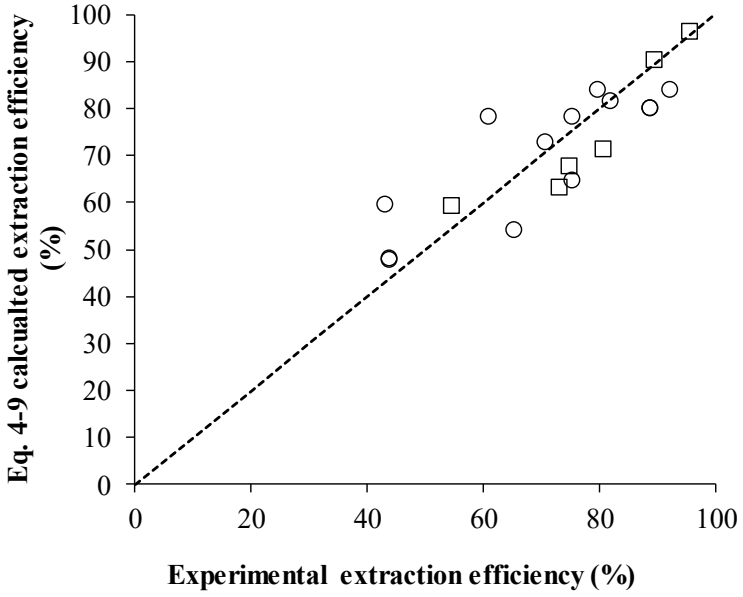

Figure 4.8: Parity plot of the extraction efficiency calculated from multiple linear regression (Eq. (4-9)) and experimental extraction efficiency for (□) cuttings and (○) simulated cuttings

The parity plot shows good agreement between the experimental and calculated values, and the AARD between the calculated and measured values is 10.2 %. The parity plot also shows that there is no discernable difference between the extraction efficiency results for the cuttings and simulated cuttings.

The results of the regression imply that increasing the solids content of the slurry will increase the extraction efficiency. Fortin (2003) showed a higher naphthalene removal rate in the lab-scale version of the current column when the solids concentration of the processed slurry increased from 0.3 wt% to 7 wt%.

In batch systems, reducing the solids content of slurries is known to decrease the extraction efficiency. Jones (2010) determined that increasing the mass ratio of water to cuttings from 0.5:1 to 5:1 decreased the extraction efficiency from 90 % to 35 %. Saintpere and Morillon Jeanmaire (2000) reported a reduction in extraction efficiency as the water content of the cuttings was increased beyond 10 – 15 %. These results are also consistent with batch extraction of organics from soil slurries (Laitinen 1999; Akgerman and Yeo 1993). The effect of water in supercritical systems is complex, but in highly dilute systems, the reduction in extraction efficiency is generally attributed to the water limiting contact between the supercritical fluid and the solute of interest (Saldana et al. 2005). Design changes to the batch-system by Jones (2010) allowed improved contact between the SC CO_2 and the slurry, which improved the extraction efficiency of a 1:1 slurry from 61 % to 98 %.

Increasing the solids content of the slurry is easily achieved in theory, but the current pilot system set up limited the concentration of solids that could be fed into the system, as described in Section 4.3.2. The design of the feed tank and mixer, and the large diameter of the slurry pump inlet line, resulted in blockages of flow to the pump. It is recommended to test higher solids content slurries, but the slurry feed tanks and pipes upstream of the pump will need to be re-designed to accommodate the higher concentrations of solids. The added benefit of being able to process higher solids content slurries increases the overall cuttings throughput, which is especially important for reducing costs of a commercial scale system.

The regression equation also suggests that increasing the CO_2 density will increase the column extraction efficiency. In the range of conditions tested, density can be increased by increasing pressure and/or decreasing temperature. Density affects the extraction by changing the fluid properties of the solvent and, therefore, changing the solubility of the solute. Chapter 3 has shown that the solubility of n-hexadecane and D822 increase with

increasing density (pressures up to 24.2 MPa at temperatures of 40 °C and 50 °C), as described by the Chrastil equation. For future experiments, it is recommended to investigate the effect of higher pressures on the extraction efficiency. Lowering temperature should be less of a priority for future tests because the current temperature (~40 °C) is the minimum temperature required to achieve >31 °C (supercritical temperature for CO_2) along the length of the vessel. Additionally, controlling temperature accurately in the current experimental set up is difficult.

The results of the regression also imply that increasing the oil content of the cuttings solids will increase the extraction efficiency. For the current pilot-scale system, when using simulated cuttings, increasing the oil content of the solids is simply a matter of adding more oil when the cuttings are prepared. However, a commercial system would be processing slurries made from cuttings delivered from drilling rigs. The oil content of the cuttings would be variable, depending on the source and the solids handling equipment in use at a drilling rig. Therefore, it would not be worthwhile testing the oil on solids process parameter directly.

Collecting a large data set with statistical analysis in mind was not an objective of this study. To that end, the limitations of the data and the regression should be considered. First, the experiments were not conducted in random order. From run no. 35 to 78b, the operators were gaining familiarity with the system, which in turn would improve the performance of the column. Also, most of the process parameters did not vary over a large range, which makes detecting their effect as statistically significant difficult. Finally, the regression is missing a key process parameter: slurry level. It is expected that measuring level and improving level control would have a major positive effect on the column performance results (as in the improvements from Fortin (2003) to Forsyth (2006)). The current column has no level measurement because of technological limitations. It is recommended to continue searching for a suitable level measurement method.

The average of the individual average RSD values for the extraction efficiencies of Table 4.5 is 18.2 %. In comparison, the RSD on the extraction efficiency data for the batch extractions

on cuttings slurries in Jones (2010) range from 0.5 to 20 %. Both the range and the average of the individual average RSD values are quite reasonable considering the increased complexity of the continuous system and the novelty of its operation. For the two runs with a high RSD (Run 37 and 56b) there are two samples out of five with quite distinct extraction efficiencies that appear to be a result of slurry pump flow/slurry level. The extraction efficiency of the individual samples for Run 37 are 22.9, 34.4, 20.7, 68.5, and 69.2 %. From Figure 4.9, the timing of the last samples (Samples 4 and 5) occurred during a period of time where the slurry pump speed had been reduced after a period of time of being relatively high. The reduction in speed would correspond to a reduction in slurry level at the bottom of the vessel, resulting in more height available for mass transfer. The vessel does not have active level measurement, so the slurry pump speed is only an indirect measure. This explanation is only one possible, but likely, reason as to why the last two samples had a much better efficiency and further supports the need for a better slurry level measurement.

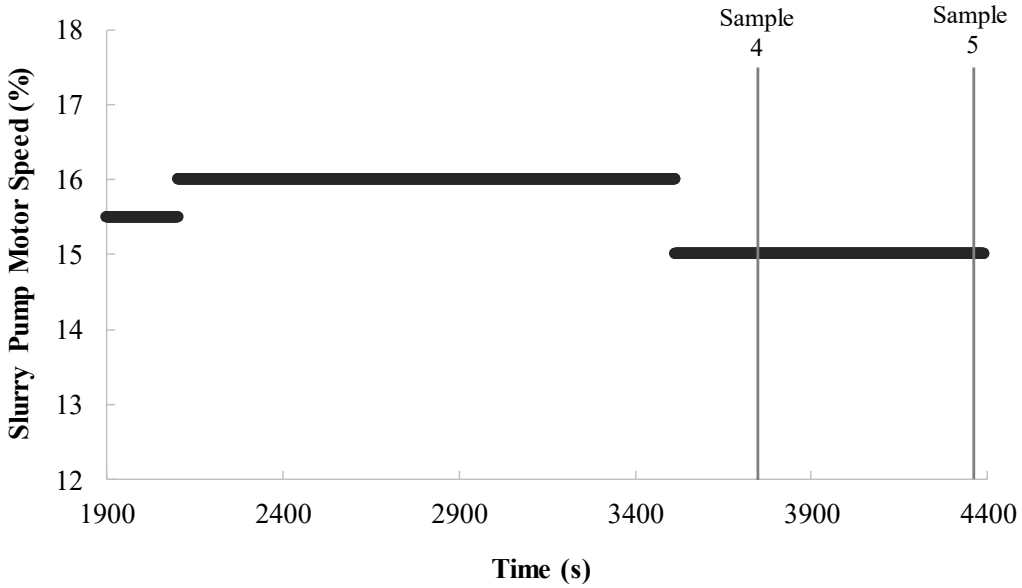

Figure 4.9: Slurry Pump Speed during Run 37, with timing of Sample 4 and Sample 5

For Run 56b, the last two of five samples had the lowest extraction efficiencies. The five extraction efficiencies calculated from the five individual samples were 85.5, 85.8, 82.6, 35.8, and 15.6 %. Lab notes on the final two samples (Sample 4 and 5) record the observation of

an increased smell of diesel. The last two samples were taken during a period when the system was being prepared for a test of the control system. The test requires a long period where the slurry pump speed is held constant, then increased significantly. More information on the control system development and testing is available in Roodpeyma (2017). Figure 4.10 shows the details of the slurry pump speed and the timing of Samples 4 and 5. During the long period of time at 14.5 %, the vessel was likely slowly filling (i.e., reducing the length of column available for efficient extraction). Again, this period of time of constant pump speed was in preparation for a control system test where the speed was increased for a very short time to 17.5 %, as shown in Figure 4.10.

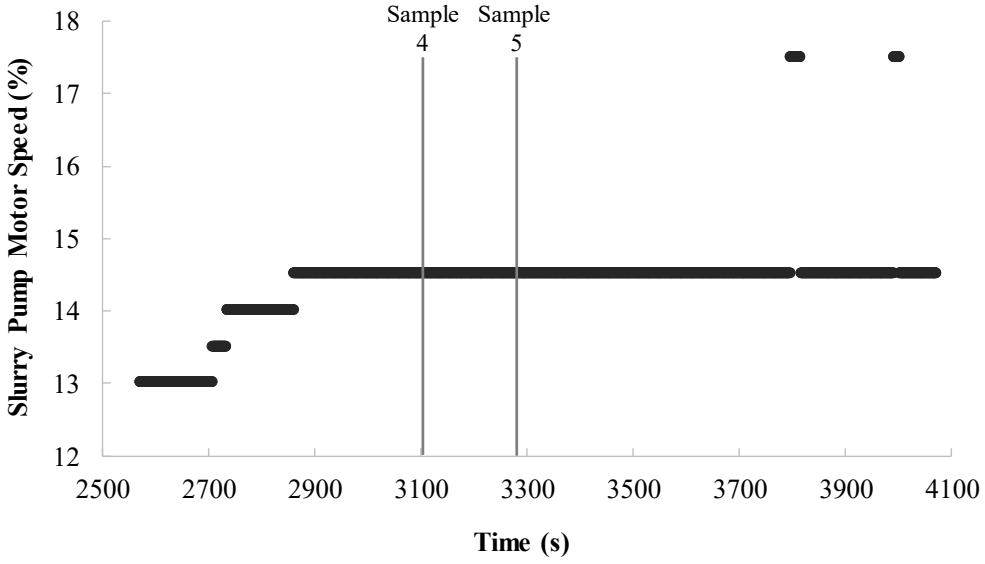

Figure 4.10: Slurry Pump Speed during Run 56b, with timing of Sample 4 and Sample 5

4.4.5 Overall Volumetric Mass Transfer Coefficients

This section discusses the results of the overall mass transfer coefficient (*ka*) calculation, investigates the important process parameters that affect *ka*, and tests the assumptions of the *ka* derivation.

The *ka* values in Table 4.5 range from 1.21×10^{-5} to 9.69×10^{-4} s^{-1}. There are no direct comparison *ka* values in the literature because of the novelty of the physical system; that is,

a pilot-scale, baffle tray column in supercritical service being used for the removal of oil from drill cuttings slurries. However, the *ka* values calculated are consistent with overall mass transfer coefficient values calculated on the lab-scale, batch system at the University of Alberta for drill cuttings only. The values for the batch system ranged from 10^{-5} to 10^{-4} s^{-1}, up to a maximum of 2.5×10^{-4} s^{-1} (Street et al. 2013). Similarly, the values are consistent with the lab-scale countercurrent column developed at the University of Guelph for the removal of polyaromatic hydrocarbons from soil slurries: Fortin (2003) determined overall volumetric mass transfer values from 10^{-5} to 10^{-4} s^{-1}, to a maximum of 4.6×10^{-4} s^{-1}. Forsyth (2006) improved upon the system design by Fortin (2003) by implementing a level control system and the overall mass transfer coefficient values improved by an order of magnitude, to a maximum of 5.1×10^{-3} s^{-1}. It has been shown that the level control is an important variable in mass transfer and improvements to level control on the current column could be expected to increase *ka* here as well.

The individual RSD values for the *ka* data in Table 4.5 have an overall average of 19.2 %. Again, considering the complexity of the system, this magnitude of RSD seems reasonable. The highest individual RSD values correspond to the same runs (37 and 56b) with the highest RSD in the extraction efficiency. As with extraction efficiency, the last two samples of five in both cases were distinctly different most likely as a result of the slurry pumps speed and corresponding changes in the slurry level at the bottom of the vessel. When the level of slurry at the bottom of the column is high, the carbon dioxide is no longer the continuous phase, instead bubbling up through slurry which is less efficient for mass transfer.

For additional comparison to the literature, Fair (1993) provides a heat transfer-mass transfer analogy to estimate mass transfer in baffle columns in gas-liquid service, Eq. (4-10):

$$HTU = \frac{C_p}{(C_1)(\dot{m}_L)^{0.44}} \left(\frac{Sc}{Pr}\right)^{2/3} \quad \textbf{(4-10)}$$

The inputs are the gas specific heat (C_p), liquid mass velocity ($\dot{m}_L$), Schmidt number (Sc), and Prandtl number (Pr). C_1 is a constant, equal to 0.0025, for English units (C_p in BTU·lb^{-1}·°F^{-1}; $\dot{m}_L$ in lb·h^{-1}·ft^{-2}). The Prandtl number requires the specific heat, dynamic viscosity, and thermal conductivity of the gas; in this case, all were provided for CO_2 at extraction conditions from the Fundamental Equation of State (Span and Wagner 1996). Similarly, the density and dynamic viscosity for the Schmidt number were provided for CO_2 at extraction conditions from the Fundamental Equation of State (Span and Wagner 1996). The Schmidt number also requires a diffusion coefficient for the drilling oil in CO_2, which was estimated from a correlation provided by Lin and Tavlarides (2010). Lin and Tavlarides (2010) tested a variety of correlations against experimental measurements of diffusion of diesel fuel and other surrogate compounds in SC CO_2 at 313.15 to 373.15 K and pressures up to 30 MPa. The correlation of Evans et al. (1979) was recommended by Lin and Tavlarides (2010) for calculating the diffusion of diesel in SC CO_2 and is shown in Eq. (4-11):

$$\frac{D_{12}}{T} = \alpha \eta_2^{\beta} \qquad \textbf{(4-11)}$$

Where D_{12} is the diffusion coefficient of diesel in CO_2 in m^2·s^{-1}, T is the temperature in K, and η_2 is the dynamic viscosity of CO_2 in Pa·s, from the Fundamental Equation (Span and Wagner 1996). Regressing the data from Lin and Tavlarides (2010) for diesel fuel, $\alpha = 18.6 \times 10^{-14}$ and $\beta = -0.51$.

Using Eq. (4-10) and (4-11), a *ka* was calculated for each set of experimental extraction conditions in the current system. Figure 4.11 shows a parity plot of the measured and calculated *ka* values.

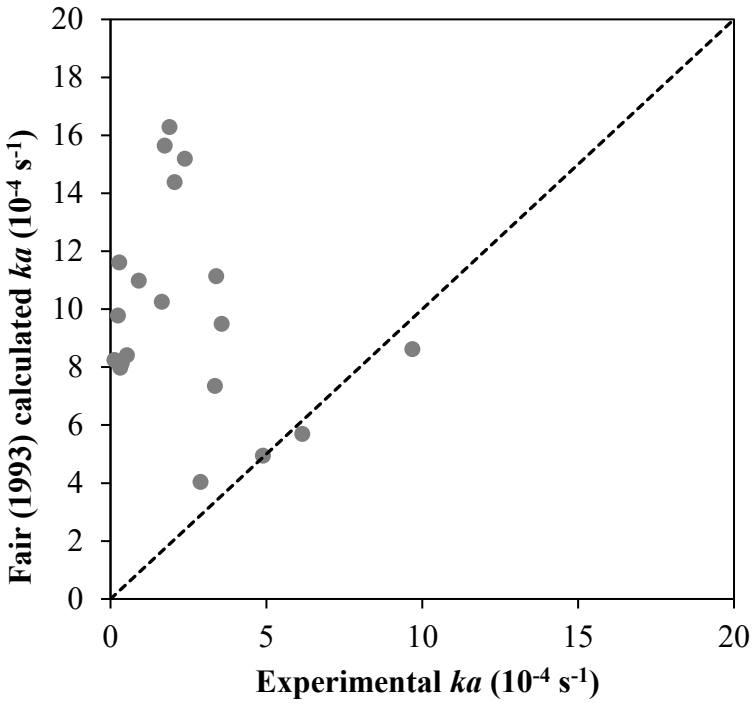

Figure 4.11: Parity plot of experimental *ka* values and *ka* values calculated from the heat transfer-mass transfer analogy provided by Fair (1993)

From Figure 4.11, most of the values of *ka* calculated from Fair (1993) tend to overestimate the experimentally obtained *ka* values. The AARD between the experimental and calculated values is 1365 %. Although the AARD is high, there are some important differences between the systems in the correlation of Fair (1993) and the current system, which would impact mass transfer. These differences include the sizes and geometries of vessels; the geometries and arrangement of baffles; and the operating phases (gas-liquid system for Fair (1993) versus liquid-supercritical fluid for the current experiments). Also, the heat transfer-mass transfer analogy provided by Fair (1993) is based on three small heat transfer data sets from sieve tray columns.

Finally, the overall AARD for the diffusion coefficient correlation for diesel in SC CO_2 proposed by Lin and Tavlarides (2010) is <8 % in the range of temperatures and pressures tested. However, the study has experimental data points for D_{12} at 313.15 K at 10 MPa. If the

experimental values are is used in the mass transfer calculation of Fair (1993), the *ka* values are on average 338 % larger.

Figure 4.12 compares the experimental *ka* values with those calculated with the method of Fair (1993), based on gas mass velocity. There is a clear relationship between the *ka* predicted by the method of Fair (1993) and the gas mass velocity that is not clearly seen in the experimental *ka*. Some of the experimental data points at the lower gas mass velocities seem to agree, while others do not.

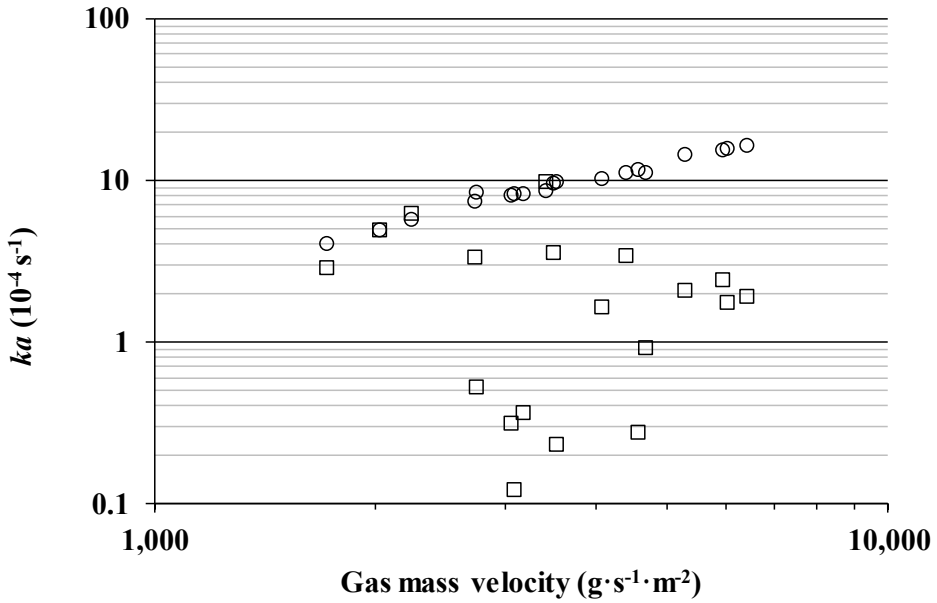

Figure 4.12: *ka* versus gas mass velocity for the experimental data (□) and calculated by the method of Fair (1993) (○)

A similar relationship is not seen in spray or sieve tray columns in supercritical service (Lahiere and Fair 1987). Studying the extraction of ethanol and isopropyl alcohol from water using SC CO_2, Lahiere and Fair (1987) found no relationship between the flow of SC CO_2 and the column mass transfer efficiency. The data set was also small (12 data points) and covered a small range of flows (approximately 2,000 to 15,000 $g \cdot s^{-1} \cdot m^{-2}$).

There is the possibility that none of the data sets (present work included) cover a large enough range of flows to accurately capture the effect of the flow of CO_2 on the mass transfer

efficiency. Density may be playing a role in the observed effect as the density difference between phases in supercritical columns is much less than that of gas-liquid columns.

Also, in the data used by Fair (1993) to develop the correlation, the columns were operated near flooding, which is known to be a beneficial operating region for mass transfer. The experimental CO_2 flow rates were much too low to compare to the flood capacity data provided in Fair (1993) and no evidence of flooding was observed under the flow conditions tested. Flooding would be observed as an escalation in pressure drop over the length of the column, to the point that flow can no longer enter. It would be recommended to attempt different flows to determine the flooding points of the current column. However, the current design of the column entrances seems to be limiting the flows to below flooding. The current openings for the inlet piping are 3.2 mm (¼"), which was the maximum size possible while maintaining the integrity of the lid when the column was under pressure. The relatively small openings create a restriction on the flow that when the flow rates are increased, a large increase in pressure is observed in the inlet lines but not the column. In order to test flows to determine the flooding point, the current column entrances will need to be modified.

The overall logarithmic average for the *ka* data in Table 4.5 is 2.44×10^{-4} s^{-1}. The AARD between the logarithmic average and the measured values is 308 %. As with the extraction efficiency data, a multiple linear regression was undertaken to provide a better estimate for *ka* as related to the extraction process conditions and to form initial recommendations for process conditions to test in future work. The regression was undertaken in MS Excel using the same step-wise elimination procedure as the regression for extraction efficiency (Section 4.4.4). The result is Eq. (4-10).

$$ka = -0.00061 - 0.00142\,(\ln \rho) + 0.0162\left(C_{s,sl}\right) + 7.18 \times 10^{-6}\left(C_{oil,s}\right) \qquad \textbf{(4-10)}$$

where $C_{s,sl}$ is the slurry solids content ($g_s \cdot 100g_{sl}^{-1}$) and $C_{oil,s}$ is the initial oil on solids ($g_{oil} \cdot 100g_{s,dry}^{-1}$). The adjusted R^2 of the equation is 0.70. Figure 4.11 shows a parity plot with reasonable agreement between the calculated and experimental *ka* values and, as with the

extraction efficiency results, there does not appear to be a discernable difference between the cuttings and simulated cuttings.

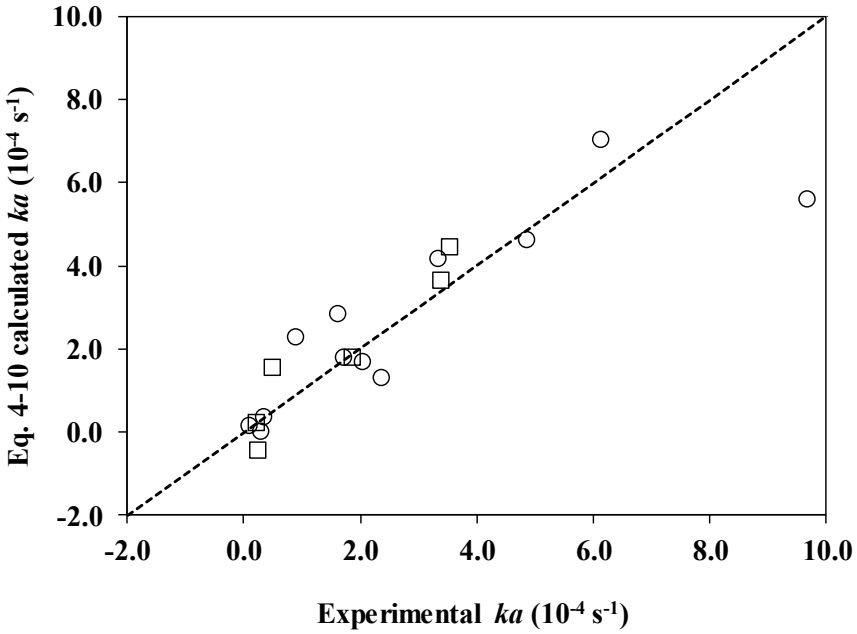

Figure 4.13: Parity plot of *ka* calculated from Eq. 4-10 versus experimental *ka* for (□) cuttings and (○) simulated cuttings

According to the regression results, an improved *ka* can be achieved by decreasing the density, increasing the solids content of the slurry, and increasing the oil content of the cuttings solids. These were also important extraction parameters identified by the regression of the extraction efficiency results. A discussion of increasing the solids content and oil content is provided in Section 4.4.4.

Interestingly, decreasing the density is the opposite action as to what was indicated by the regression of the extraction efficiency data. The mass transfer of oil to SC CO_2 is a balance between the mass flux (which is an efficiency-like measure), *ka*, and the driving force concentration difference, as in Eq. (4-3). Decreasing density would improve *ka* directly through the ρ term, but also by decreasing solubility, C^* (all other values being held constant). However, increasing *ka* can also be achieved by increasing the mass flux, *n* (again, all other

values being held equal). The regression of the current data shows that, for *ka,* the direct ρ/solubility effect is governing. And, while *ka* is an important measure of the column performance and necessary for scale-up, the most important aspect to the technology development is the extraction of oil from cuttings. Therefore, it is recommended that future experiments focus on increasing density to improve the efficiency.

The regression results also allow another viewpoint on variability in calculated *ka*. Owing to the wide variety of extraction conditions and limited control of some of them, no runs are true replicates. However, if only density, slurry solids content, and oil on solids are considered (as the most significant factors), then there is one set of three runs that can be compared: Runs 58, 59, and 61 (density from 0.7991 – 0.8201 $g \cdot mL^{-1}$; solids content 1.9 – 2.3 $g_s \cdot 100g_{sl}^{-1}$; oil on solids 12.9 – 18.0 $g_{oil} \cdot 100g_{s,dry}^{-1}$). The average *ka* for Runs 58, 59, and 61 is 20.60×10^{-5} s^{-1} and the AARD between the individual run *ka* and the average is 10.4 %.

Eq. (4-10) does calculate two negative *ka* values, which is impossible in reality and shows the limitations of the regression at this point in the technology development. However, if the size and collection method of the data set is considered, it is not appropriate to suggest that the regression could be used as a predictor for *ka* values. Rather, the regression can identify important extraction parameters effecting *ka* and, therefore, help direct future research.

The AARD between the values calculated from the regression and the measured values is 55.6 %, which is a substantial improvement over the logarithmic average. It is worth noting that the prediction of mass transfer coefficients in *any* column, supercritical or otherwise, is by and large an empirical data fitting exercise (Wang et al. 2005). For example, despite intensive study (in comparison to baffle columns), correlations for mass transfer in packed columns under gas-liquid service typically achieve AARD values no better than ±20 to 30 % (for example, the correlations of Onda et al. (1968), or Bravo and Fair (1982) are commonly used).

4.4.6 Sensitivity Analysis for *ka*

The calculation of *ka* is subject to uncertainties related to the measurement of the input variables, which should be investigated to determine how representative of the column the *ka* result is. This section will examine the impact of uncertainties in the measured pressure and temperature (impacting density and solubility); slurry and CO_2 flow rates; slurry level; solubility (Chrastil correlation); and the concentration of the oil in the exiting CO_2 flow.

Pressure and Temperature

Pressure and temperature have an impact on the mass transfer coefficient calculation through the density and solubility. Pressure and temperature values, as reported in Table 4.5, are overall averages of the readings from sensors in the top and bottom of the column. While the top and bottom pressure sensors read the same (within the standard deviation), the temperature sensors typically have different readings. It is difficult to determine if the average of the top and bottom temperature sensor values is a good representation of the column conditions. If the bottom sensor is reading a localized cold area due to the incoming CO_2, then the average is an underrepresentation of the temperature in most of the column. The temperature difference between the top and bottom of the column eventually settles to approximately 10 °C, with the bottom sensor reading lower due to its proximity to the incoming CO_2. However, in the absence of data to provide an alternate, the average value was used. The typical standard deviation for the pressure and temperature averages is 0.3 MPa and 1.3 °C, respectively.

Although pressure and temperature are intertwined in the density and solubility, for purposes of determining impacts on *ka*, they were considered separately. For pressure, investigating the impact of three standard deviations (± 0.9 MPa) is reasonable for a starting point. Pressure has the greatest impact on density at the lowest pressure values tested (i.e., 10 MPa; Runs 41a, 55a, and 56a). For Run 55a, a 0.9 MPa decrease in pressure resulted in a C^* which is smaller than C. This result is a mathematical and physical impossibility. The ΔC became positive when the pressure decreased only 0.7 MPa. Thus, the experimental data confirms that the variation in pressure is slightly better than three standard deviations. For

Runs 41a and 56a, a 0.7 MPa decrease in pressure resulted in an average increase in *ka* of 89 % and a maximum increase of 105 %. As decreases in pressure resulted in increases in *ka*, the values of *ka* in Table 4.5 are conservative.

If pressure increased by 0.7 MPa, the greatest effect is again at the lowest pressure tested (10 MPa). For the three runs at this pressure, the worst case is Run 55a where the *ka* is decreased by 54 %. On average, the decrease in *ka* for the three runs as a result of a 0.7 MPa pressure increase is 36 %.

Temperature changes also have the greatest impact at low pressures (10 MPa). If the temperature increased 10 °C (representing the change from top to bottom sensor of the vessel), the density decreased such that C becomes larger than C^* for Run 55a. An average temperature increase of 4.2 °C resulted in a positive ΔC , which shows the temperature variation in the column is likely less than 10 °C. Considering Runs 41a and 56a, the average increase in *ka* as a result of a 4.2 °C temperature increase is 239 % and the maximum is 289 %. Again, the positive results of this sensitivity analysis are that the temperature measurement is better than 10 °C and the *ka* values in Table 4.5 are conservative with respect to increases in temperature. Decreases in temperature of 4.2 °C at 10 MPa decreased the *ka* by an average of 48 % and a maximum (Run 55a) of 67 %.

A summary of the sensitivity analysis for the pressure and temperature changes are shown in Table 4.7.

Table 4.7: Summary of impacts to *ka* as a result of uncertainties in pressure and temperature

Input	Uncertainty	Δ *ka* (%)	
		average	maximum
Pressure	+ 0.7 MPa	-36	-54
	- 0.7 MPa	89	105
Temperature	+ 4.2 °C	239	289
	- 4.2 °C	-48	-67

Flow rates, solubility, and oil concentration in CO_2

Table 4.8 summarizes the impact of uncertainties in solubility (through the calculation of solubility using the Chrastil correlation from Chapter 3, and not pressure and temperature directly), oil concentration in the CO_2, and the flow rates on *ka*. Compared to pressure and temperature, these parameters have a much lower impact on *ka*. Average changes to *ka* ranged from -1.0 to 11.1 % with the worst case being a 14.1 % increase as a result of uncertainty in the Chrastil correlation.

Table 4.8: Summary of impacts to *ka* as a result of uncertainties in flow rates, oil content in CO_2, and solubility

Input	Uncertainty (%)	Δ *ka* (%) average	Δ *ka* (%) maximum
Q_{sl}	+ 10	+10.7	+13.6
	- 10	-10.5	-12.7
Q_{CO2}	+ 20	-1.0	-4.9
	- 20	+1.4	+7.4
Slurry oil content	+ 10	-8.6	-10.9
	- 10	+8.5	+10.3
Solubility calculation (Chrastil correlation)	+ 9.4	-9.0	-10.9
	- 9.4	+11.1	+14.1

The flowrates for CO_2 and slurry through the column were calculated from the pumps using the stroke length, speed, and inner bore diameter. This calculation is a standard calculation method for piston pumps, and their volumetric efficiency is commonly expected to be near 100 % for most of their lifespan (Bourgoyne Jr. et al. 1986). However, there is no flowrate verification in the system as flowmeters suitable for small diameter piping, cold, and low flows could not be easily sourced. So, for Q_{sl}, a conservative uncertainty of ± 10 % was considered.

Although the calculation for *ka* assumed that the water in the slurry is inert, water does play a role. For the flow of CO_2, its mutual solubility in water is important. Spycher et al. (2003) give the solubility of SC CO_2 in water as approximately 0.025 mol CO_2 · mol water^{-1} (0.06 gCO_2 · g water^{-1}) for the range of the extraction conditions tested here. The result is, on

average, that 15 % of the flow of CO_2 is lost to the slurry. This loss, plus the possibility of some loss in volumetric efficiency, was considered as an uncertainty in Q_{CO2} of ±20 %.

Although the SC CO_2 is also soluble in oil, this loss of flow was not considered because the flow of oil is much lower than that of water. Increased losses of CO_2 due to a loss of slurry level at the bottom of the vessel was also not considered because this represents a system upset condition wherein no samples are taken.

For the oil content in the slurry (used to calculate *C*), an uncertainty of ±10 %, representing 3 standard deviations on the cold shake method, was used to assess the change in *ka*. For the solubility measurement, an uncertainty of ± 9.4 % was used as this is the AARD of the Chrastil correlation from Chapter 3.

Slurry Level

The calculation of *ka* has an input *H,* which represents the length of the column available for mass transfer. Lacking better information, *H* was set for the internal physical length of the column. However, during normal operation, there is always an amount of slurry maintained at the bottom of the column. In this continuous slurry environment, the mass transfer would be less efficient, and *ka* would be impacted negatively. It is difficult to apply an uncertainty to *H* because the level is not constant during the run. As mentioned previously, the current column set up does not have level sensing equipment and maintaining level requires operators to observe the slurry out flow for an increased presence of CO_2 (indicating a need for a higher slurry pump speed). Decreasing amounts of CO_2 in the slurry out flow mean the column is filling and the pump speed should be decreased. All this said, using the largest possible *H* (physical length of column) means that the *ka* values calculated are conservative.

4.5 Conclusion and Recommendations

Towards the overall objective of demonstrating SC CO_2 extraction in a continuous, pilot-scale, baffle tray column as a treatment for oily drill cuttings, the primary purpose of Chapter 4 was to provide a first quantification of the column performance. Fifteen slurry extraction

experiments were successfully completed on the extraction system presented in Chapter 2. With respect to the objectives, the following conclusions and recommendations can be made:

A suitable cold shake method was adapted from the literature to analyse slurry samples of high water content

Both a wrist-action shake and a wrist-action shake + ultrasonic extraction with toluene were tested. Based on the recovery of spiked samples and the standard deviations, the wrist-action shake only was selected. The recovery of the method was 96.4 % ± 2.7 %, which was well above the QA/QC requirement of > 80 % in the CCME Canada-wide Standard for Petroleum Hydrocarbons in Soil. In comparison with the commonly used Dean Stark method, the wrist-action shake has a lower processing time, uses less consumables, and is more suitable for higher water contents.

Extraction efficiencies were successfully measured and values up to 95.8 % were achieved.

The range of extraction efficiencies was from 36.6 to 95.8 %, with an overall average RSD of 18.2 %. The values are consistent with literature results for batch systems treating drill cuttings and drill cuttings slurries. Variability in slurry level likely resulted in the highest individual RSD values. It is recommended that an appropriate slurry level measurement be sourced to improve consistency of extraction efficiency in the column.

Overall volumetric mass transfer coefficients (ka) were successfully measured and values of up to 9.69 × 10^{-4} s^{-1} were achieved.

The calculated *ka* values ranged from 1.21 × 10^{-5} s^{-1} to 9.69 × 10^{-4} s^{-1}, with an overall average RSD of 19.2 %. The novelty of the system prevents direct comparison to literature values, but the range is consistent in terms of order of magnitude with results from the lab-scale, batch SC CO_2 extraction of oil from cuttings and the lab-scale continuous SC CO_2 extraction of naphthalene from soil slurries. High variabilities in *ka* for some of the extraction runs are caused by the results from single samples. These samples were taken when the slurry level in the vessel was distinctly different than the rest of the experiment, leading to changes in efficiency by increasing or reducing the available length of the column for mass transfer. This

result further reinforces the recommendation to source an appropriate slurry level measurement.

The experimentally calculated ka values are roughly consistent with the calculated values from the mass transfer correlation for baffle columns in gas-liquid service (Fair 1993).

The AARD between the predicted and the experimentally calculated values was 1365 %. However, the correlation by Fair (1993) is based on a small data set for columns of different geometries and operating conditions than the current column and requires a diffusion coefficients, which were calculated from another correlation (Lin and Tavlarides 2010). Considering these variations, the AARD seems reasonable.

The data for the correlation of Fair (1993) were generated from columns operating near flooding, which is known to be beneficial for mass transfer and was not observed in the collection of the current data. It is recommended that future extraction experiments include tests of higher flow rates to find the capacity limits of the column and likely improve the mass transfer. The current column entrance design appears to be limiting the flows to well below flooding, so the design will need modification prior to these tests.

A basic multiple linear regression was completed on the calculated extraction efficiency and ka data.

Both regressions showed that density, slurry solids content, and oil on solids were important process parameters and both regressions provide an estimate of extraction efficiency and *ka* that is an improvement over the average values. In particular, the AARD of the *ka* regression is 55.6 %. In the context of the substantial literature surrounding *ka* correlations for packed columns (typically ± 20 – 30 %), the regression result is very promising for the technology presented in this thesis.

While neither regression is currently suitable for prediction purposes, they can be used to inform recommendations on future work. Both regressions suggested an increase in slurry solids content and oil content on solids would improve extraction efficiency and *ka*. Increasing the slurry solids content would require adjustments in the current slurry feed

system to prevent the settling of solids in the piping. Increasing the oil content of the solids should not be prioritized for future experiments because any commercially viable system would need to handle a variety of cuttings with different oil contents.

While density was found to be an important factor in both regressions, they did not agree on whether increasing or decreasing density should be prioritized for future work. As extraction efficiency is the ultimate measure of system improvement, higher densities should be tested. Because temperature is harder to control on the current system the higher densities should be tested by increasing the system pressure.

The calculated ka values are ± 30 to 60 %.

The variation in calculated *ka* as a result of errors in process variable measurement, petroleum hydrocarbon analysis, and solubility calculation is on average ± 1 % to 48 %. Much higher maximum variations were found for errors in pressure and temperature measurement, but they were isolated to the extraction runs with the lowest density. The calculated *ka* values in those cases were conservative with respect to the pressure and temperature measurement errors. Further, the comparison of three runs with similar important process conditions (density, slurry solids content, and initial oil on solids) had an AARD of 10.4 %. Finally, the RSD on any single calculated *ka* ranged from 2.43 – 56.0 %. Because the column lacks a suitable slurry level measurement, the variation in calculated *ka* due to slurry level changes (changes to *H* in the *ka* calculation) was not considered. However, the reported *ka* values are conservative with respect to slurry level.

Chapter 5: Conclusions and Recommendations

The overall aim of the research was to demonstrate a continuous SFE process for the treatment of hydrocarbon-contaminated drill cuttings. Chapter 5 summarizes the conclusions and recommendations toward this goal.

5.1 Conclusions

The three objectives of this research have been fulfilled. Regarding the objectives, the following are the main claims of the thesis:

1. A pilot-scale, continuous SFE process for the extraction and recovery of hydrocarbons from drill cuttings was successfully built, commissioned, and operated.

Updated design work (modifications to flow specifications, lab layout, P&ID, control philosophy, operation manual and HAZOP) was completed successfully. Construction of the process was also successful, despite the challenges in procuring equipment for a novel SFE process at pilot-scale. A total of 82 experimental runs were completed, with the majority aimed at gathering data for mass transfer and control studies. Over the course of these runs, the process operated at pressures up to 17.9 MPa; temperatures up to 45.4°C; slurry flow rates from 2.0 to 3.4 $L \cdot min^{-1}$ at pump conditions; and CO_2 flow rates from 0.64 to 2.0 $L \cdot min^{-1}$ at pump conditions. The slurry solids concentration varied between 0.16 to 3 wt%. The experimental run durations varied from 7 to 43 minutes, with total run times of well over 1 h (start up, steady state, cleaning, shut down). The process successfully demonstrated extraction of hydrocarbon from slurried cuttings under safe and reliable operation. The novel SFE process built for this project, has been demonstrated to be a solution to the drill cuttings problem, and is a major step towards development of a commercial-scale process.

2. The solubility of drilling fluid D822 in SC CO_2 was successfully measured.

A semi-flow method for the measurement of drilling fluid solubility was successfully developed and validated against literature data for nC16. Using the developed method, the solubility of D822 in SC CO_2 was measured at 35 °C, 40 °C and 50 °C over 10.4 MPa to 24.2

MPa. The solubility of D822 increased with increasing pressure, to a maximum of 0.146 g·g^{-1} at 24.2 MPa at 40°C. The D822 solubility data were successfully modeled using the Chrastil equation, resulting in coefficients of A=-3513.53 K, B=-28.61, and C=5.58 with an AARD of 9.4 %. The Chrastil model is recommended for use in calculating solubilities of D822-like drilling fluids in SC CO_2. The Chrastil model was used to estimate the interfacial drilling fluid concentration when calculating mass transfer coefficients for the continuous SFE process.

3. The performance of the continuous SFE process was successfully quantified by extraction efficiency and overall volumetric mass transfer coefficient.

Chapter 4 provides a first quantification of the column performance from 15 extraction experiments that were completed on the extraction system presented in Chapter 2. The first successfully completed task towards quantifying the continuous SFE process performance was the adaptation of a cold-shake solvent extraction method from the literature to determine the hydrocarbon content of cuttings. The developed method met the recovery requirements for the CCME Canada-wide Standard for Petroleum Hydrocarbons in Soil and is faster, requires less consumables, and more suitable for high water content slurries than the Dean-Stark Method that was previously used to determine the hydrocarbon content of cutting.

The range of extraction efficiencies was from 36.6 to 95.8 %, with an overall average RSD of 18.2 %. The values are consistent with literature results for batch systems treating drill cuttings and drill cuttings slurries. The calculated *ka* values ranged from 1.21×10^{-5} s^{-1} to 9.69×10^{-4} s^{-1}, with an overall average RSD of 19.2 %. The novelty of the system prevents direct comparison to literature values, but the range is consistent in terms of order of magnitude with results from the lab-scale, batch SC CO_2 extraction of oil from cuttings and the lab-scale continuous SC CO_2 extraction of naphthalene from soil slurries. The experimental results were also roughly consistent with a mass transfer correlation from the literature for baffle tray columns in gas-liquid service. Considering the impacts of process variable measurement, petroleum hydrocarbon analysis, and solubility calculation as well as the range of the run average RSD values, the calculated ka values are ± 30 to 60 %.

The extraction efficiency and *ka* data were analysed using a linear regression. Both regressions showed that density, slurry solids content, and oil on solids were important process parameters and both regressions provide an estimate of extraction efficiency and ka that is an improvement over the average values.

5.2 Recommendations

The research has yielded the following recommendations for future work towards improving the continuous SFE process technology:

1. An appropriate slurry level measurement device or method should be found. A constant level of slurry will likely improve the column performance and will improve the consistency of the hydrocarbon extraction.
2. Higher flow rates of CO_2 and slurry should be tested to determine the column flooding limit. Operating near flooding is known to be beneficial for mass transfer. The current column entrance design appears to be limiting the flows to well below flooding, so the design will need modification prior to these tests.
3. Future experiments should prioritize increasing the slurry solids content and increasing density by testing higher pressures. Increasing the slurry solids content would require adjustments in the current slurry feed system to prevent the settling of solids in the piping.
4. The continuous SFE process developed should be tested for the removal of hydrocarbons from other soil slurries.

References

Advantage Mud Systems Ltd. n.d. Base Oil comparison for Invert Muds [online]. Available from http://www.advantagemud.com/documents/Pds/Oil%20Mud%20Products/Base%20Oils%20Inverts.pdf [cited December 22, 2016].

Aim, K., and Fermeglia, M. 2003. Solubility of Solids and Liquids in Supercritical Fluids. In The Experimental Determination of Solubilities, Wiley Series in Solution Chemistry Volume 6. Edited by G. T. Hefter and R. P. T. Tomkins. John Wiley & Sons, Ltd., Etobicoke, ON. pp. 493–555.

Alberta Energy Regulator (AER). 2019. Directive 050: Drilling Waste Management [online]. Available from https://www.aer.ca/documents/directives/Directive050.pdf [accessed 14 March 2020].

Akgerman, A., and Yeo, S. 1993. Supercritical Extraction of Organic Components from Aqueous Slurries. *In* Supercritical Fluid Engineering Science. *Edited by* E. Kiran et al. American Chemical Society, Washington, DC. pp. 294 – 304.

Bourgoyne Jr., A. T., Millheim, K. K., Chenevert, M. E., and Young Jr., F. S. 1986. Applied Drilling Engineering. Society of Petroleum Engineers, Richardson, TX.

Bravo, J. L., and Fair, J. 1982. Generalized Correlation for Mass Transfer in Packed Distillation Columns. Industrial & Engineering Chemistry Process Design and Development, **21**(1): 162 – 170.

Brunner, G. 2010. Applications of Supercritical Fluids. Annual Review of Chemical and Biomolecular Engineering, **1**: 321 – 342.

Brunner, G. 2005. Supercritical Fluids: Technology and Application to Food Processing. Journal of Food Engineering, **67**: 21 – 33.

Burke, J., and Veil, J. A. 1995. Synthetic-based Drilling Fluids have Many Environmental Pluses. Oil & Gas Journal, **93**(48): 59 – 64.

Canadian Association of Petroleum Producers (CAPP). 2019. Statistics: Wells and Metres/Feet Drilled by Province [online]. Available from https://www.capp.ca/resources/statistics/ [accessed 14 March 2020].

Canadian Council of Ministers of the Environment (CCME). 2008. Canada-Wide Standards for Petroleum Hydrocarbons (PHC) in Soil [online]. Available from https://www.ccme.ca/files/Resources/csm/phc_cws/phs_standard_1.0_e.pdf [accessed 28 April 2019].

Chandler, K., Pouillot, F. L. L., and Eckert, C. A. 1996. Phase Equilibria of Alkanes in Natural Gas Systems. 3. Alkanes in carbon dioxide. Journal of Chemical Engineering Data, **41**: 6–10.

Charoensombut-Amon, T., Martin, R. J., and Kobayashi, R. 1986. Application of a Generalized Multiproperty Apparatus to Measure Phase Equilibrium and Vapor Phase Densities ofSsupercritical Carbon Dioxide in n-Hexadecane Systems up to 26 MPa. Fluid Phase Equilibria, **31**: 89 – 104.

Chimowitz, E. H. 2005. Introduction to Critical Phenomena in Fluids. Oxford University Press, Don Mills, ON.

Chrastil, J. 1982. Solubility of Solids and Liquids in Supercritical Gases. Journal of Physical Chemistry, **86**(15): 3016 – 3021.

de Haan, A. B. 1991. Supercritical Fluid Extraction of Liquid Hydrocarbon Mixtures. PhD Thesis, Faculty of Chemical Technology and Materials Science, Delft University of Technology, Delft, Netherlands.

Dohrn, R., Peper, S., and Fonseca, J. M.S. 2010. High-pressure Fluid-Phase Equilibria: Experimental Methods and Systems Investigated (2000-2004). Fluid Phase Equilbria, **288**: 1–54.

D'Souza, R., Patrick, J. R., and Teja, A. S. 1988. High Pressure Phase Equilibria in the Carbon Dioxide - n-Hexadecane and Carbon Dioxide - Water Systems. The Canadian Journal of Chemical Engineering, **66**: 319 – 323.

Eldridge, R. B. 1996. Oil Contaminant Removal from Drill Cuttings by Supercritical Extraction. Industrial Engineering & Chemistry Research, **35**(6): 1901 – 1905.

Eppig, C. P., Putnam, B. M., de Filippi, R. P. 1984. Apparatus for Removing Organic Contaminants for Inorganic-rich Mineral Solids. US Patent #4,434,028

Esmaeilzadeh, F., Goodarznia, I., and Daneshi, R. 2008. Solubility Calculation of Oil-contaminated Drill Cuttings in Supercritical Carbon Dioxide using Statistical Associating Fluid Theory (PC-SAFT). Chemical Engineering Technology, **31**(1): 66 – 70.

Eustaquio-Rincón, R., and Trejo, A. 2001. Solubility of n-Octadecane in Supercritical Carbon Dioxide at 310, 313, 333, and 353 K, in the range 10-20 MPa. Fluid Phase Equilibria, **185**: 231 – 239.

Evans, D. F., Tominaga, T., and Chan, C. 1979. Diffusion of Symmetrical and Spherical Solutes in Protic, Aprotic, and Hydrocarbon Solvents. Journal of Solution Chemistry, **8**(6): 461 – 478.

Fair, J. R. 1993. How to Design Baffle Tray Columns. Hydrocarbon Processing, **75**(5): 75 – 80.

Fonseca, J. M. S., Dohrn, R., and Peper, S. 2011. High-pressure Fluid-phase Equilibria: Experimental Methods and Systems Investigated (2005–2008). Fluid Phase Equilibria, **300**: 1–69.

Fortin, M. M. 2003. Fully-Continuous Supercritical Fluid Extraction of Napthalene from Soil Slurries. M. Sc. Thesis, University of Guelph, Guelph, Canada.

Forsyth, V. C. 2006. Fully-Continuous Supercritical Fluid Extraction of PAHs from Soil Slurries. M. Sc. Thesis, University of Guelph, Guelph, Canada.

Gibsons Energy. 2016. D822 Safety Data Sheet [online]. Available from http://gibsons.msdsbinders.com/CustomBinder/ViewMsds/9199ec03-a796-40c4-8140-f7068c0cec7e/19783/Gibson%20D822%20-%20Gibson%20Energy%20Limited [accessed 27 June 2016].

Goodarznia, I., and Esmaeilzadeh, F. 2006. Treatment of Oil-contaminated Drill Cuttings of South Pars Gas Field in Iran using Supercritical Carbon Dioxide. Iranian Journal of Sciene and Technology Transaction B – Engineering, **30**(B5): 607 – 611.

Gupta, R. B., and Shim, J.-J. 2007. Solubility in Supercritical Carbon Dioxide. CRC Press, Boca Raton, Fla.

Hawari, J., Beaulieu, C., Ouellette, D., Pontbriand, Y., Halasz, A. M., and Van Tra, H. 1995. Determination of Petroleum Hydrocarbons in Soil: SFE versus Soxhlet and Water Effect on Recovery. International Journal of Environmental Analytical Chemistry, **60**(2-4): 123 – 137.

Holscher, I. F., Spee, M., and Schneider, G. M. 1989. Fluid-phase Equilibria of Binary and Ternary Mixtures of CO_2 with Hexadecane, 1-Dodecanol, 1-Hexadecanol, and 2-Ethoxy-ethanol at 333.2 K and 393.2 K and at Pressures up to 33 MPa. Fluid Phase Equilibria, **90**: 149 – 162.

Hunstman Corp. 2015. Products for Oilfield Applications [online]. Available at http://www.huntsman.com/performance_products/Media%20Library/global/files/Products%20for%20Oilfield%20Applications%202015%20brochure.pdf [accessed 28 April 2019].

International Association of Oil & Gas Producers (IAOGP). 2003. Environmental Aspects of the Use and Disposal of Non Aqueous Drilling Fluids Associated with Offshore Oil & Gas Operations [online]. Available from https://www.iogp.org/bookstore/product/environmental-aspects-of-the-use-and-disposal-of-non-aqueous-drilling-fluids-associated-with-offshore-oil-gas-operations/ [accessed 14 March 2020].

Jones, C. R. 2010. Treatment of Oily Drill Cuttings Slurries using Supercritical Carbon Dioxide. M.Sc. Thesis, Department of Civil and Environmental Engineering, University of Alberta, Edmonton, Alberta.

Kautz, C. B., Schneider, G. M., Shim, J.-J., Wagner, B., and Tuma, D. 2008. Solubilities of a 1,4-Bis(alkylamino)-9,10-anthaquinone series in Compressed Carbon Dioxide. Journal of Chemical Engineering Data, **53**: 2356 – 2371.

King, M. B., Kassim, K., Bott, T. R., Sheldon, J. R.,and Mahmud, R. S. 1984. Prediction of Mutual Solubilities of Heavy Components with Super-critical and Slightly Sub-critical Solvents: the Role of Equations of State and Some Applications of Simple Expanded Lattice Model at Subcritical Temperatures. Berichte der Bunsengesellschaft fur physikalische Chemie, **88**: 812 – 820.

Kolmetz, K., Sloley, A. W., Zygula, T. M., Ng, W. K., and Faessler, P. W. 2004. Design Guidelines for Distillation Columns in Fouling Service. *In* Proceedings of The 16th Ethylene Producers Conference, New Orleans, USA, April 26, 2004.

Kordikowski, A., and Schneider, G. M. 1993. Fluid Phase Equilibria of Binary andTternary Mixtures of Supercritical Carbon Dioxide with Low-volatility Organic Substances up to 100 MPa and 393 K: Cosolvency Effects and Miscibility Windows. Fluid Phase Equilibria, **90**: 149 – 162.

Kumar, S. K., and Johnston, K. P. 1988. Modelling the Solubility of Solids in Supercritical Fluids with Density as the Independent Variable. Journal of Supercritical Fluids, **1**: 15 – 22.

Lahiere, R. J., and Fair, J. R. 1987. Mass-Transfer Efficiencies of Column Contactors in Supercritical Extraction Service. Industrial & Engineering Chemistry Research, **26**(10): 2086 – 2092.

Laitinen, A. 1999. Supercritical Fluid Extraction of Organic Compounds from Solids and Aqueous Solutions. PhD Thesis, Department of Chemical Technology, University of Helsinki, Finland.

Laitinen, A., Michaux, A., and Aaltonen, O. 1994. Soil Cleaning by Carbon Dioxide Extraction: a Review. Environmental Technology, **15**(8): 715 – 727.

Larson, L. L., Silva, M. K., Taylor, M .A., and Orr, F. M. Jr. 1989. Temperature Dependence of L1/L2/V Behaviour in CO_2/Hydrocarbon Systems. SPE Reservoir Engineering, **4**: 106 – 114.

Lee, J. I., and Sigmund, P.M. 1979. Phase Behavior and Displacement Studies of Carbon Dioxide-Hydrocarbon Systems. Research report RR-37, Petroluem Research Institute, Calgary, Alberta.

Lin, R., and Tavlarides, L. L. 2010. Diffusion Coefficients of Diesel Fuel and Surrogate Compounds in Supercritical Carbon Dioxide. Journal of Supercritical Fluids, **52**(1): 47 – 55.

Lopes, B. L. F., Sánchez-Camargo, A. P., Ferreira, A. L. K., Grimaldi, R., Paviani, L. C., and Cabral, F. A. 2012. Selectivity of Supercritical Carbon Dioxide in the Fractionation of Fish Oil with a Lower Content of EPA+DHA. Journal of Supercritical Fluids, **61**: 78–85.

Lopez Gomez, J. J. 2004. The Use of Supercritical Fluid Extraction for the Treatment of Oil Contaminated Drilling Waste. M.Sc. Thesis, Department of Civil and Environmental Engineering, University of Alberta, Edmonton, Alberta.

Ma, B., Wang, R., Ni, H., and Wang, K. 2019. Experimental study on Harmless Disposal of Waste Oil Based Mud Using Supercritical Carbon Dioxide Extraction. Fuel, **252**: 722 – 729.

Massetti, F., Nardella, A., Raffaele, T., and Guarneri, A. 2006. Method for the Removal and Recovery of the Oily Component of Drill Cuttings using Liquid CO_2. United States Patent #7,128,169.

McHugh, M. A., and Krukonis, V. J. 1994. Supercritical Fluid Extraction: Principles and Practice, second edition. Butterworth-Heinemann, Boston, MA.

Montero, G. A., Giorgio, T. D., and Schnelle, K. B. 1996. Scale-up and Economic Analysis for the Design of Supercritical Fluid Extraction Equipment for Remediation of Soil. Environmental Progress, **15**(2): 112 – 121.

National Energy Board, Canada-Nova Scotia Offshore Petroleum Board, and Canada-Newfoundland and Labrador Offshore Petroleum Board. 2010. Offshore Waste

Treatment Guidelines [online]. Available at https://www.cer-rec.gc.ca/bts/ctrg/gnthr/2010ffshrwstgd/2010ffshrwstgd-eng.pdf [accessed 14 March 2020].

Nieuwoudt, I., and du Rand, M. 2002. Measurement of Phase Equilibria of Supercritical Carbon Dioxide and Paraffins. Journal of Supercritical Fluids, **22**: 185 – 199.

Odusanya, O. O. 2003. Supercritical Carbon Dioxide Treatment of Oil Contaminated Drill Cuttings. M.Sc. Thesis, Department of Civil and Environmental Engineering, University of Alberta, Edmonton, Alberta.

Onda, K., Takeuchi, H., and Okumoto, Y. 1968. Mass Transfer Coefficients Between Gas and Liquid in Packed Columns. Journal of Chemical Engineering of Japan, **1**(1): 56 – 62.

Phelps, C. L., Smart, N. G., and Wai, C. M. 1996. Past, Present, and Possible Future Applications of Supercritical Fluid Extraction Technology. Journal of Chemical Education, **73** (12): 1163 – 1168.

Ran, H. B., Sabet, J. K., and Varaminian, F. 2019. Study of Solubility in Supercritical Fluids: Thermodynamic Concepts and Measurement Methods – A Review. Brazilian Journal of Chemical Engineering **36**(4): 1367 – 1392.

Railroad Commission of Texas (RCT). 2001. Waste Minimization in the Oil Field [online]. Available from https://www.rrc.state.tx.us/media/5707/wastemin.pdf [accessed 14 March 2020].

Restek Corp. 2002. Technical Guide, Operating Hints for Using Split/Splitless Injectors [online]. Available from https://www.restek.com/pdfs/59880A.pdf [accessed 28 April 2019].

Reverchon, E., Russo, P., and Stassi, A. 1993. Solubilities of Solid Octacosane and Triacontane in Supercritical Carbon Dioxide. Journal of Chemical & Engineering Data, **38**: 458 – 460.

Roodpeyma, M. 2017. Development, Modelling and Control of a Continuous Pilot Scale Supercritical Fluid Extraction Process. PhD Thesis. Department of Civil & Environmental Engineering, University of Alberta, Edmonton, Alberta, Canada.

Rosenthal, A. 2012. Safe Design of a Continuous Supercritical Extraction System for the Extraction of Drilling Fluid from Drill Cuttings. M.Sc. Thesis, Department of Engineering, University of Guelph, Guelph, Ontario, Canada.

Saldana, M. D. A., Nagpal, V., and Guigard, S. E. 2005. Remediation of Contaminated Soils using Supercritical Sluid Extraction: A Review (1994-2004). Environmental Technology **26**: 1013 – 1032.

Saintpere, S., and Morillon-Jeanmaire, A. 2000. Supercritical CO_2 Extraction Applied to Oily Drill Cuttings. *In* Proceedings of 2000 SPE Annual Technical Conference and Exhibition, Dallas, Texas, Oct. 1–4, 2000, SPE #63126.

Seaton, S., and Hall, J. 2005. Recovery of Oil from Drilled Cuttings by Liquefied Gas Extraction. *In* SPE International Symposium on Oilfield Chemistry, Houston, TX, 2 – 4 February 2005.

Seaton, S., Morris, R., Blonquist, J., and Hogan, B. 2006. Analysis of Drilling Fluid Base Oil Recovered from Drilling Waste by Thermal Desorption. *In* 13th International Petroleum Environmental Conference, San Antonio, TX, 16 – 19 October 2006.

Shi, Q., Jing, L., and Qiao, W. 2015. Solubility of n-Alkanes in Supercritical CO_2 at Diverse Temperature and Pressure. Journal of CO_2 Utilization, **9**: 29 – 38.

Sigma-Aldrich. 2014. Hexadecane Safety Data Sheet [online]. Available from http://www.sigmaaldrich.com/MSDS/MSDS/DisplayMSDSPage.do?country=CA&language=en&productNumber=H0255&brand=SIGMA&PageToGoToURL=http%3A%2F%2Fwww.sigmaaldrich.com%2Fcatalog%2Fproduct%2Fsigma%2Fh0255%3Flang%3Den, [accessed 17 October 2016].

Schmitt, W. J., and Reid, R. C. 1988. The Solubility of Paraffinic Hydrocarbons and Their Derivatives in Supercritical Carbon Dioxide. Chemical Engineering Communications, **64**: 155–176.

Schwab, A. P., Su, J., Wetzel, S., Pekarek, S., and Banks, M. K. 1999. Extraction of Petroleum Hydrocarbons from Soil by Mechanical Shaking. Enivronmental Science & Technology, **33**(11): 1940 – 1945.

Škerget, M., Knez, Z., and Knez-Hrnčič, M. 2011. Solubility of Solids in Sub- and Supercritical Fluids: a Review. Journal of Chemical Engineering Data, **56**: 694–719.

Span, R., and Wagner, W. 1996. A New Equation of State for Carbon Dioxide Covering the Fluid Region from the Triple-Point Temperature to 1100 K at Pressures up to 800 MPa. Journal of Physical and Chemical Reference Data, **25**(6): 1509 – 1596.

Spycher, N., Pruess, K., and Ennis-King, J. 2003. CO_2-H_2O Mixtures in the Geological Sequestration of CO_2. I. Assessment and Calculation of Mutual Solubilities from 12 to 100°C and up to 600 bar. Geochimica and Cosmochimica Acta, 67(16): 3015 – 3031.

Street, C. G. 2008. Extraction of Hydrocarbons from Drilling Waste Using Supercritical Carbon Dioxide. M.Sc. Thesis, Department of Civil and Environmental Engineering, University of Alberta, Edmonton, Alberta.

Street, C. G., Guigard, S. E., Kapila, M., Smith, A., Bingham, R., and Stiver, W. H. 2013. Mass Transfer Coefficients for the Removal of Oil from Drill Cuttings Using Supercritical

Carbon Dioxide. *In* Proceedings of the Tenth Conference on Supercritical Fluids and Their Applications, Naples, Italy. April 29 – May 6, 2013, pp. 427 – 432.

Thar Process. 2019. Thar Process, Inc. and 51st Parallel Inc. Announce the Creation of Canada's Largest Cannabinoid-Based Toll Processor: Thar Extracts Alberta ULC [online]. Available at https://www.prnewswire.com/news-releases/thar-process-inc-and-51st-parallel-inc-announce-the-creation-of-canadas-largest-cannabinoid-based-toll-processor-thar-extracts-alberta-ulc-300976143.html [accessed 14 March 2020].

Tunnicliffe, I., and Joy, R. M. 2007. Cleaning and Supercritical Cleaning of Hydrocarbon-containing Materials. United States Patent #7,175,716.

United States Environmental Protection Agency (USEPA). 2019. Management of Exploration, Development and Production Wastes: Factors Informing a Decision on the Need for Regulatory Action [online]. Available from https://www.epa.gov/sites/production/files/2019-04/documents/management_of_exploration_development_and_production_wastes_4-23-19.pdf [accessed 14 March 2020].

USEPA. 2011. Regulating Petroleum Industry Wastewater Discharges in the United States and Norway [online]. Available from https://nepis.epa.gov/Exe/ZyPDF.cgi/P100B9AW.PDF?Dockey=P100B9AW.PDF [accessed 14 March 2020].

USEPA. 2007. Method 3350C Ultrasonic Extraction [online]. Available at https://www.epa.gov/sites/production/files/2015-12/documents/3550c.pdf [accessed 14 March 2020].

USEPA. 2000. Profile of the Oil and Gas Extraction Industry [online]. Available from https://archive.epa.gov/compliance/resources/publications/assistance/sectors/web/pdf/oilgas.pdf [accessed 14 March 2020].

Veil, J. A. 2002. Drilling Waste Management: Past, Present, and Future. *In* SPE Annual Technical Conference and Exhibition, San Antonio, TX, 29 September – 2 October 2002.

Venter, M. J., Willems, P., Kareth, S., Weidner, E., Kuipers, N. J. M., and de Haan, A. B. 2007. Phase Equilibria and PhysicalPproperties of CO_2-saturated Cocoa Butter Mixtures at Elevated Pressures. Journal of Supercritical Fluids, 41: 195 – 203.

Wang, G. Q., Yuan, X. G., and Yu, K. T. 2005. Review of Mass-Transfer Correlations for Packed Columns. Industrial & Engineering Chemistry Research, **44**(23): 8715 – 8729.

Whittaker A. 1985. The Mud Circulating System. *In* Theory and Applications of Drilling Fluid Hydraulics. *Edited by* A. Whittaker. The EXLOG Series of Petroleum Geology and Engineering Handbooks, vol 1. Springer, Dordrecht, Netherlands.

Zhao, S., and Zhang, D. 2014. An Experimental Investigation into the Solubility of *Moringa oleifera* Oil in Supercritical Carbon Dioxide. Journal of Food Engineering, **138**:1–10.

Zupan, T., and Kapila, M. 2000. Thermal Desorption of Drill Muds and Cuttings in Ecuador: the Environmentally and Financially Sound Solution. *In* SPE International Conference on Health, Safety & Environment in Oil & Gas Exploration and Production, Stavanger, Norway, 26 – 28 June 2000.

Zytner, R. G., Salb, A., Brook, T. R., Leunissen, M., and Stiver, W. H. 2001. Bioremediation of Diesel Fuel Contaminated Soil. Canadian Journal of Civil Engineering, **28**(suppl. 1): 131 – 140.

Appendix A: Line Specifications

Appendix Table A.1: Line specification in the SFE process

Item	Drawing reference	Description	Supplier	Service	Material
12.7 mm (½″) flexible hose	LN-2001	Connected directly after the CO_2 tank	Swagelok	CO_2	Plastic
19.1 mm (¾″) tubing (2.8 mm wall thickness)	LN-2002	CO_2 tank to CO_2 pump rigid line	Pinacle/ Swagelok	CO_2	SS
19.1 mm (¾″) tube	LN-2003	Cauldron brass tubing	Swagelok	CO_2	Brass
12.7 mm (½″) flexible hose	LN-2004	Coming out of the cauldron	Swagelok	CO_2	Plastic
6.4 mm (¼″) tubing (1.7 mm wall thickness)	LN-2005	CO_2 pump to extraction vessel main line	Pinacle/ Swagelok	CO_2	SS
3.2 mm (1/8)″ tubing (0.7 mm wall thickness)	LN-2006	Extended CO_2 inlet line in to the extraction vessel	Pinacle/ Swagelok	CO_2	SS
6.4 mm (¼″) tubing (1.7 wall thickness)	LN-2007	Extraction vessel by-pass line	Pinacle/ Swagelok	CO_2	SS
50.8 mm (2″) flexible hose	LN-3001	Outlet of slurry tank FT-3601	Mcmaster-Carr	Slurry	Plastic
50.8 mm (2″) flexible hose	LN-3002	Outlet of slurry tank FT-3602	Mcmaster-Carr	Slurry	Plastic
50.8 mm (2″) flexible hose	LN-3003	Outlet of water tank FT-3603	Mcmaster-Carr	Slurry	Plastic
50.8 mm (2″) nipples, elbows and tees	LN-3004	Rigid line after FT-3602	Pinacle	Slurry	SS
50.8 mm (2″) nipples, elbows and tees	LN-3005	Rigid line after FT-3601	Pinacle	Slurry	SS
50.8 mm (2″) nipples, elbows and tees	LN-3006	Rigid line after FT-3603	Pinacle	Slurry	SS
50.8 mm (2″) nipples, elbows and tees	LN-3007	Rigid joint line after FT-3601 and FT-3602	Pinacle	Slurry	SS
50.8 mm (2″) nipples, elbows and tees	LN-3008	Slurry pump inlet	Pinacle	Slurry	SS
19.1 mm (¾″) tubing (2.8 mm wall thickness)	LN-3009	Slurry pump outlet	Pinacle/ Swagelok	Slurry	SS
19.1 mm (¾″) tubing (2.8 mm wall thickness)	LN-3010	Slurry/water tank by-pass line	Pinacle/ Swagelok	Slurry	SS
9.5 mm (3/8″) flexible hose	LN-3011	Flexible line at the end of 9.6 mm (¾″) slurry line (LN-3009)	Swagelok	Slurry	Plastic

Appendix Table A.1: Line specifications in the SFE process, continued

Item	Drawing reference	Description	Supplier	Service	Material
6.4 mm (¼″) tubing (1.7 wall thickness)	LN-3012	Slurry inlet to extraction vessel	Pinacle/ Swagelok	Slurry	SS
6.4 mm (¼″) tubing (1.7 wall thickness)	LN-4001	CO_2 outlet from extraction vessel	Pinacle/ Swagelok	CO_2/Oil	SS
6.4 mm (¼″) tubing (1.7 wall thickness)	LN-4002	CO_2 line after bypass and into separator	Pinacle/ Swagelok	CO_2/Oil	SS
9.5 mm (3/8″) tubing	LN-4003	High pressure line in and out of the metering valve (MV-4303)	Zimco	CO_2/Oil	SS
3.2 mm (1/8)″ tubing (0.7 mm wall thickness)	LN-4004	CO_2 inlet extended tubing into separator	Swagelok	CO_2/Oil	SS
3.2 mm (1/8)″ tubing (0.7 mm wall thickness)	LN-4005	Product out extended tubing from separator	Swagelok	Oil	SS
6.4 mm (¼″) tubing (1.7 wall thickness	LN-4006	Product main line out from separator	Pinacle/ Swagelok	Oil	SS
3/8″ flexible and removable hose	LN-4007	Required for pumping out oil from separator	Fisher	Oil	Plastic
6.4 mm (¼″) tubing (1.7 wall thickness)	LN-4008	CO_2 outlet line from separator	Pinacle/ Swagelok	CO_2	SS
6.4 mm (¼″) tubing (1.7 wall thickness)	LN-4009	Separator by-pass line	Pinacle/ Swagelok	CO_2/Oil	SS
6.4 mm (¼″) tubing (1.7 wall thickness)	LN-4010	CO_2 line to fume hood	Pinacle/ Swagelok	CO_2/Oil	SS
3.2 mm (1/8)″ tubing (0.7 mm wall thickness)	LN-5001	Manifold	Pinacle/ Swagelok	Slurry/CO_2	SS
6.4 mm (¼″) tubing (1.7 wall thickness)	LN-5002	Extraction vessel to LN-5003	Pinacle/ Swagelok	Slurry/CO_2	SS
19.1 mm (¾″) tubing (2.8 mm wall thickness)	LN-5003	LN-5002 to slurry tanks	Pinacle/ Swagelok	Slurry/CO_2	SS

Appendix B: Valve Specifications

Appendix Table B.1: Valve specification in the SFE process

Item	Drawing reference	Location	Function	Service	Supplier
6.4 mm (¼″) relief valve	RV-1301	Extraction vessel (top)	Pressure relief	CO_2/Slurry	Swagelok
6.4 mm (¼″) relief valve	RV-1302	Extraction vessel (bottom	Pressure relief	CO_2/Slurry	Swagelok
19.1 mm (¾″) check valve	CV-2301	LN-2002	Flow direction	CO_2	Swagelok
6.4 mm (¼″) check valve	CV-2302	LN-2005	Flow direction	CO_2	Swagelok
6.4 mm (¼″) relief valve	RV-2303	LN-2005	Pressure relief	CO_2	Swagelok
6.4 mm (¼″) ball valve	BV-2304	LN-2005	Isolation	CO_2	Swagelok
6.4 mm (¼″) ball valve	BV-2305	LN-2007	Isolation	CO_2	Swagelok
19.1 mm (¾″) ball valve	BV-2306	LN-2002	Isolation	CO_2	Swagelok
19.1 mm (¾″) relief valve	RV-2307	LN-2002	Pressure relief	CO_2	Praxair
19.1 mm (¾″) relief valve	RV-2308	CO_2 pump	Pressure relief	CO_2	Cat pumps
19.1 mm (¾″) ball valve	BV-2309	LN-2002	Drain	CO_2	Swagelok
6.4 mm (¼″) ball valve	BV-2310a	LN-2005	Drain	CO_2	Swagelok
6.4 mm (¼″) three-way ball valve	BV-2310b	LN-2005	Back pressure prevention	CO_2	Swagelok
50.8 mm (2″) ball valve	BV-3301	LN-3005	Isolation	Slurry	Pinacle
50.8 mm (2″) ball valve	BV-3302	LN-3004	Isolation	Slurry	Pinacle
19.1 mm (¾″) relief valve	RV-3304	LN-3009	Relief of pressure	Slurry	Pumps and pressure
19.1 mm (¾″) check valve	CV-3305	LN-3009	Flow direction	Slurry	Western Gauge and Instruments Ltd.
19.1 mm (¾″) ball valve	BV-3306	LN-3009	Isolation	Slurry	Swagelok
19.1 mm (¾″) ball valve	BV-3307	LN-3010	Isolation	Slurry	Pinacle
19.1 mm (¾″) ball valve	BV-3308	LN-3010	Isolation	Slurry	Swagelok
50.8 mm (2″) ball valve	BV-3309	LN-3006	Isolation	Slurry	Pinacle
19.1 mm (¾″) ball valve	BV-3310	LN-3010	Isolation	Slurry	Swagelok

Appendix Table B.1: Valve specification in the SFE process, continued

Item	Drawing reference	Location	Function	Service	Supplier
19.1 mm (¾″) ball valve	BV-3311	LN-5003	Isolation	Slurry/CO_2	Swagelok
19.1 mm (¾″) ball valve	BV-3312	LN-3010	Isolation	Slurry	Swagelok
19.1 mm (¾″) ball valve	BV-3313	LN-5003	Isolation	Slurry/CO_2	Swagelok
50.8 mm (2″) check valve	CV-3314	LN-3006	Flow direction	Slurry	Pinacle
50.8 mm (2″) ball valve	CV-3315	LN-3005	Flow direction	Slurry	Pinacle
50.8 mm (2″) ball valve	CV-3316	LN-3004	Flow direction	Slurry	Pinacle
6.4 mm (¼″) ball valve	BV-3317	LN-3012	Isolation	Slurry	Swagelok
50.8 mm (2″) ball valve	BV-3318	LN-3008	Drain	Slurry	Pinacle
19.1 mm (¾″) ball valve	BV-3319	LN-3009	Drain	Slurry	Pinacle
50.8 mm (2″) plastic ball valve	BV-3320	FT-3601	Isolation	Slurry	McMaster-Carr
50.8 mm (2″) plastic ball valve	BV-3321	FT-3602	Isolation	Slurry	McMaster-Carr
50.8 mm (2″) plastic ball valve	BV-3322	FT-3603	Isolation	Slurry	McMaster-Carr
6.4 mm (¼″) ball valve	BV-4301	LN-4001	Isolation	CO_2	Swagelok
6.4 mm (¼″) ball valve	BV-4302	LN-4009	Isolation	CO_2	Swagelok
9.5 mm (3/8″) metering valve	MV-4303	LN-4003	Metering	CO_2	Autoclave
6.4 mm (¼″) relief valve	RV-4304	Separator	Pressure relief	CO_2	Swagelok
6.4 mm (¼″) ball valve	BV-4305	LN-4006	Isolation	CO_2	Swagelok
6.4 mm (¼″) ball valve	BV-4306	LN-4002	Isolation	CO_2	Swagelok
6.4 mm (¼″) ball valve	BV-4307	LN-4008	Isolation	CO_2	Swagelok
6.4 mm (¼″) ball valve	BV-5301	LN-5001	Isolation	Slurry/CO_2	Swagelok
6.4 mm (¼″) ball valve	BV-5302a	LN-5002	Manifold	Slurry/CO_2	Swagelok
6.4 mm (¼″) ball valve	BV-5302b	LN-5002	Manifold	Slurry/CO_2	Swagelok

Appendix Table B.1: Valve specification in the SFE process, continued

Item	Drawing reference	Location	Function	Service	Supplier
6.4 mm (¼″) ball valve	BV-5302c	LN-5002	Manifold	Slurry/CO_2	Swagelok
6.4 mm (¼″) ball valve	BV-5303	LN-5001	Drain	Slurry/CO_2	Swagelok

Appendix C: Instrumentation Specifications

Appendix Table C.1: Instrumentation specification in SFE process

Item	Drawing reference	Location	Function	Supplier	Temperature rating (°C)	Pressure rating (MPa)
Level sensor	LI-1401	Extraction vessel	IRC (on/off)	Corr Instruments	0 to 100	44.8
Pressure sensor	PI-1402	Extraction vessel	IRC	Digikey	-40 to 125	34.5
Temperature sensor	TI-1403	Extraction vessel	IRC	Omega	J type	N/A
Pressure sensor	PI-1404	Extraction vessel	IRC	Omega	15 to 70	34.5
Level sensor	LI-1405	Extraction vessel	IRC (on/off)	Corr Instruments	0 to 100	44.8
Level sensor	LI-1406	Extraction vessel	RC (on/off)	Corr Instruments	0 to 100	44.8
Temperature gauge	TI-1407	Extraction vessel	I	McMaster-Carr	0 to 100	N/A
Temperature gauge	TI-1408	Extraction vessel	I	McMaster-Carr	0 to 100	N/A
Temperature gauge	TI-1409	Extraction vessel	I	McMaster-Carr	0 to 100	N/A
Temperature sensor	TI-1410	Extraction vessel	IR	Omega	J type	N/A
Heating tape	HX-1411	Extraction vessel (bottom)	C (on/off)	Omega	232 (max)	N/A
Pressure sensor	PI-2403	CO_2 pump	I	Cat pumps	N/A	68.9
Temperature sensor	TI-2404	LN-2002	IR	Omega	J type	N/A
Pressure sensor	PI-2405	LN-2002	IR	Digikey	-40 to 125	34.4
Pressure sensor	PI-2406	LN-2005	IRC	Wika	0 to 50	34.4
Temperature sensor	TI-2407	LN-2005	IR	Omega	J type	N/A
Temperature sensor	TI-2408	LN-2005	IR	Omega	J type	N/A
Chiller	HX-2409	CO_2 pump	IC	Cole-Parmer	-35 to 100	N/A
Cauldron (dry ice)	HX-2410	LN-2003	C	N/A	Optional based on amount of dry ice used	N/A
Temperature sensor	TI-3401	FT-3601	IR	Omega	J type	N/A
Temperature sensor	TI-3402	FT-3602	IR	Omega	J type	N/A

Appendix Table C.1: Instrumentation specification in SFE process, continued

Item	Drawing reference	Location	Function	Supplier	Temperature rating (°C)	Pressure rating (MPa)
Level switch	LI-3403	FT-3601	IR (on/off)	Omega	N/A	N/A
Level switch	LI-3404	FT-3602	IR (on/off)	Omega	N/A	N/A
Pressure sensor	PI-3405	LN-3008	IR	Omega	15 to 70	34.4
Pressure sensor	PI-3406	LN-3009	IRC	Omega	15 to 70	34.4
Flow meter	FI-3407	LN-3008	IRC	Simark Controls	-20 to 80	0.1 – 3
Temperature sensor	TI-3407	LN-3008	IR	Omega	J type	N/A
Level switch	LI-3408	FT-3603	IR (on/off)	Omega	N/A	N/A
Temperature sensor	TI-3410	LN-3009	IR	Omega	J type	N/A
Temperature sensor	TI-3411	FT-3603	IR	Omega	J type	N/A
Pressure sensor	PI-4402	Separator	IRC	Digikey	-40 to 125	34.4
Temperature sensor	TI-4403	Separator	IR	Omega	J type	N/A
Pressure sensor	PI-4406	LN-4002	I	Swagelok	N/A	34.4
Heating tape	HX-4407	MV-4303	C (on/off)	Omega	N/A	N/A
Heating tape	HX-4408	LN-4002	C	Omega	232 (max)	N/A
Temperature sensor	TI-5401	LN-5003	IR	Omega	J type	N/A
Pressure sensor	PI-5403	LN-5003	IR	Omega	15 to 70	34.4
Pressure sensor	PI-5404	LN-5001	I	Swagelok	N/A	6.9

Appendix D: List of Priority 1, 2, 3, and 4 Alarms

Appendix Table D.1: List of Priority 1, 2, 3, and 4 alarms in the SFE process

Alarm ID	Condition	Action	Related to
Priority 1 alarm			
EAH1-CO_2	CO_2 Level > 9,500 ppm	System is interlocked to shut down and the control system to operate in Emergency mode. (Kill switch should be used if automated shutdown fails.)	The Lab
Priority 2 alarms			
PAH2-1402	27 MPa < PI-1402	System is interlocked to shut down and the control system to operate in Emergency mode. (Kill switch should be used if automated shutdown fails.)	Extraction vessel
PAH2-2406	27 MPa < PI-2406	System is interlocked to shut down and the control system to operate in Emergency mode. (Kill switch should be used if automated shutdown fails.)	CO_2 Pump Outlet
PAH2-3406	27 MPa < PI-3406	System is interlocked to shut down and the control system to operate in Emergency mode. (Kill switch should be used if automated shutdown fails.)	Slurry Pump Outlet
PAH2-4402	20 MPa < PI-4402	System is interlocked to shut down and the control system to operate in Emergency mode. (Kill switch should be used if automated shutdown fails.)	Separator
TAH2-1403	85 °C < TI-1403	System is interlocked to shut down and the control system to operate in Emergency mode. (Kill switch should be used if automated shutdown fails.)	Extraction Vessel
LAH2-1401	LI-1401 activated	System is interlocked to shut down and the control system to operate in Emergency mode. (Kill switch should be used if automated shutdown fails.)	Extraction Vessel
Priority 3 alarms			
PAH3-1402	22 MPa < PI-1402	Troubleshoot for blockages or other failures. Shutdown if there is evidence of a blockage or unable to correct condition. Correct pressure if no evidence of blockage or other failure: change pressure set-point, open BV-4303 to relieve pressure, switch restrictor	Extraction vessel
PAH3-2405	3.1 MPa < PI-2405	Shutdown (because relief valve is not working correctly)	CO_2 Pump Inlet
PAL3-2405	PI-2405 < 2.5 MPa	Shutdown immediately and ensure sufficient CO_2 available.	CO_2 Pump Inlet
PAH3-2406	22 MPa < PI-2406	Troubleshoot for blockages or other failures. Shutdown if there is evidence of a blockage or unable to correct condition. Correct pressure if no evidence of blockage or other failure: change pressure set-point, open BV-4303 to relieve pressure, switch restrictor	CO_2 Pump Outlet
TAL3-1410	TI-2407 < 31 °C	Check related cooling and heating facilities. Shutdown if abnormal condition is not corrected or if temperature decreases.	CO_2 Pump Outlet

Appendix Table D.1: List of priority 1, 2, 3, and 4 alarms in the SFE process, continued

Alarm ID	Condition	Action	Related to
TAH3-2407	60 °C < TI-2407	Check related cooling and heating facilities. Shutdown if abnormal condition is not corrected or if temperature increases. If no failure is found and extraction vessel temperature is safe and stable, the experiment may continue.	CO_2 Pump Outlet
PAH3-3406	22 MPa < PI-3406	Troubleshoot for blockages or other failures. Shutdown if there is evidence of a blockage or unable to correct condition. Correct pressure if no evidence of blockage or other failure: change pressure set-point, open BV-4303 to relieve pressure, switch restrictor	Slurry Pump Outlet
TAH3-3410	60 °C < TI-3410	Check related cooling and heating facilities. Shutdown immediately if abnormal condition is not corrected or if temperature increases above 85 C. If no failure is found and extraction vessel temperature is safe and stable, the experiment may continue.	Slurry Pump Outlet
PAH3-4402	8 MPa < PI-4402	Troubleshoot for blockages or other failures. Shutdown if there is evidence of a blockage or unable to correct condition. Correct pressure if no evidence of blockage or other failure: change pressure set-point, open BV-4303 to relieve pressure.	Separator
TAL3-4403	TI-4403 < 0 °C	Increase temperature of heating jacket on metering valve. Shutdown if abnormal condition is not corrected or if temperature decreases.	Separator
LAL3-3408	LI-3408 on in water tank	Shutdown. Or quickly add some water to the water tank.	Slurry Pump Inlet
TAH3-1403	60 °C < TI-1403	Shutdown if abnormal condition is not corrected or if temperature approaches 85 °C. If no failure is found and extraction vessel temperature is safe and stable, the experiment may continue.	Extraction vessel
PAL3-4402	PI-4402 < 1 MPa	Shut down if abnormal condition is not corrected or if pressure is still decreasing during normal operations	Separator
Priority 4 alarms			
PAL4-1402	PI-1402 < 6 MPa	Troubleshoot for blockages, leaks or other failures. Shutdown if there is evidence of a blockage or unable to correct condition. Correct pressure if no evidence of blockage or other failure: change pressure set-point, change setting of BV-4303 to increase pressure, ensure adequate CO_2 supply available	Extraction vessel
LAH4-1405	LI-1405 is on (i.e., level past 16 cm)	Ensure the system is responding correctly: slurry exit flow should be greater than delivery flow. Troubleshoot for evidence of blockages or leaks. Shutdown if level does not decrease or if slurry exit flow is less than delivery flow.	Extraction vessel

Appendix Table D.1: List of priority 1, 2, 3, and 4 alarms in the SFE process, continued

Alarm ID	Condition	Action	Related to
LAL4-1406	LI-1406 is off (i.e., level is below 5 cm)	Ensure the system is responding correctly: slurry exit flow should be less than delivery flow. Troubleshoot for evidence of blockages or leaks. Shutdown if level does not increase or if slurry exit flow is greater than delivery flow or if CO_2 continuously escapes from slurry return line.	Extraction vessel
FAHL4-3407	FI-3407 (mass flow) is: (+/- 30%) of flow indicated by slurry pump RPM	Watch slurry level and pump RPM. Verify the sensors are working correctly. Ensure the system is responding correctly to extraction vessel pressure and slurry level.	Slurry Pump Inlet

Appendix E: Overall Volumetric Mass Transfer Sample Calculations

This appendix provides sample calculations for the overall volumetric mass transfer coefficients. One sample of Run 35 (Table 4.5) is considered.

Recall from Chapter 4 that the equation to calculate *ka* is:

$$ka = \frac{-Q \ln\left(\frac{C^* - C}{C^*}\right)}{A_x H \rho}$$

where Q is the mass flow of CO_2 through the column ($g_{CO2} \cdot s^{-1}$), C is the concentration of oil in the CO_2 exiting the column ($g_{oil} \cdot g_{CO2}^{-1}$), C^* is the interface mass fraction of oil in the CO_2 ($g_{oil} \cdot g_{CO2}^{-1}$), A_x is the cross-sectional area of the column (m^2), ρ is the CO_2 density at column conditions ($g \cdot m^{-3}$), and H is the height of the column (m). Q is calculated by converting the motor speed of the CO_2 pump to a mass flow rate using the volume of the pistons and the CO_2 density at the pumping conditions, provided by the Fundamental Equation of State (Span and Wagner 1996).

For Run 35 (Table 4.5), Q = 16.9 $g_{CO2} \cdot s^{-1}$. For the extraction conditions of 13.5 MPa and 41.3 °C, ρ=742.89 $kg \cdot m^{-3}$ (742 890 $g \cdot m^{-3}$) from the Fundamental Equation of State (Span and Wagner 1996). A_x was taken from the engineering drawings provided for the column as 0.0055 m^2. H was taken to be 2.2 m, which was determined from the drawings minus a small adjustment for the slurry and CO_2 inlet depths.

C^* can be determined from the Chrastil correlation determined in Chapter 3 wherein C^* is equivalent to y. Recall from Chapter 3, the linear form of the Chrastil equation is:

$$\ln y = C \ln \rho + \left(\frac{A}{T} + B\right)$$

where y is the solubility of solute (either $g \cdot g^{-1}$ or $mol \cdot mol^{-1}$), ρ is the density of the supercritical solvent ($kg \cdot m^{-3}$), T is the temperature (K), and A (K), B (unitless), and C (unitless) are constants. The results of Chapter 3 found A=-3513.53 K, B=-28.61, and C=5.58 for D822 solubility in supercritical carbon dioxide. For the extraction conditions of Run 35:

$$\ln y = 5.58 \ln(742.89 \text{ kg} \cdot \text{m}^{-3}) + \left(\frac{-3513.53 \text{ K}}{(41.3 + 273.15)\text{K}} - 28.61\right)$$

$$\ln y = -2.896$$

$$y = 0.0552 \text{ g}_{oil} \cdot \text{g}_{CO2}^{-1} = C^*$$

C is the concentration of oil in the exiting CO_2 flow from the column and is calculated as:

$$C = \frac{Q_{sl}\left(C_{sl,in} - C_{sl,out}\right)}{Q}$$

where Q_{sl} is the mass flow of slurry through the column ($g_{sl} \cdot s^{-1}$), $C_{sl,in}$ is the mass fraction of oil in the slurry entering the column ($g_{oil} \cdot g_{sl}^{-1}$), and $C_{sl,out}$ is the mass fraction of oil in the slurry leaving the column ($g_{oil} \cdot g_{sl}^{-1}$). The slurry flow rate is calculated by converting the motor speed of the slurry pump to a mass flow rate using the volume of the pistons and assuming a slurry density of 1 $g \cdot mL^{-1}$. For Run 35, Q_{sl} = 45.2 $g_{sl} \cdot s^{-1}$. From the petroleum hydrocarbon analysis, $C_{sl,in}$ = 0.000503 $g_{oil} \cdot g_{sl}^{-1}$ and $C_{sl,out}$ = 0.0001599 $g_{oil} \cdot g_{sl}^{-1}$. Therefore,

$$C = \frac{45.2 \text{ g}_{sl} \cdot \text{s}^{-1}(0.000503 \text{ g}_{oil} \cdot \text{g}_{sl}^{-1} - 0.0001599 \text{ g}_{oil} \cdot \text{g}_{sl}^{-1})}{16.9 \text{ g}_{\text{CO2}} \cdot \text{s}^{-1}}$$

$$C = 9.17 \times 10^{-4} \text{ g}_{oil} \cdot \text{g}_{co2}^{-1}$$

Then,

$$ka = \frac{-(16.9\ \mathrm{g_{CO2}} \cdot \mathrm{s^{-1}}) \ln\left(\frac{0.0552\ \mathrm{g}_{oil} \cdot \mathrm{g}_{CO2}^{-1} - 9.17\ \times 10^{-4}\ \mathrm{g}_{oil} \cdot \mathrm{g}_{co2}^{-1}}{0.0552\ \mathrm{g}_{oil} \cdot \mathrm{g}_{CO2}^{-1}}\right)}{(0.0055\ \mathrm{m^2})(2.2\ \mathrm{m})\ (742\ 890\ \mathrm{g}_{CO2} \cdot \mathrm{m^{-3}})}$$

$$ka = \ 3.14 \times 10^{-5}\ \mathrm{s^{-1}}$$